2001

Robust decentralized control of power systems through excitation systems and thyristor controlled series capacitors

Lingling Fan
West Virginia University

Robust Decentralized Control of Power Systems through Excitation Systems and Thyristor Controlled Series Capacitors

by

Lingling Fan

Dissertation submitted to the
College of Engineering and Mineral Resources
at West Virginia University

in partial fulfillment of the requirements
for the degree of

Doctor of Philosophy
in
Electrical Engineering

Professor Asadollah Davari, Ph.D.
Professor Ronald Klein, Ph.D.
Professor Powsiri Klinkhachore, Ph.D.
Professor John E. Sneckenberger, Ph.D.
Professor Ali Feliachi, Ph.D., Chair

Lane Department of Computer Science and Electrical Engineering

Morgantown, West Virginia
2001

Keywords:
robust control, decentralized control, power systems

Abstract

Robust Decentralized Control of Power Systems through Excitation Systems and Thyristor Controlled Series Capacitors

by

Lingling Fan
Doctor of Philosophy in Electrical Engineering

West Virginia University

Professor Ali Feliachi, Ph.D., Chair

The objective of this work is robust decentralized control of power systems through excitation systems and Thyristor Controlled Series Capacitors (TCSC). Hence the dissertation consists of two parts. In the first part an algorithm for the design of nonlinear decentralized excitation control is developed based on a feedback linearization technique. Feedback linearization technique is applied in excitation control of each generator to obtain an interconnected system where subsystems have linear system matrices and interconnections are represented by nonlinear terms. Different ways of achieving decentralization are investigated: (1) linear robust control combined with observer decoupled state space (2) disturbance accommodation control. While linear robust control guarantees the subsystem's stability when the interconnection terms are bounded within certain values, disturbance accommodation control is based on linear models of the interconnection terms. Nonlinear simulations are performed on a three-machine nine-bus power system. The simulation results demonstrate the effectiveness of the proposed methodologies.

In the second part, indices for control signal selection and mode effectiveness and interaction are developed. They are applied in Thyristor Controlled Series Capacitor damping control, which is to improve inter-area oscillation damping over a range of operating conditions, for evaluating local signals. Residues not only represent the combination of state controllability and observability but also represent the eigenvalue sensitivity with respect to controller parameters. Hence residues are suitable to be utilized to develop indices or criteria for control signal selection and controller siting. The indices are the effectiveness of the controller over a wide range of operating conditions and the interaction of the controller with oscillation modes other than the critical ones. Controller configuration design is also investigated: one is lead-lag structure design and the other is multi-step design.

Two case studies are performed to explain and demonstrate the effectiveness of the proposed methodologies. The first power system is the two-area four-machine inter-area oscillation benchmark system. A poor damping oscillation can be observed in the tie-line. Three typical operating conditions are chosen to testify the robustness and effectiveness of the controller. The results show that for a TCSC installed on the tie-line, the better signal is the absolute value of

active power which not only is robust but has less interaction with the other oscillation modes. The second is the western U.S. power system (WSCC). The system has three inter-area oscillation modes near 0.7 Hz. The proposed conditions and indices are utilized to find the optimal placement, signal for a TCSC damping controller. Both root locus analysis and nonlinear simulation results show that TCSC damping controller is effective in stabilizing the most critical inter-area modes.

The indices proposed in this dissertation are general and can be used for signal selection and siting of other devices, such as Static Var Compensator, Unified Power Flow Controller and etc. The uncertainty shown in the case studies in this dissertation are variations of load conditions. It can also be variations of topologies. While the variation of load conditions can be considered as unstructured uncertainty the variations of the topologies can be considered as structured uncertainty. With variation of topologies included in case studies, the proposed indices are shown to be applicable to both structured and unstructured uncertainty. The damping controller proposed in this dissertation is to use local measurement as input signals. Local measurements can be obtained by phasor measurement units (PMU). The feasibility of these control schemes using PMU should be investigated using discrete control techniques. Meanwhile, the measurement errors, control signal delays are not considered in this dissertation. Further work can take above factors into consideration.

Acknowledgements

I am grateful to have this opportunity to acknowledge the people who helped me in completing my Ph.D. degree.

My first thanks go to Dr. Ali Feliachi, who has advised me for more than two years, providing me constant guidance and contribution to my academic progress, from whom I learned research ability, communication ability and diligence, which benefit my career.

I would like to express my appreciation to Dr. Klein, who provided me a great opportunity to come to West Virginia University and provided support to both my husband and me continuously.

My thanks go to Dr. Davari, Dr. Klink and Dr. Sneckenberger for their invaluable support and serving as my committee members.

My thanks go to National Science Foundation under grant ECS-9870041 and Department of Energy (WV DOE/EPSCoR State Implementation Award) for funding the projects I was involved and providing financial support.

Special thanks goes to my colleagues Karl Schoder and Azra Hasanovic for their help.

Not even a word can express my gratefulness to my family. Without their backup and support, it is impossible for me to finish this program. I wish my father could live and see this day as he always wished me to be successful.

Finally, my thanks go to my husband for his being my partner in my life, encouraging me all the time and sharing my failure and success.

Contents

Acknowledgements **iv**

List of Figures **viii**

List of Tables **x**

1 Introduction **1**
1.1 Problem description 1
1.2 Approach 4
1.3 Outline 4

2 Literature survey **6**
2.1 Introduction 6
2.2 Excitation control for stability enhancement 6
2.2.1 Feedback linearization technique 9
2.2.2 Decentralization techniques 10
2.2.3 Observer decoupled state space 12
2.3 TCSC damping controller for inter-area oscillations 12
2.3.1 Inter-area oscillations 12
2.3.2 Signal selection and controller siting 13
2.3.3 Controller structure 14
2.4 Conclusion 16

3 Nonlinear decentralized control of excitation systems **17**
3.1 Introduction 17
3.2 Feedback linearization theory 18
3.2.1 Input-state linearizable 18
3.2.2 Conditions for input-state linearization 19
3.3 Nonlinear synchronous generator model and its mapped linear system 19
3.3.1 One-axis model 20
3.3.2 Subtransient model 24
3.4 Linear robust controller design 26
3.5 Observer decoupled state space (ODSS) 28
3.5.1 Physical meaning of dynamic rotor angle reference δ_{ei} 28

3.5.2 Calculation of the new state variable through local measurements 31
3.6 Linear robust design and ODSS case study 32
3.7 Disturbance accommodation control 33
3.7.1 DAC Theory 35
3.7.2 Modeling interface variable 36
3.7.3 Design of a disturbance-utilization controller for output regulator problem . . 39
3.7.4 Case study 44
3.8 Conclusion 46

4 TCSC damping controller 49
4.1 Introduction 49
4.2 Power system model with TCSC damping controller 52
4.3 Modal analysis 54
4.4 Robust residue-based damping controller 58
4.4.1 Signal selection 58
4.4.2 Controller design 60
4.5 Case study – a two-area four-machine power system 62
4.5.1 Operating conditions 64
4.5.2 Indices for signal selection 65
4.5.3 Damping controller design 69
4.6 Case study – the western U.S. power system 77
4.6.1 Introduction 77
4.6.2 WSCC system 79
4.6.3 Damping enhancement via TCSC 83
4.6.4 TCSC siting and signal selection 83
4.7 Conclusion 87

5 Interaction between excitation and TCSC damping controllers 90

6 Conclusions 96

References 99

A Synchronous generator models 104
A.1 Classical generator model 104
A.2 Two-axis generator model 106
A.3 One-axis generator model 106

B Proof of Theorem 3.2 107
B.1 Intuitive proof of necessity part 107
B.2 Proof of sufficiency part 109

C Solution of Riccati equation 3.19 111

D Solving Kx, Ky, Kz 113

E Two-area four-generator test system data **115**

F WSCC system data **117**

Approval Page **122**

List of Figures

1.1 Power system controller classes . . . 2

2.1 Diagram of conventional excitation control . . . 7
2.2 Bode diagram of a phase-lead unit . . . 8
2.3 Lead-lag controller structure . . . 15

3.1 Feedback linearization diagram . . . 19
3.2 Block diagram of direct axis of subtransient generator model. . . . 22
3.3 Block diagram of quadrature axis of subtransient generator model. . . . 23
3.4 The plant and controller interconnection . . . 26
3.5 A two-generator power system . . . 29
3.6 Equivalent two-generator power system . . . 30
3.7 A synchronous machine connected with its terminal bus . . . 31
3.8 A three-machine nine-bus power system . . . 32
3.9 Time response of relative rotor angles . . . 33
3.10 Time response of electric torques and excitation voltages . . . 34
3.11 Time reponse of the new state variables . . . 34
3.12 Interface variables w_2 . . . 36
3.13 Interface variable w_3 . . . 37
3.14 K_x versus time . . . 42
3.15 K_y versus time . . . 42
3.16 K_z versus time . . . 43
3.17 Time response of the relative rotor angles of the open-loop system . . . 44
3.18 Machine angles when a nonlinear controller is installed at machine #2 . . . 45
3.19 Excitation voltage of machine #2 . . . 46
3.20 Machine angles when nonlinear controllers are installed at machines #2 and #3 . . . 47
3.21 Excitation voltages of machines #2 and #3 . . . 47
3.22 Machine angles when nonlinear controllers are installed at machines #2 and #3 . . . 48
3.23 Excitation voltages of machines #2 and #3 . . . 48

4.1 Configuration of a TCSC . . . 50
4.2 Impedance vs. firing angle α characteristic of the TCSC. . . . 51
4.3 Closed-loop feedback system . . . 57
4.4 Residue plot . . . 59

4.5 Closed-loop system diagram . . . 62
4.6 Two-area test power system . . . 63
4.7 Eigenvalues of the open-loop system . . . 64
4.8 Variation of proposed effectiveness index vs. the tie-line active power . . . 66
4.9 $SI^i_{\lambda 31}$ vs. the tie-line active power . . . 66
4.10 $SI^i_{\lambda 33}$ vs. the tie-line active power . . . 67
4.11 $SI^i_{\lambda 42}$ vs. the tie-line active power . . . 68
4.12 $SI^i_{\lambda 44}$ vs. the tie-line active power . . . 68
4.13 Robust desgin illustration . . . 70
4.14 Root locus with absolute value of active power flow as variable (gain = 0 to 2, with a step of 0.1) . . . 71
4.15 Root locus with voltage magnitude as variable, (gain = 0 to 10, each step 1) . . . 72
4.16 Dynamic response of relative rotor angles in case 1 . . . 73
4.17 Dynamic response of relative rotor angles in case 2 . . . 73
4.18 Dynamic response of relative rotor angles in case 3 . . . 74
4.19 Dynamic response of u – B_tcsc . . . 74
4.20 Dynamic response of relative rotor angles in case 1 . . . 75
4.21 Dynamic response of relative rotor angles in case 2 . . . 75
4.22 Dynamic response of u – B_tcsc . . . 76
4.23 Root locus of two types of design . . . 78
4.24 WSCC system . . . 80
4.25 Root locus of the system with TCSC controller . . . 86
4.26 Generator rotor speeds of WSCC reduced system with no TCSC . . . 86
4.27 Generator rotor speeds of WSCC reduced system with TCSC . . . 87
4.28 Tie-line power flow of WSCC reduced system with no TCSC . . . 88
4.29 Tie-line power flow of WSCC reduced system with TCSC . . . 88
4.30 TCSC damping controller output . . . 89

5.1 Open-loop system poles. . . . 91
5.2 Open-loop power system dynamic performance. . . . 92
5.3 Dynamic performance of relative rotor angles. . . . 92
5.4 Dynamic response of excitation controller system output. . . . 93
5.5 Root locus of the system with TCSC controller . . . 94
5.6 Dynamic performance of relative rotor angles. . . . 94
5.7 Dynamic response of TCSC damping controller output . . . 95

A.1 Phasor diagram . . . 105
A.2 Classical equivalent circuit of a generator . . . 105
A.3 Transient equivalent circuit of a generator . . . 106

List of Tables

3.1 Eigenvalues of Electromechanic Oscillation Modes 37

4.1 The dominant oscillation modes 63
4.2 Three Operating Conditions (values in pu) 64
4.3 Residues' magnitude and phase of the inter-area mode 65
4.4 Angle of residues with input signal: |P| 69
4.5 One-step design approach 77
4.6 Two-step design approach 77
4.7 Eigenvalue analysis results of local oscillation modes 81
4.8 Eigenvalue analysis results of inter-area oscillation modes 82
4.9 Mode shapes of inter-area oscillation modes 82
4.10 Residues when active power through tie-lines used as input signal of the controller in case 1 83
4.11 Residues when active power through tie-lines used as input signal of the controller in case 2 84
4.12 Residues when current magnitude used as input signal of the controller in case 1 . . 84
4.13 Residues when current magnitude used as input signal of the controller in case 2 . . 85

5.1 Test descriptions 91

E.1 Bus Data 115
E.2 Transformer and Line Data 116
E.3 Generator Data 116
E.4 Exciter Data 116

F.1 Bus Data (1) 117
F.2 Bus Data (2) 118
F.3 Transformer Data 119
F.4 Line Data 120
F.5 Generator of Classical Model 120
F.6 Generator of Detail Model 121
F.7 Exciter Data 121

Chapter 1

Introduction

1.1 Problem description

Modern power systems are nonlinear large-scale systems, with power plants and control stations interconnected through transmission lines. Stability is a major concern for large-scale power systems. When power systems are subject to a perturbation or a disturbance, such as a loss of a generator, a loss of a line or a fault, control schemes are designed to alleviate the transient behavior and steer the system to a stable condition. That adjustment to the new operating condition is called transient period. If the generators maintain synchronism at the end of the transient period, then the system is stable [4]. Stability can be further classified into transient stability and dynamic stability. Transient stability has a unique definition when applied to power systems. It relates with major disturbances and it may include specific countermeasures in the way of selective relay and other emergency control or security measures [27]. The system is called transient stable for a large disturbance, e.g., the three-phase fault, the loss of a transmission line, if following this disturbance and countermeasure, it will settle down to a stable and viable equilibrium point. Transient stability analysis examines the dynamic behavior of a power system for as much as several seconds following a disturbance and is concerned with the electrical distribution network, the electrical loads, and the electromechanical equations of motion of the interconnected generators. Transient stability can be further classified as first swing stability and oscillation stability. The system is called first swing stable if its synchronous generators will not lose synchronism during the first swing of their rotor angles. The system is called oscillation stable if the following oscillations can be dampened. A power system is dynamic stable if it remains stable when subject to small disturbances (change of load). Unlike transient stability, dynamic stability tends to be a property of the state of the

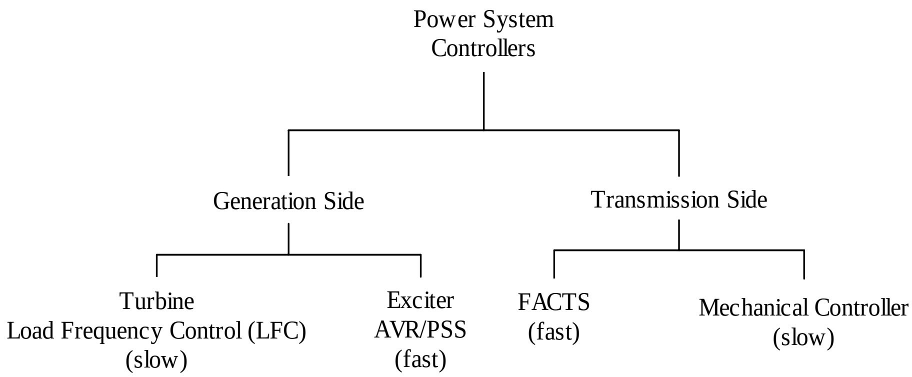

Figure 1.1: Power system controller classes

system. There is no distinct boundary between transient stability and dynamic stability.

To improve the stability of power systems, controllers are widely used in power systems. These controllers can be categorized into two classes: controllers installed on the generator side, e.g., Automatic Voltage Regulator (AVR)/Power System Stabilizer (PSS) and controllers installed on the transmission line side, e.g., Flexible Alternative Current Transmission System (FACTS) devices. There are two basic control schemes on the generator side. One is Load Frequency Control (LFC) or turbine-governor control which is used to keep the frequency of the generator at its rated value, e.g., 60 Hz in United State and 50 Hz in Europe. The other is excitation control. Due to the relatively large time constant of the turbine, the LFC control cannot act fast enough to improve transient stability of the systems. On the other hand, the excitation control can act very fast since the exciter's time constant is relatively small.

The excitation system plays an important role in power system control. With AVR, the excitation system can regulate the terminal voltage. With PSS – which uses rotor speed error, frequency error or power as input – the excitation system can provide oscillation damping to power systems.

Most of those control schemes are based on linear power system models which are valid around a certain operating point. A power systems is actually a nonlinear system, and therefore, with a change of operating point, these control schemes designed for a specific operating point may lose their effectiveness to stabilize the power system. Even when the operating point does not change, when the feedback gains increase, the resulting stability region may vanish. This may be due to the neglected nonlinearity creating an unstable limit cycle around an asymptotically stable equilibrium [34].

Large power systems have numerous subsystems, especially power plants and control stations which are located in different geographical areas. Centralized control needs all information from every subsystem. Thus extra communication links are required, which will introduce high cost and unreliability. Therefore, the decentralized control structure is more attractive. In the past years, the feasibility of decentralized control has been studied and various control schemes proposed [63].

Nonlinear control technologies have been introduced and applied in power systems. Among them, Feedback linearization seems to be an attractive methodology. By applying feedback linearization technique, nonlinear systems are mapped to linear ones while retaining some internal dynamics. Control schemes based on linear systems can then be applied. The control law has to be mapped back to the original nonlinear system. The mapping needs information of the whole system. The problem then arises, that decentralized control scheme cannot be reasonably achieved. Research has to be done to design the nonlinear controller while maintaining decentralization and robustness.

While excitation control improves the stability of synchronous machines, FACTS-based control is expected to stabilize tie-line oscillations. FACTS concepts were introduced into power systems with the advent of high voltage power electronics technology, microprocessors and microelectronics. FACTS is designed to overcome the limitations of present mechanically controlled AC power transmission systems. The main purpose of FACTS devices is to increase transmission capacities and control abilities of power flows. By using reliable high-speed power electronics controllers, FACTS technology also offers improvements in power system oscillation damping.

Since FACTS devices are installed in transmission lines which link distinct geographical areas, the FACTS-based control will be able to stabilize inter-area oscillations which cannot be controlled through generator controllers with only local measurements.

This dissertation investigates (1) the application of nonlinear control theory combined with linear control techniques to design decentralized controllers for excitation systems and (2) the siting, signal selection and controller design of the damping control of a Thyristor Controlled Series Capacitor (TCSC) — a kind of device of FACTS to obtain a robust controller using only local measurements.

1.2 Approach

The approach of this research is described here. First, each generator is considered as a subsystem described with a set of differential equations which includes mathematical terms of interconnection. Feedback linearization technique is applied to the generator model, resulting in a partially linear model, i.e., it is linear except for the interconnection terms. Two methods to handle the nonlinear terms are investigated to achieve a robust decentralized control scheme. These two methods are the linear robust design method and Disturbance Accommodation Control method.

Second, the purpose of FACTS-based controllers is to dampen inter-area oscillations for a wide range of operating conditions. Several oscillation modes may exist in power systems. The controllers are expected to dampen critical modes — the most poorly damped modes — while having less effect on the other oscillation modes. Indices for selecting signals are proposed and a control structure is investigated. A modal analysis method is used to identify oscillation modes, calculate mode shapes and obtain residues of input-output channels. Residues represent the system sensitivity with respect to the controller parameters such as gain. Therefore, residues are very useful quantities. Based on residue's phase and magnitude information, conditions and indices for signal selection can then be derived and used to determine the appropriate signal for implementation. Case studies on two power systems are performed to illustrate the effectiveness of the proposed methodology. One is a two-area four-generator power system which presents a poorly damped inter-area oscillation. The other is the western U.S. power system (WSCC) which contains three 0.7 Hz inter-area oscillation modes. Both linear analysis and nonlinear simulations will be performed to the two power systems.

1.3 Outline

This dissertation is organized as follows. A literature survey is given in Chapter 2. In Chapter 3, feedback linearization theory is introduced. Each synchronous generator is considered as a subsystem and its excitation system is designed based on feedback linearization combined with linear control techniques such as linear robust control and disturbance accommodation control.

In Chapter 4, a linearized power system model including TCSC is developed. TCSC damping control is designed to dampen inter-area oscillations using local measurements. Two indices and a constraint for signal selection and siting are proposed. Residue based controller structure is then designed as cascaded lead-lag units. In order to make the critical oscillation modes be closer to the expected values, multi-step control design is also presented. Damping enhancement of a two-area four-machine power system and the WSCC system is presented.

Chapter 5 discusses the two control schemes for the two-area four-machine power system. Chapter 6 concludes the dissertation.

Chapter 2

Literature survey

2.1 Introduction

In this chapter, a literature survey of work related to the problem investigated in this dissertation is performed. The survey is organized in two sections. In the first section, work related to improving the stability of power systems through excitation control is reviewed. Then, work related to damping power system inter-area oscillations using Thyristor Controller Series Capacitor (TCSC) is given.

2.2 Excitation control for stability enhancement

Synchronous generators are important elements in power systems. An exciter controls the generated electromagnetic flux linkage of a generator. Thus the exciter will affect not only the output voltage but the power factor and current magnitude. The conventional excitation system control includes automatic voltage regulator (AVR) and power system stabilizer (PSS) as shown in Fig. 2.1.

The AVR is a continuously acting proportional system consisting of sensors and amplifiers. With the generator terminal voltage magnitude V_t as a feed back signal, the AVR helps to control the output of the exciter so that the generator terminal voltage magnitude changes in a desired way. The PSS is an auxiliary controller that adds damping to local electromechanical oscillations that are destabilized by high gain, fast acting exciters. PSS is often in the form [17]

$$G_s(s) = \frac{k_0\tau_0 s}{1+\tau_0 s}\frac{1+\alpha_1\tau_1 s}{1+\tau_1 s}\frac{1+\alpha_2\tau_2 s}{1+\tau_2 s}$$

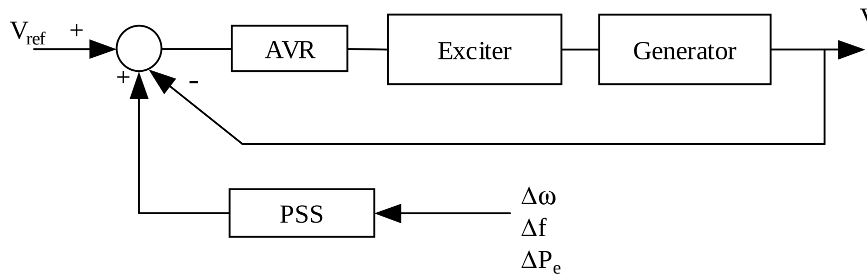

Figure 2.1: Diagram of conventional excitation control

The first term is a reset term to assure no permanent offset in PSS's output due to a prolonged frequency error. The remaining terms are lead-compensation pairs to improve the phase lag through the system from the constant reference voltage magnitude V_{ref} to angular speed ω. Input signals of PSS can be angular speed deviation $\Delta\omega$, frequency deviation Δf or generated power deviation ΔP_e. The frequency domain analysis, e.g., Bode diagram was used to determine the parameters of PSS for PSS to provide adequate phase margin at the oscillation frequency [37]. Bode diagram of a phase-lead unit in the form of

$$G(s) = \frac{1+\alpha\tau s}{1+\tau s}, \quad \alpha > 1$$

is shown in Fig. 2.2 [53].

The phase that the lead unit G(s) can provide is given by

$$\begin{aligned}
\angle G(j\omega) &= \frac{1+j\alpha\tau\omega}{1+j\tau\omega} = \tan(\alpha\tau\omega) - \tan(\tau\omega) \\
&= \tan\frac{(\alpha-1)\tau\omega}{1+\alpha\tau^2\omega^2} = \tan\frac{\alpha-1}{\frac{1}{\tau\omega}+\alpha\tau\omega} \\
&\leq \tan\frac{\alpha-1}{2\sqrt{\alpha}} \\
\text{when } \frac{1}{\tau\omega} &= \alpha\tau\omega, \angle G(j\omega) = \tan\frac{\alpha-1}{2\sqrt{\alpha}}
\end{aligned}$$

Therefore, the corresponding values of $\omega_{\max}$ and $\phi_{\max}$ are

$$\omega_{\max} = \frac{1}{\tau\sqrt{\alpha}}$$

and

$$\phi_{\max} = \sin^{-1}\frac{\alpha-1}{\alpha+1}$$

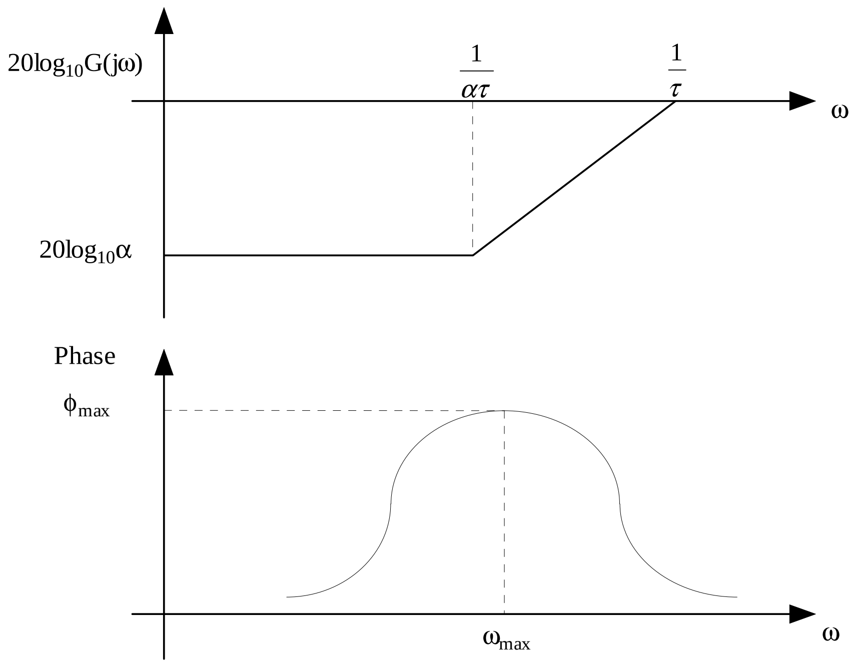

Figure 2.2: Bode diagram of a phase-lead unit

Hence, if the oscillation frequency is known and the desired phase of PSS is known, the parameters of PSS can be determined easily.

Usually PSS is designed as an auxiliary controller of a known AVR to obtain the desired damping characteristic. PSS and AVR can also be designed simultaneously [9] [23] [46]. In [23], a coordinated AVR/PSS called four-loop regulator was designed, which can not only damp oscillations but also achieve voltage regulation by defining a performance index including voltage deviation and frequency deviation. The control law is obtained by optimizing the performance index and hence the regulator is actually a linear quadratic state feedback controller with four state variables feeding back. To make this regulator more widely applicable in an industrial point of view, it was put in the standard AVR and PSS structure in [9] and was tested for damping in the 10-generator 37-bus New England power system model in [46]. Test results showed that the controller was efficient to dampen oscillations.

As a matter of fact, part of the work of this dissertation is to design excitation control for stability improvement. Treating AVR and PSS as a single system will certainly make the design procedure more systematic and easier for new techniques to be applied. The proposed work uses feedback linearization and a decentralized control structure — These concepts will be surveyed.

2.2.1 Feedback linearization technique

Many control designs of nonlinear systems are performed using linear control system tools applied to a linearized model of the original system around an operating point. The controller is designed for this specific operating condition and it is expected to be effective around this point. With significantly changing operating conditions, several controllers have to be designed and be switched on or off according to operating conditions. Nonlinear control theories have been investigated in power system excitation control to overcome the disadvantage of controllers based on linear control theories. Among these theories are neural network based controller [52], variable structure control [12] and feedback linearization control technique [41]. The neural network based controller utilizes neural networks as a nonlinear function to map an input to an output. Though the concept of design is easy to understand, the determination of the neural network parameters involves heavy computation. As for large-scale power systems with all kinds of different scenarios, the computation time will be huge and hence that kind of controller is not realistic. A variable structure control has more than one control schemes to switch to according to certain criteria. However since the switching cannot occur exactly at the required time, chattering usually occurs which will deteriorate the dynamic responses of power systems.

Feedback linearization is an approach to algebraically transform a nonlinear system dynamics into a fully or partly linear dynamic system so that linear control techniques can be applied [49]. The feedback linearization control technique was first applied to excitation systems to improve power system stability of a single-machine infinite-bus power system. The original nonlinear system has a feedback equivalence to a linear controllable system [41]. Instead of the traditional machine angle, the rotor speed, and the transient voltage as state variables, the deduced linear model after feedback linearization has the machine angle, the rotor speed and the generated power as state variables and the excitation voltage as a control input. When the order of the generator model is low, the relative degree of the output –machine rotor angle – may be the same as the order of the system, thus no remaining dynamics exist when the mapping occurs. And the state feedback controller can stabilize the system well. When the machine model has a high order, e.g., when a hydro-turbine is included as discussed in [2], non-stable internal dynamics exist. More control effort has to be done to guarantee the stability of the power system. In the case discussed in [2], an additional signal related to the gate position is fed back to the controller. In most other high order cases, the internal dynamics are stable and no extra control effort is required.

Feedback linearization technique has also been applied to a multi-machine power systems. In [48], variable structure controllers were designed to accommodate the parameter uncertainties such as generator parameters and operating conditions. In [13], a state feedback controller was designed. The controllers in [13] and [48] were claimed to use only local measurements. However, to map the linear controller back to the original nonlinear system, tremendous information from "everywhere" is needed. Research has been done on combining feedback linearization technique and decentralization technique; see [57], [58], [22] and [59]. Those decentralization techniques are addressed in the next section.

2.2.2 Decentralization techniques

The controller structure needs to be feasible for implementation. A decentralized structure is a structure in which control stations use only local measurements to generate the control signals.

The class of nonlinear interconnected systems considered here consists of m interconnected subsystems, each described by

$$\dot{x}_i = f_i(t, x_i) + g_i(t, x), i = 1, 2, ..., m$$

where $f_i(t, x_i)$ depends only on subsystem i and $g_i(t, x)$ is related with the entire remaining system, and therefore is called the interconnection term.

Here $x_i(.) \in R^{n_i}$ and x_i is the state variable vector of subsystem i;

x is the state variable vector of the entire system, $x = (x_1^T, ..., x_m^T)^T$;

m is the number of the subsystems;

$n_1 + ... + n_m = n$ is the sum of the subsystems.

In [32], Lyapunov's function method is utilized for design of decentralized controllers for an interconnected system and an M-matrix condition is derived. With M-matrix condition satisfied, the decentralized controller can stabilize the interconnected system. In the first step, the system is decomposed into smaller isolated subsystems, by ignoring interconnections, each described by:

$$\dot{x}_i = f_i(t, x_i), i = 1, 2, ..., m$$

Local stabilizers are then designed for m isolated systems using existing control methods. For linear invariant systems, pole-placement method and linear quadratic method may be used. Assume that the closed-loop local systems are stable, then Lyapunov function V_i exists which satisfies

$$\dot{V}_i = \frac{\partial V_i}{\partial t} + \frac{\partial V_i}{\partial x_i} f_i(t, x_i) \le -\alpha_i \phi_i^2(x_i)$$

$$\left\| \frac{\partial V_i}{\partial x_i} \right\| \le -\beta_i, \text{ where } \alpha_i, \beta_i \text{ are positive constants and } \phi_i(x_i) \text{ is a smooth function}$$

In the second step, the information of the interconnections are included. The interconnection terms $g_i(t, x)$ are assumed to satisfy the bound

$$\|g_i(t, x)\| \le \sum_{i=1}^{m} \gamma_{ij} \phi_j(x_j), \text{ where } \gamma_{ij} \text{ is a constant}$$

Then if matrix S defined by $S_{ij} = \begin{cases} \alpha_i - \beta_i \gamma_{ii}, i = j \\ -\beta_i \gamma_j, i \neq j \end{cases}$ is an M-matrix; that is, the leading principal minors of S are positive:

$$det \begin{bmatrix} s_{11} & s_{12} & \dots & s_{1k} \\ s_{21} & & & \\ \dots & & & \\ s_{k1} & \dots & \dots & s_{kk} \end{bmatrix} > 0, k = 1, 2, ..., m,$$

then the system is globally uniformly asymptotically stable.

Lyapunov's direct method is usually utilized to design decentralized control for excitation systems; for example, in [40]. In [57] and [22], feedback linearization techniques are applied to the subsystems to cancel or alleviate the nonlinearity. The nonlinear terms that are not measurable and that are associated with the rest of the system are kept. These nonlinear interconnection terms are assumed to be bounded, and their bounds are approximated by linear functions. Static feedback controller or dynamic feedback controller are thus designed which will satisfy the Lyapunov functions.

The above decentralization approaches are based on solving n machine Riccati equations. The satisfactory condition is that all machines should have the same kind of controller. Then the question is how to design the controller when one considers only one local synchronous generator's excitation control.

Other decentralization techniques combined with feedback linearization technique have also been investigated. In [18], interconnections are treated as disturbance or noises. And then H∞ design is applied to the subsystem. There exists a state feedback controller, which guarantees that the H∞ norm of the transfer matrix from the "noise" to the desired variables is less than a certain bound. The advantage of this approach is that only one subsystem is in consideration when designing the nonlinear controller.

2.2.3 Observer decoupled state space

Proposed by Zaborsky, et. al. [66], the observer decoupled state space (ODSS) concept has been used with the feedback linearization technique to achieve decentralization. It provides a way of recovering the information that one cannot measure locally [13]. This concept applies a specific transformation to large, nonlinear systems with a network structure, such as a power system. A power system will be transferred from state space $Z = \{z\}$ into an observer decoupled state space $Z_e = \{z_e\}$, where the state variables are locally measurable. This transformation is diffeomorphic; that is, the original differential function is smooth and its inverse exists and is smooth. Under proper and practical assumptions, generators are modeled by the classical model, so the two spaces are equivalent. At equilibrium, the two coordinates coincide pair by pair for each state variable. Everywhere else, the state vectors of the two coordinates are distinct. Hence, the observer decoupled state space Z_e can be treated as a moving target to be tracked by Z. During the tracking process, no knowledge of the equilibrium state is needed.

Due to the structure of the power system model, subsets z_{ei} of target state z_{el} connected with a particular bus (node) can be computed at the local bus i using information which can be measured at this local bus itself. So z_e is decoupled as far as its observation is concerned.

The rotor angle in a power system is a good signal for feedback stability control. The post-fault equilibrium needs to be known. Load flow is a way to calculate the equilibrium point. Yet it takes a long time and needs information on the post-fault network, so that it is not suitable for on-line control. In this situation, ODSS can provide a dynamic rotor angle that converges to a desired post-fault value much faster.

2.3 TCSC damping controller for inter-area oscillations

2.3.1 Inter-area oscillations

Inter-area oscillations are electromechanical oscillations of a group of generators in one area against a group of generators in another area [33]. These oscillations tend to be of low frequency in the range of 0.1 to 0.8 Hz. System structure such as the tie-line impedance and the power flow through the tie-lines determines the natural frequency and damping of the inter-area mode. For a two-area system, the nature frequency and damping ratio of the inter-area mode decrease as the tie-line impedance or power flow is increased. Excitation systems and load characteristics affect the nature of inter-area oscillations too.

Inter-area oscillations may induce instability to power systems and thus need to be dampened. Yang and Feliachi [63] used controllability and observability to identify inter-area oscillations from other oscillations. The most difficult type of oscillations to be dampened are those not controllable and not observable simultaneously at one location. Since AVR/PSS uses local signals as its feedback control signals, it might not be possible to dampen this type of inter-area oscillations. Research has been done to solve this kind of problem. A signal from the "other" control station is used [63]. An extra communication link is needed and the cost will increase dramatically. Thus, new methods to control inter-area oscillations have to be pursued.

More and more FACTS devices are used nowadays to regulate power flows in power systems and they are usually installed in transmission lines. Their controllability to inter-area oscillation is stronger than PSS. Among FACTS devices, Thyristor Controlled Series Capacitor (TCSC) has been used in long transmission lines to reduce the electrical distance, which will increase the amount of power transmitted and improve the dynamic stability of the system using supplementary control [35]. Investigators have used different supplementary control input signals for inter-area oscillation damping purposes.

The siting, signal selection and controller design are three topics related to FACTS-based stabilizers' effect on inter-area oscillations. Modal analysis is the most popular tool in analysis and synthesis of controllers.

2.3.2 Signal selection and controller siting

For some types of controllers, such as state feedback controllers, the input signals to the controller will be the states of the power system. The controller thus is a centralized one and may be difficult to implement. There are a lot of methods for input signal selection. For linear plant models in state-space description, state controllability and state observability have been used as criteria to choose input/output of the controller. These two quantities could be combined together as residues. Another rule for input signal selection is to adapt to changing operating conditions. The rule is that the input/output signals should be selected to yield a large minimum singular value [65].

Most TCSC damping controllers use simple structure and simple signals. In [36], the input signal—an emulated power swing angle synthesized from local measurements of voltage and current – was recommended. This control signal is also used in [56] and [64]. In [14] and [38], the input signal is synthesized from the generator's speed. This synthesized speed requires a remote signal, which will need extra communication links. Local measurements are also used as signals, such as tie-line power [15] and bus voltage magnitude [61].

Local signals are preferred. The effectiveness of these signals should be investigated to find out the appropriate signal for inter-area oscillations. Several different indices have been proposed for input signal selection and controller siting. As an example, modal analysis of the linearized open-loop power system is used in [20] where controllability is used as an index for siting and observability is used as an index for signal selection. Another index is based on an additional damping torque coefficient induced by TCSC damping controller[62]. This is also based on modal analysis but it is performed in the frequency domain. Modal decomposition is used to isolate the swing mode and then the system is represented by a block diagram based on transfer functions. Three indices are proposed in [36]. They are phase influence, maximum damping influence and natural phase influence. These indices are used to pick the equivalent impedances to determine a synthesized power angle.

To make the control signal robust over a wide range of operating conditions, an index based on approximate residues of linearized models at different operating points is proposed in [61]. This approximate residues index describes the effectiveness of the controller. If it is kept in a small range when the operating condition changes, then the control signal is robust. Otherwise, the control signal is not robust with respect to variation of the operating conditions.

2.3.3 Controller structure

Besides signal selection and controller siting, controller structure should be designed appropriately. The conventional low-order controller is an attractive structure for control engineers. Even when controllers are obtained by use of Linear Quadratic Gaussian method, the proposed control law is transformed to a conventional lead-lag low-order control structure [46].

Lead-lag control structure is a widely used structure, e.g., PSSs were designed in such control structure [37]. A lead-lag controller consists of a washout unit to eliminate the steady-state error and lead-lag units as shown in Fig. 2.3.

The residue of the open-loop system at a certain oscillation mode has a phase which determines the direction of movement of the oscillation mode's root locus. The two lead-lag units provide phase compensation to make the direction of movement to be toward the negative real axis. There are two design requirements that should be taken into consideration. First, fixed-parameter controllers are preferred. Second, different operating conditions are considered. To simplify the

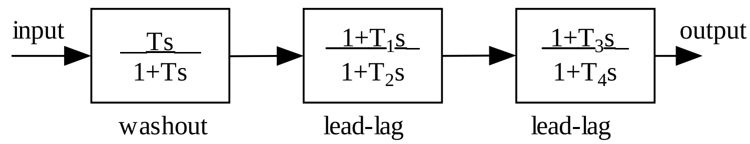

Figure 2.3: Lead-lag controller structure

design requirements, only two extreme conditions are considered. If in these two cases, the controller has satisfactory performance then the controller will have satisfactory performance in all the other cases. The assumption is that the phase compensation should be monotonic [63].

Systematic robust design methods have been applied to achieve robust controllers which can accommodate the change of network structure and operating conditions. Reference [8] gives a comparison of the classical phase compensation approach, the $\mu-$synthesis approach, and a linear matrix inequality (LMI) technique for multiple power system stabilizer design to dampen an inter-area oscillation. The inter-area oscillation is unstable in the open-loop system and cannot be stabilized using only one conventional PSS due to a right half zero (RHZ) close to the unstable pole. The two conclusions are (1) a lower-order centralized design by use of LMI matches the performance of a higher-order centralized design by use of $\mu-$synthesis, and (2) a centralized design achieves the same damping enhancement with much smaller gains than the decentralized gain.

The H∞ control design method is applied to design a TCSC damping controller in [55]. The uncertainty considered is the transmission strength variation and a structured uncertainty model is built based on the loss of a transmission line while the nominal model is built based on the nominal structure and a specific operating condition. The uncertainty model in [45] is an unstructured uncertainty representing variations of operating conditions. Besides uncertainty, model error is another issue to be considered in robust control. In [51] linear quadratic gaussian (LQG) control methodology is applied to design the robust TCSC damping controller against model error, which was modeled as white noise. However LQG method did not address uncertainties other than white noise adequately and thus is not practical.

In a word, systematic robust control is designed based on specific uncertainty. Power systems can possess a large number of topological configurations and steady-state operating points. It is difficult for a controller to be robust against all the variations.

Besides linear design methods, nonlinear design methods for TCSC are also proposed. In [15] a static neural network is established with several integral units to emulate the inverse system of the original nonlinear system. The Proportional, Integral and Derivative (PID) control design is then performed to stabilize the pseudo-linear system. The disadvantage of this design is that huge data should be collected for the parameters of the neural network to be “trained”.

2.4 Conclusion

In the literature survey, feedback linearization technique is investigated as a new control methodology for excitation control. To achieve a decentralized control structure, it should be utilized along with decentralized techniques or ODSS. The decentralized techniques preferred are the simple and practical ones and the algorithms for nonlinear excitation control are developed in Chapter 3. TCSC damping controller signal selection, siting, and controller synthesis are also investigated and the algorithm developed are shown in Chapter 4.

Chapter 3

Nonlinear decentralized control of excitation systems

3.1 Introduction

Primary control, such as AVR/PSS or turbine-governor in a power system is designed to respond to relatively minor disturbances in an automatic way. By use of set points, primary control will stabilize system in a specified regime. However, if the post-fault operating condition is far from the normal condition, a controller tuned in normal condition may not operate as expected.

Nonlinear control schemes have been applied to power systems to make controllers operate in a wide range. Among them, feedback linearization technique enables the nonlinear power system model to be transformed into a linear system model. Thus linear control techniques can be applied.

When not all information is available, a totally linear system model can not be obtained. Instead, nonlinear interconnection terms have to be taken into consideration. The first way in this chapter is to model the interconnection terms as bounded disturbances. Then linear robust control method is applied. The second way is to model the interconnection terms as wave-form type disturbances that can be expressed in state-space form. Linear quadratic regulator is then designed.

Observer decoupled state space (ODSS) concept is also used in this chapter to obtain a dynamic equilibrium point of rotor angle. The application of ODSS is shown in the case study.

3.2 Feedback linearization theory

3.2.1 Input-state linearizable

Consider an n dimension system,

$$\dot{\mathbf{x}} = f(\mathbf{x}) + g(\mathbf{x})u, \;\; y = h(\mathbf{x}) \tag{3.1}$$

where x represents a n dimensional state vector, $x = [x_1, x_2, ..., x_n]^T$, u is the scalar control input, f and g are nonlinear vector functions of the states, h is a scalar function of the states and y is the output of interest. If the original system can be transformed to a canonical form when applying a transformation $z = \phi(x)$, where

$$\begin{bmatrix} z_1 \\ z_2 \\ ... \\ z_m \end{bmatrix} = \begin{bmatrix} \phi_1(x) \\ \phi_2(x) \\ ... \\ \phi_m(x) \end{bmatrix} = \begin{bmatrix} h(x) \\ L_f^1 h(x) \\ ... \\ L_f^{m-1} h(x) \end{bmatrix}$$

with $L_f^k h(x) \triangleq \bigtriangledown[L_f^{k-1}].f(x)$

$L_f^k h(x) \neq 0 \;\; \text{for } k = 0, ..., m-1$

$L_f^k h(x) = 0 \;\; \text{for } k = m, ..., n$

then the system is said to be input-state linearizable.

The dynamics of the new system can be expressed in canonical form

$$\begin{aligned} \frac{d}{dt}\begin{bmatrix} z_1 \\ z_2 \\ ... \\ z_m \end{bmatrix} &= \begin{bmatrix} z_2 \\ z_3 \\ ... \\ \alpha(z) + \beta(z) \end{bmatrix} = Az + bv, \\ y &= z_1 \end{aligned} \tag{3.2}$$

where $z = [z_1, z_2, ..., z_m]^T$ is called the linearizing input state. Also $\alpha(z) = L_f^m h[\phi^{-1}(z)]$,and $\beta(z) = L_g L_f^{m-1} h[\phi^{-1}(z)] \neq 0$ are called the linearizing control law, where

$$A = \begin{bmatrix} 0 & 1 & 0 & .. & 0 \\ 0 & 0 & 1 & .. & .. \\ .. & .. & .. & .. & .. \\ 0 & 0 & 0 & .. & 1 \\ 0 & 0 & 0 & .. & 0 \end{bmatrix}, b = \begin{bmatrix} 0 \\ 0 \\ .. \\ 0 \\ 1 \end{bmatrix}$$

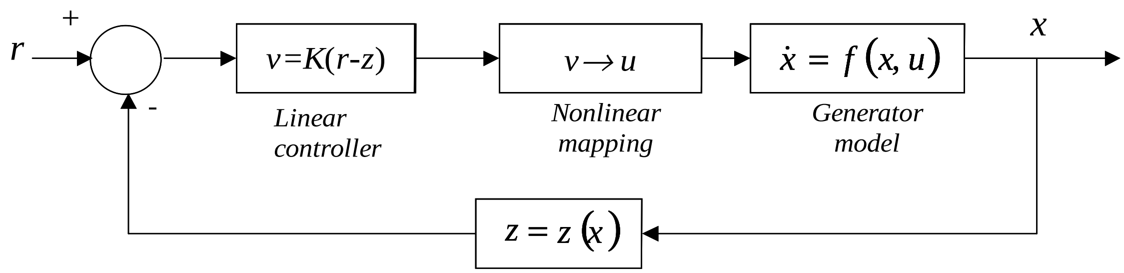

Figure 3.1: Feedback linearization diagram

The transformed linear dynamics have the canonical form. Since all linear controllable systems are equivalent to the canonical form through a linear state transformation and pole placement, therefore if the nonlinear system of Eq. 3.1 can be transformed into a linear system, it is input-state linearizable. The diagram of feedback linearization is shown in Fig. 3.1.

3.2.2 Conditions for input-state linearization

Reference [49] gives the conditions for input-state linearization.

Theorem 3.1 The nonlinear system in Eq. 3.1, with $f(x)$ and $g(x)$ being smooth vector fields, is input-state linearizable if and only if there exists a region Ω such that the following conditions hold:

- the vector field $\{\mathbf{g}, ad_f\mathbf{g}, ..., ad_f^{n-1}\mathbf{g}\}$ are linearly independent in Ω
- the set $\{\mathbf{g}, ad_f\mathbf{g}, ..., ad_f^{n-2}\mathbf{g}\}$ is involutive in Ω

The one-axis third order synchronous generator model has been proved to be input-state linearizable if the state is a vector of rotor angle δ, rotor speed ω and generating power P_e.

3.3 Nonlinear synchronous generator model and its mapped linear system

The synchronous generator is a key component in power systems. Feedback linearization technique law varies when the model varies. There are several models available for synchronous generators. As the one-axis model is input-state linearizable without internal dynamics remaining, this model has been studied in most of the literature on feedback linearization control in excitation control [13] [59]. In this dissertation, both the one-axis model and the full-order synchronous generator model will be studied.

3.3.1 One-axis model

Consider a power system that comprises N generating unit. Each unit is modeled using the one-axis model. For the i-th machine in the power system, the state space model is expressed as follows (subscript i is neglected for simplicity).

$$\begin{aligned} \frac{d\delta}{dt} &= \omega_0 (\omega - 1) \\ \frac{d\omega}{dt} &= \frac{1}{2H} (P_m - P_e) \\ \frac{dE'_q}{dt} &= \frac{1}{T'_{d0}} (E_{fd} - E) \end{aligned} \tag{3.3}$$

where

δ : rotor angle

ω: rotor speed

P_m : mechanical power

P_e : electrical power

E'_q : direct axis stator EMF corresponding to the field flux linkage

E_{fd} : stator EMF corresponding to the excitation voltage

E : stator EMF corresponding to the open circuit current, $E = E'_q - (x_d - x'_d)I_d$

T'_{do} : direct axis transient open circuit time constant

H : constant angular moment of inertia in second

The interaction of this generator with the rest of the system is through the electrical power P_e which is given by

$$P_e = E'_q I_q + (x'_d - x_q) I_q I_d$$

where

I_d: d-axis current of the stator

I_q: q-axis current of the stator

Excitation voltage E_{fd} is the input to the system.

Exact feedback linearization technique are applied to the state-space model of each machine. The new state variables are defined as:

$$\begin{aligned} \xi_1 &= \delta - \delta_0 \\ \xi_2 &= \omega_0 (\omega - 1) \\ \xi_3 &= \frac{\omega_0}{2H} (P_m - P_e) \end{aligned} \tag{3.4}$$

Then

$$\begin{aligned} \frac{d\xi_1}{dt} &= \xi_2 \\ \frac{d\xi_2}{dt} &= \xi_3 - \frac{D}{2H}\xi_2 \\ \frac{d\xi_3}{dt} &= v + w \end{aligned} \tag{3.5}$$

where w is the interfacing term, a function of the differential of the currents, which relates to the state variables of the rest of the system and cannot be obtained directly from the one-axis generator model.

$$w = -\frac{\omega_0}{2H}\left(E'_q \dot{I}_q + (x'_d - x_d)(I_q \dot{I}_d + \dot{I}_q I_d)\right) \tag{3.6}$$

and

$$v = \alpha + \beta E_{fd} \tag{3.7}$$

where

$$\begin{aligned} \alpha &= \frac{\omega_0}{2H}\frac{1}{T'_{d0}} E I_q \\ \beta &= -\frac{\omega_0}{2H}\frac{1}{T'_{d0}} I_q \end{aligned} \tag{3.8}$$

Then the subsystem dynamics in the coordinate system become:

$$\dot{\xi} = A\xi + Bv + Ew \tag{3.9}$$

where

$$A = \begin{bmatrix} 0 & 1 & 0 \\ 0 & 0 & 1 \\ 0 & 0 & 0 \end{bmatrix}, B = \begin{bmatrix} 0 \\ 0 \\ 1 \end{bmatrix}, E = \begin{bmatrix} 0 \\ 0 \\ 1 \end{bmatrix}$$

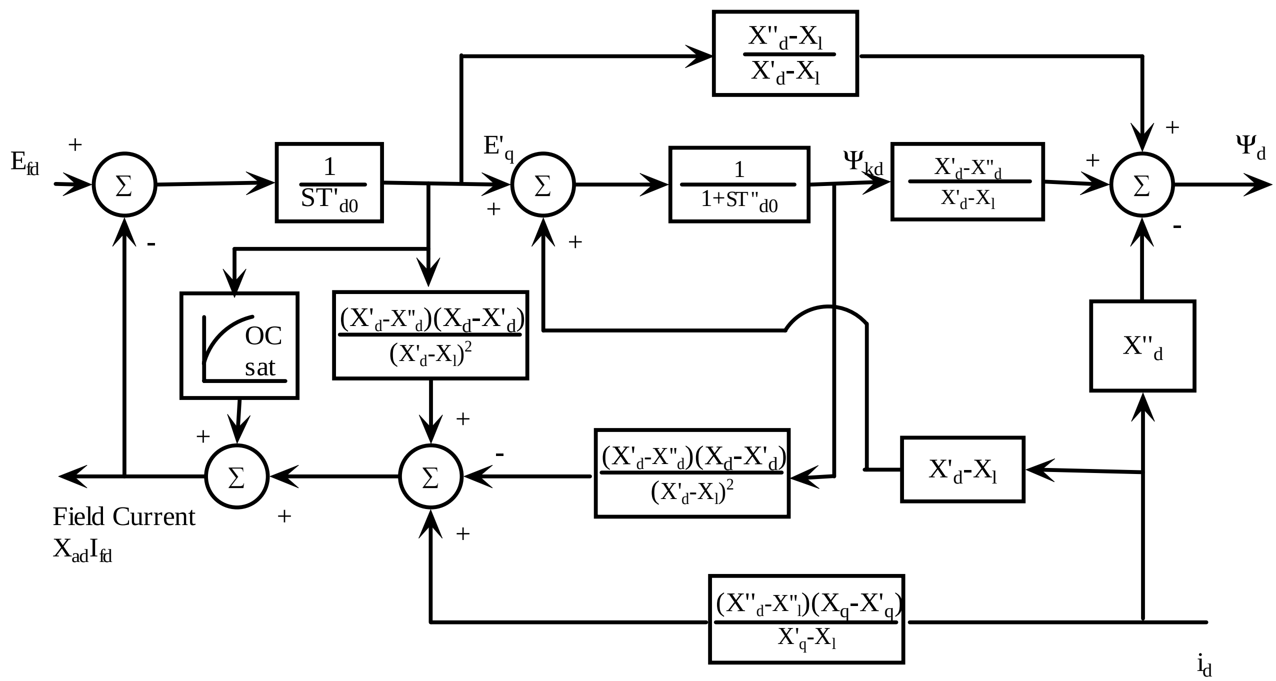

Figure 3.2: Block diagram of direct axis of subtransient generator model.

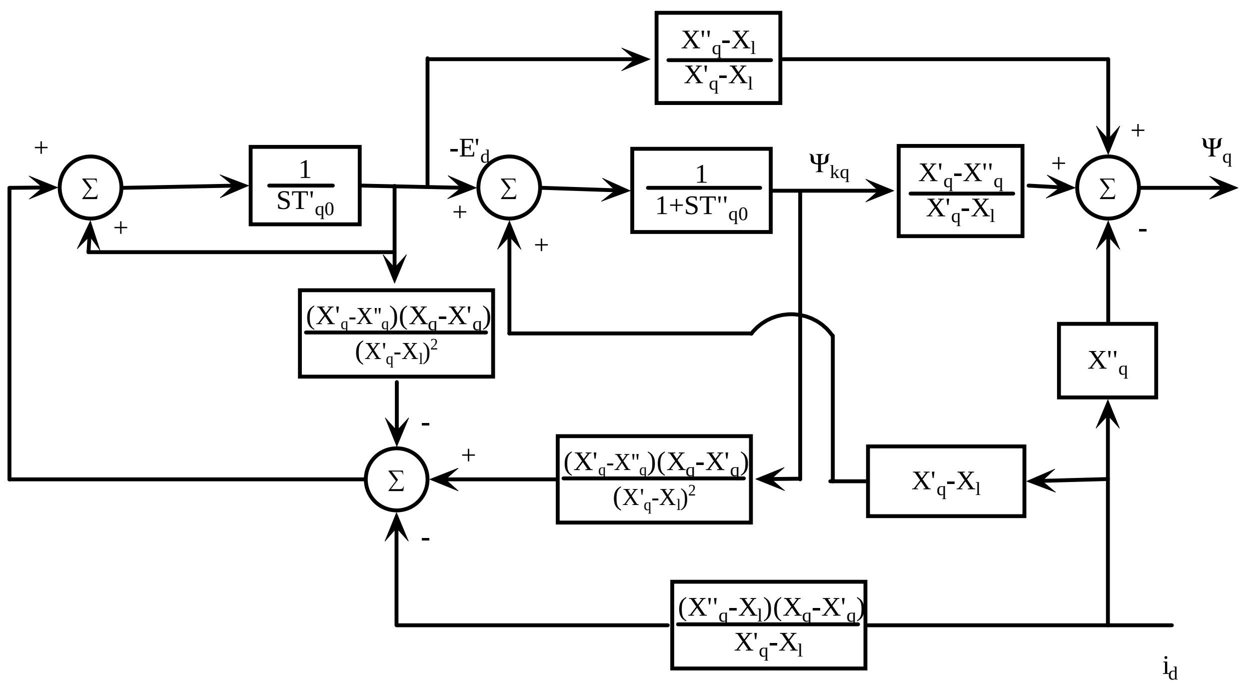

Figure 3.3: Block diagram of quadrature axis of subtransient generator model.

3.3.2 Subtransient model

In subtransient model, a synchronous generator is modeled as a voltage source behind subtransient reactance. The model be expressed in the block diagrams in Fig. 3.2 and Fig. 3.3 [4].

Besides the swing equations, the model includes four differential equations.

$$
\begin{aligned}
\dot{E}'_q &= \frac{1}{T'_{d0}}(K_d E'_q + E_{FD} + x_{xd} i_d - K_d \Psi_{kd} + E_\Delta) \\
\dot{\Psi}_{kd} &= -\Psi_{kd} + E'_q - i_d(x'_d - x_l) \\
\dot{E}'_d &= -\frac{1}{T'_{q0}}(E'_d + K_q E'_d - x_{xq} i_q + K_q \Psi_{kq}) \\
\dot{\Psi}_{kq} &= -\frac{1}{T''_{q0}}(\Psi_{kq} - E'_d - i_q(x'_q - x_l))
\end{aligned}
\tag{3.10}
$$

where

$$K_d = \frac{(x_d - x'_d)(x'_d - x''_d)}{(x'_d - x_l)^2} \tag{3.11}$$

$$K_q = \frac{(x_q - x'_q)(x'_q - x''_q)}{(x'_q - x_l)^2} \tag{3.12}$$

$$x_{xd} = \frac{(x_d - x'_d)(x'_d - x_l)}{x'_d - x_l} \tag{3.13}$$

$$x_{xq} = \frac{(x_q - x'_q)(x'_q - x_l)}{x'_q - x_l} \tag{3.14}$$

where

$i_d(t), i_q(t)$	direct-axis and quadrature-axis currents
$x_d(t), x_q(t)$	direct-axis and quadrature-axis reactances
$x'_d(t), x'_q(t)$	direct-axis and quadrature-axis transient reactances
$x''_d(t), x''_q(t)$	direct-axis and quadrature-axis subtransient reactances
E'_q	direct-axis stator EMF corresponding to the field flux linkage
E'_d	quadrature-axis stator EMF corresponding to Q circuit flux linkage
Ψ_{kd}, Ψ_{kq}	direct-axis and quadrature-axis subtransient flux linkages

The outputs of the diagram Ψ_d, Ψ_q are expressed as follows.

$$\begin{aligned} \Psi_d &= \frac{x_d'' - x_l}{x_d' - x_l} E_q' + \frac{x_d' - x_d''}{x_d' - x_l} \Psi_{kd} + i_d x_d'' \\ \Psi_q &= -\frac{x_q'' - x_l}{x_q' - x_l} E_d' + \frac{x_q' - x_q''}{x_q' - x_l} \Psi_{kq} - i_q x_q'' \end{aligned} \tag{3.15}$$

The electrical power generation P_e is expressed as follows.

$$P_e = i_q \Psi_d - i_d \Psi_q \tag{3.16}$$

The new state variables after feedback linearization are the same as those in one-axis model. Due to the difference of the two models, differential equation of ξ_3 is expressed as follows.

$$\begin{aligned} \frac{d\xi_3}{dt} &= -\frac{\omega_0}{2H}\frac{dT_e}{dt} = -\frac{\omega_0}{2H} \begin{bmatrix} i_q \left(\frac{x_d'' - x_l}{x_d' - x_l} \dot{E}_q' + \frac{x_d' - x_d''}{x_d' - x_l} \dot{\Psi}_{kd} + \dot{i}_d x_d'' \right) \\ -i_d \left(-\frac{x_q'' - x_l}{x_q' - x_l} \dot{E}_d' + \frac{x_q' - x_q''}{x_q' - x_l} \dot{\Psi}_{kq} - \dot{i}_q x_q'' \right) \end{bmatrix} + \frac{\omega_0}{2H_i} \left(\dot{i}_q \Psi_d - \dot{i}_d \Psi_q \right) \\ &= \alpha + \beta E_{fd} + w \end{aligned} \tag{3.17}$$

where

$$\begin{aligned} \alpha &= -\frac{\omega_0}{2H} \begin{bmatrix} i_q \left(\frac{x_d'' - x_l}{x_d' - x_l} \frac{1}{T_{d0}'} (K_d E_q' + x_{xd} i_d - K_d \Psi_{kd} + E_\Delta) + \frac{x_d' - x_d''}{x_d' - x_l} \dot{\Psi}_{kd} \right) \\ -i_d \left(-\frac{x_q'' - x_l}{x_q' - x_l} \dot{E}_d' + \frac{x_q' - x_q''}{x_q' - x_l} \dot{\Psi}_{kq} \right) \end{bmatrix} \\ \beta &= -\frac{\omega_0}{2H} \frac{x_d'' - x_l}{x_d' - x_l} \frac{1}{T_{d0}'} i_q \\ w &= \frac{\omega_0}{2H} \left(\dot{i}_q (\Psi_d - i_d x_q'') - \dot{i}_d (\Psi_q + i_q x_d'') \right) \end{aligned}$$

The study of synchronous generator models shows that the more complicate the model, the more information should be taken care, which will increase the difficulty of implementation of the controller. Depending on the special needs of a power system, a different study model of the generator is to be selected with accuracy and simplicity as trade-offs. When feedback linearizing technique is applied to one-axis model, the original third order model is mapped to a third order model and no inner dynamics exist. However, the subtransient model has sixth order and it is also mapped to a third order model. Inner dynamics exist. Due to the characteristics of electric circuits of synchronous generator, these inner dynamics are stable and no control effort is necessary to take care of the dynamics. Therefore, the control design procedure based on both models are same. The following controller design is based on the one-axis generator model.

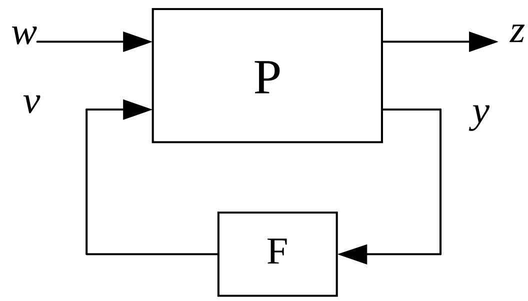

Figure 3.4: The plant and controller interconnection

3.4 Linear robust controller design

For each subsystem, one now has a set of differential equations as shown in Eq. 3.9. Each subsystem has an interconnection with the rest of the system. To formulate a decentralized control problem, the interconnection is considered as a disturbance and the objective of a robust controller is to be robust against the disturbance. This controller will use only local measurements as input signals. One can find that from Eq. 3.6 that the steady state value of the interconnection is zero and for each subsystem the interconnection is a single-block "uncertainty". These characteristics make it probable for the development of H_∞ methods.

The regulated variables are variables whose dependence on the disturbance one wants to minimize. The regulated variables can be chosen as the state variables and the control input $z_i = [\xi_{i1}, \xi_{i2}, \xi_{i3}, v_i]^T$, i.e., $z_i = C_i\xi_i + D_i v_i$,
where $C_i = \begin{bmatrix} 1 & 0 & 0 \\ 0 & 1 & 0 \\ 0 & 0 & 1 \end{bmatrix}, D_i = \begin{bmatrix} 0 \\ 0 \\ 1 \end{bmatrix}$.

The plant or the i-th subsystem taken into consideration is (subscript i is omitted for simplicity):

$$\begin{aligned} \dot{\xi} &= A\xi + Bv + Ew \\ z &= C\xi + Dv \end{aligned} \tag{3.18}$$

The control objective is now to minimize the effects of the disturbance w on the regulated variables z by finding an appropriate control input v as shown in Fig. 3.4, where P represents the plant and F represents the controller.

This control problem can be formulated as a H_∞ control problem. The transfer matrix from w to z, denoted by G_F, is to have a H_∞ norm strictly less that some bound γ. The H_∞ norm is equal to the L_2 induced operator norm of the closed-loop operator, i.e.

$$\|G_F\|_\infty = \sup_w \left\{ \frac{\|G_{ci}w\|_2}{\|w\|_2}, w \neq 0 \right\}$$

where G_{ci} denotes the closed-loop operator mapping w to z; $\|f\|_2 = \left(\int_0^\infty \|f(t)\|^2 \, dt \right)^{1/2}$ where $\|.\|$ denotes the Euclidian norm.

The synthesis problem is to design a controller F so that the closed-loop system is stable and $\|G_F\|_\infty < \gamma$.

In power systems, it is not desirable to feedback w since it is a complex term as shown in Eq. 3.6. Hence, a compensator described by a static state feedback law is designed to make the system internally stable. Such static state feedback control exists if, and only if, the solution of a certain algebraic Riccati equation is a positive semi-definite matrix. The design is obtained from the following theorem [54].

Theorem 3.2 Consider the system Eq. 3.18 . Let $\gamma > 0$. Assume that the system (A, B, C, D) has no invariant zeros on the imaginary axis. Then the following statements are equivalent:

1. A static feedback law $v = F\xi$ exists such that after applying this compensator to the system, the resulting closed-loop system is internally stable and the closed-loop operator G_{ci} has an H_∞ norm less than γ, i.e., $||G_{ci}||_\infty < \gamma$.

2. There is a positive semi-definite solution P of the algebraic Riccati equation

$$0 = A^T P + PA + C^T C - \begin{pmatrix} B^T P + D^T C \\ E^T P \end{pmatrix}^T \begin{pmatrix} D^T D & 0 \\ 0 & -\gamma^2 I \end{pmatrix}^{-1} \begin{pmatrix} B^T P + D^T C \\ E^T P \end{pmatrix} \tag{3.19}$$

   such that A_{cl} is asymptotically stable where:

$$A_{cl} = A - \begin{pmatrix} B & E \end{pmatrix} \begin{pmatrix} D^T D & 0 \\ 0 & -\gamma^2 I \end{pmatrix}^{-1} \begin{pmatrix} B^T P + D^T C \\ E^T P \end{pmatrix}$$

If P satisfies the conditions in part 2 then a controller satisfying the conditions in part 1 is defined by

$$F = -(D^T D)^{-1} \left(D^T C + B^T P \right) \tag{3.20}$$

Proof of the theorem is shown in Appendix. To obtain the solution of the positive semi-definite matrix P of the algebraic Riccati equation Eq. 3.19, Matlab Symbolic Toolbox is used. The procedure and codes to are shown in Appendix.

The nonlinear control scheme becomes

$$E_{fd} = \left(F \begin{bmatrix} \delta - \delta_0 \\ \omega_0 \left(\omega - 1 \right) \\ \frac{\omega_0}{2H} \left(T_m - T_e \right) \end{bmatrix} - \alpha \right) / \beta \tag{3.21}$$

3.5 Observer decoupled state space (ODSS)

From Eq. 3.21, it is obvious that rotor angle is an important variable that should be measured and fed back to the controller. The rotor angle with respect to the generator terminal voltage can be measured through the analysis of zero sequence harmonic components of the generator terminal voltage [16]. However, in Eq. 3.21, the rotor angle of a machine with respect to the reference machine is needed. Remote information has to be transmitted in order to obtain this variable. In addition, the post fault equilibrium has to be known which requires a large amount of calculation and takes a long time. ODSS technique provides a variable which can be obtained through local measurements to replace the rotor angle offset from an equilibrium point, which is difficult to measure.

3.5.1 Physical meaning of dynamic rotor angle reference δ_{ei}

The observer decoupled state space concept applied in power systems is illustrated in the system shown in Fig 3.5 that consists of two-machines connected with a tie-line, where E_i and H_i are the magnitude of the voltage source and the inertia constant respectively. Assume that the mechanical power is kept constant and both generators are modeled by classical models, i.e., a constant voltage source behind a reactance, then the swing equations can be expressed as

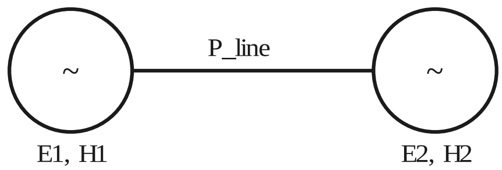

Figure 3.5: A two-generator power system

$$\begin{aligned} \frac{d\delta_1}{dt} &= \omega_0 (\omega_1 - 1) \\ \frac{d\omega_1}{dt} &= \frac{1}{2H_1} \left(P_{m1} - \frac{E_1 E_2}{x_\Sigma} \sin(\delta_1 - \delta_2) \right) \\ \frac{d\delta_2}{dt} &= \omega_0 (\omega_2 - 1) \\ \frac{d\omega_2}{dt} &= \frac{1}{2H_2} \left(P_{m2} - \frac{E_1 E_2}{x_\Sigma} \sin(\delta_2 - \delta_1) \right) \end{aligned} \tag{3.22}$$

where

δ_i : rotor angle.

ω_i: rotor speed

P_{mi} : mechanical power

E_i : voltage source magnitude

H_i : constant angular moment of inertia in second

Define dynamic reference rotor angles by:

$$\begin{aligned} \delta_{e1} &: P_{m1} - \frac{E_1 E_2}{x_\Sigma} \sin(\delta_{1e} - \delta_2) = 0 \\ \delta_{e2} &: P_{m2} - \frac{E_1 E_2}{x_\Sigma} \sin(\delta_{2e} - \delta_1) = 0 \end{aligned}$$

It is obvious to find that

$$\begin{aligned} \delta_{e1} - \delta_2 &= \delta_{10} - \delta_{20} \\ \delta_{e2} - \delta_1 &= \delta_{20} - \delta_{10} \end{aligned}$$

where δ_{10}, δ_{20} are equilibrium states.

If observation state variables δ_1', δ_2' are defined as:

$$\begin{aligned} \delta_1' &= \delta_1 - \delta_{1e} \\ \delta_2' &= \delta_2 - \delta_{2e} \end{aligned}$$

then

$$\begin{aligned} -\delta_1' + \delta_{12} &= \delta_{e1} - \delta_1 + \delta_1 - \delta_2 = \delta_{120} \\ -\delta_2' + \delta_{21} &= \delta_{e2} - \delta_2 + \delta_2 - \delta_1 = \delta_{210} \end{aligned}$$

In the two-generator system, the new state variable δ_i' represents the shift of angle with respect to the other machine. In multi-machine power system, the new state variable represents the shift of rotor angle from equilibrium with respect to the equivalent rotor angle when the rest of the system is considered as a generator.

The multi-machine power system [10] can be reduced to a two-generator system with machine i as one of the generator and all the others are combined as another generator, see Fig. 3.6 . Assume that all the lines have no loss in real power transmission.

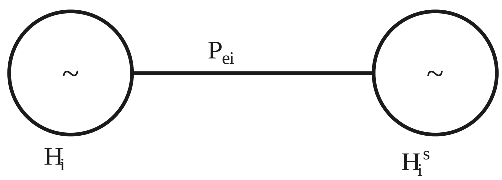

Figure 3.6: Equivalent two-generator power system

Let

$$H_i^s = \sum_{j\neq i}^{n} H_j, \;\; \delta_i^s = \frac{1}{H_i^s}\sum_{j\neq i}^{n} H_j\delta_j, \quad \omega_i^s = \frac{1}{H_i^s}\sum_{j\neq i}^{n} H_j\omega_j \tag{3.23}$$

where

δ_i^s : rotor angle of the equivalent generator

ω_i^s : rotor speed of the equivalent generator

H_i^s : constant angular moment of inertia of the equivalent generator

Then the dynamics of the equivalent generator will be:

$$\begin{aligned} \dot{\delta_i^s} &= \frac{1}{H_i^s}\sum_{j\neq i}^{n} H_j\dot{\delta_j} = \omega_0(\omega_i^s - 1) \\ \dot{\omega_i^s} &= \frac{1}{H_i^s}\sum_{j\neq i}^{n} H_j\dot{\omega_j} = \frac{1}{2H_i^s}\sum_{j\neq i}^{n}(P_{mj} - P_{ej}) = \frac{1}{2H_i^s}\left(\sum_{j\neq i}^{n}(P_{mj}) + P_{ei}\right) \end{aligned} \tag{3.24}$$

According to the two-generator power system example,

$$\delta_{ei} = \delta_i^s - \delta_{i0}^s + \delta_{i0}$$

At the equilibrium point, $\delta_{ei0} = \delta_{i0}$, which means the dynamic rotor angle reference coincides with the rotor angle.

The dynamics of δ_{ei0} are the same as δ_i^s in Eq. 3.24. Therefore, the dynamic rotor angle reference δ_{ei} is actually the center of the angles of the rest of the generators.

3.5.2 Calculation of the new state variable through local measurements

The generating power of each generator will be expressed using the d-axis voltage and terminal voltage. Assume that the d-axis transient voltage is kept constant.

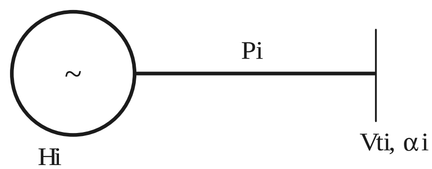

Figure 3.7: A synchronous machine connected with its terminal bus

Define a dynamic reference rotor angle by:

$$\delta_{ei} : P_{mi} - P_{ei} = P_{m0} - \frac{E'_{qi0} V_{ti}}{x'_d} \sin(\delta_{ei} - \alpha_i) = 0 \tag{3.25}$$

Now, a new observation state variable δ'_i as is defined as:

$$\delta'_i = \delta_i - \delta_{ei} \tag{3.26}$$

δ'_i is obtained from:

$$P_{mi} - P_{ei} = P_{m0} - \frac{E'_{qi} V_{ti}}{x'_d} \sin(\delta_i - \delta'_i - \alpha_i) = 0 \tag{3.27}$$

Note that the dynamic reference rotor angle δ_{ei} is an absolute angle. It cannot be calculated through measurements. Instead the new state variable δ'_i can be calculated through local measurements. Hence the controller is more attractive from an implementation point of view.

It is assumed here that the following electric variables can be measured:

V_{ti}: terminal voltage magnitude of generator i

P_{ei}: active power of generator i

Q_{ei}: reactive power of generator i

Through these measurements, the angle difference between the rotor and the terminal voltage can be obtained from Eq. 3.28.

$$\delta_i - \alpha_i = \tan^{-1} \frac{P_{ei} x_{qi}}{Q_{ei} x_{qi} + V_{ti}^2} \tag{3.28}$$

3.6 Linear robust design and ODSS case study

A three-machine nine-bus power system [4] is used to illustrate the linear robust design method, see Fig. 3.8. In addition, the offset of rotor angle is replaced with the new state proposed in Eq. 3.26.

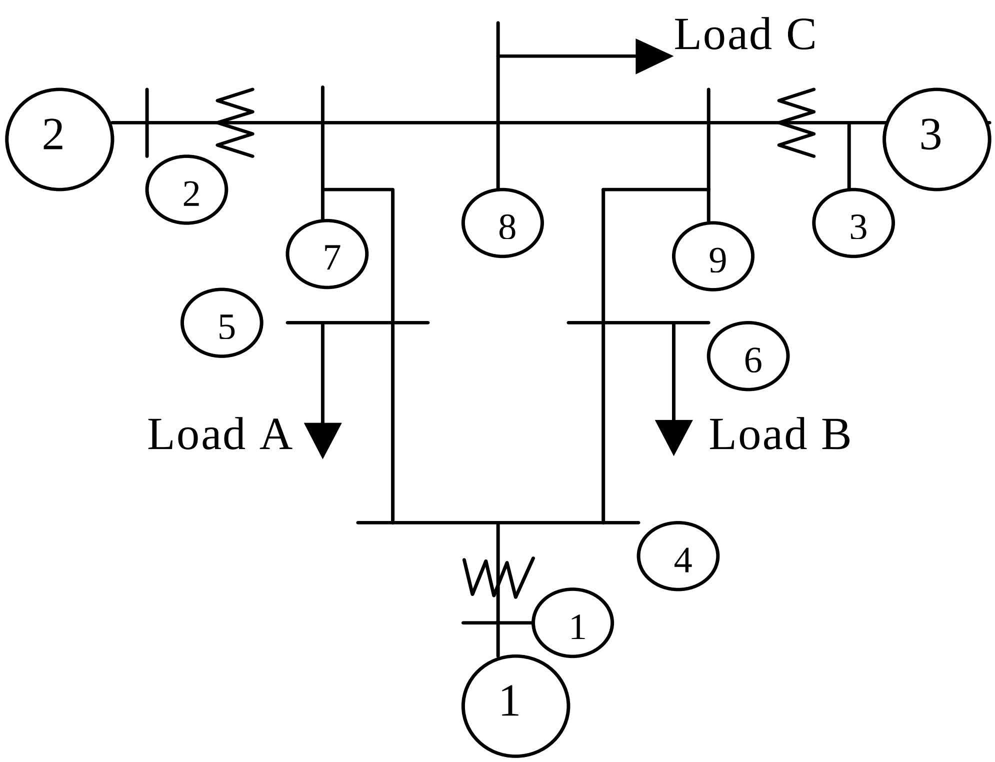

Figure 3.8: A three-machine nine-bus power system

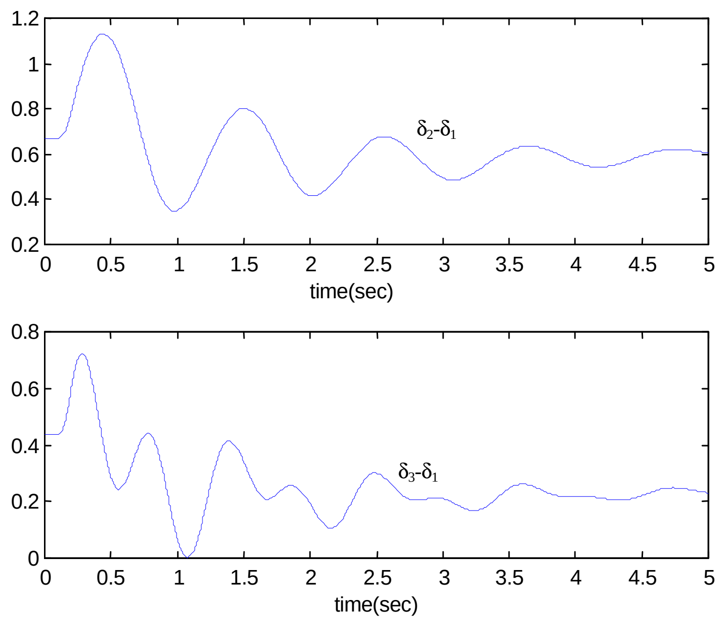

Figure 3.9: Time response of relative rotor angles

In this power system, the rotor angle of generator #1 is chosen as reference. A three-phase to ground fault is applied to bus 6. It is cleared after 0.2 second, with line 6-9 open. The proposed control strategy is applied to the excitation systems of machine 2 and machine 3. The nonlinear simulation results in Figs. 3.9, 3.10 and 3.11 show the effectiveness of the proposed controller, which is completely decentralized and can stabilize the system.

3.7 Disturbance accommodation control

The linear robust controller design method proposed in Eq. 3.4 guarantees that the subsystem remains stable if the interconnection is bounded within a certain value. In reality, the interconnection terms have wave forms. If these terms can be approximately modelled, controllers can be deduced using disturbance accommodation control (DAC) theory.

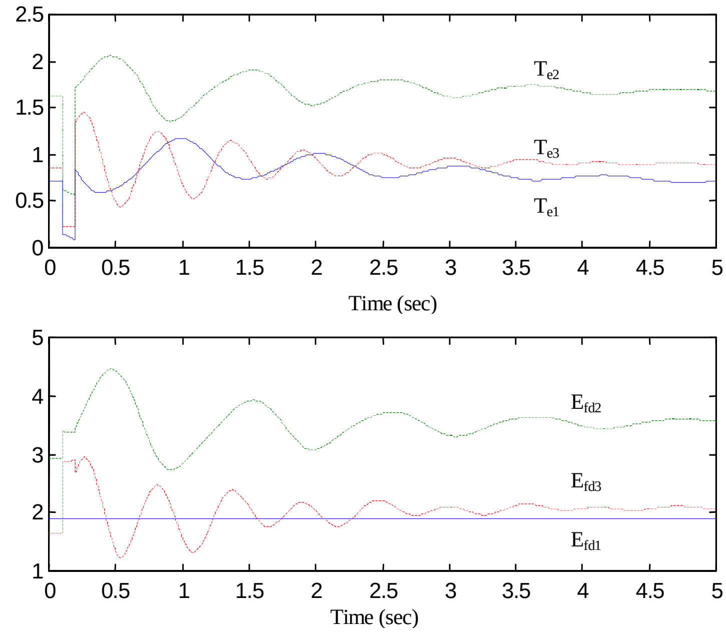

Figure 3.10: Time response of electric torques and excitation voltages

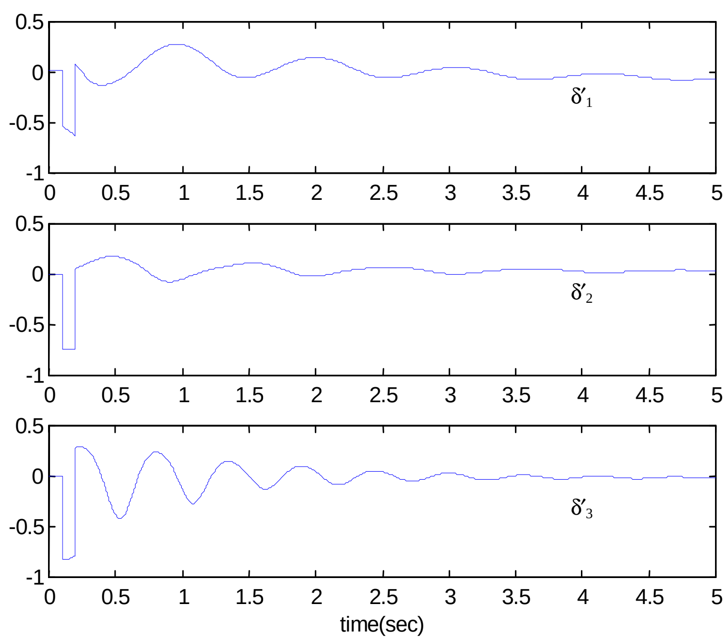

Figure 3.11: Time reponse of the new state variables

3.7.1 DAC Theory

Proposed by C. D. Johnson [30], disturbance accommodation control is to model the disturbance as a wave-form type function, build a linear model for the disturbances and then design linear control for the system.

Definition 3.1 Wave-form Type Function:

The function $w(t)$ can be called a wave-form type function if w is modeled as $w(t) = c_1 f_1(t) + c_2 f_2(t) + \ldots + c_n f_n(t)$
where the basis functions $\{f_1(t), f_2(t), \ldots, f_n(t)\}$ are completely known and the "constant" weighting coefficients $\{c_1, c_2, \ldots, c_n\}$ are totally unknown (and may jump in value from time to time). In practical applications, the $f_i(t)$ typically can be represented by a linear differential equation.

Suppose each of the chosen functions $f_i(t)$ are Laplace transformable, that is

$$f_i(s) = \frac{P_i(s)}{Q_i(s)}$$

c_i are temporarily treated as constants.

$$\begin{aligned} w(s) &= L\left[w(t)\right] = c_1 f_1(s) + c_2 f_2(s) + \ldots + c_n f_n(s) \\ &= \sum_{i=1}^{n} c_i \frac{P_i(s)}{Q_i(s)} \\ &= \frac{P(s)}{Q(s)} \end{aligned} \tag{3.29}$$

where $P(s)$ involves the coefficients c_i and

$$Q(s) = s^{\rho} + q_{\rho} s^{\rho-1} + \ldots + q_2 s + q_1 \tag{3.30}$$

$w(t)$ satisfies

$$\frac{d^{\rho} w}{dt^{\rho}} + b_{\rho} \frac{d^{\rho-1} w}{dt^{\rho-1}} +, \ldots, + b_1 w = 0 \tag{3.31}$$

where b_i,$i = 1, 2, \ldots, \rho$ are explicitly known since they are independent of c_i.

To account mathematically for c_i, $\sigma(t)$ is added to Eq. 3.31, which becomes

$$\frac{d^{\rho} w}{dt^{\rho}} + b_{\rho} \frac{d^{\rho-1} w}{dt^{\rho-1}} +, \ldots, + b_1 w = \sigma(t) \tag{3.32}$$

As a consequence, there exists a linear dynamic "state model" representation of $w(t)$.

$$\begin{aligned} w(t) &= L(t) z(t) \\ \dot{z}(t) &= M(t) z(t) + \sigma(t) \end{aligned} \tag{3.33}$$

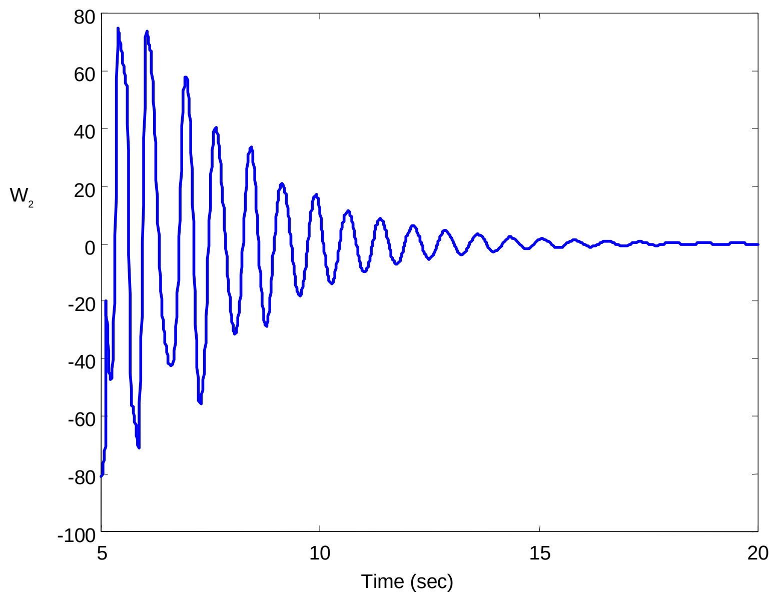

Figure 3.12: Interface variables w_2

where L and M are known matrices respectively, and $\sigma(t)$ is a sequence of completely unknown, randomly arriving, random-intensity impulses.

3.7.2 Modeling interface variable

The interconnection terms include information from the rest of the system. To decouple each subsystem, a model for the interface variables is proposed based on the disturbance accommodation control methodology. Through the simulation of the entire nonlinear power system, the dynamic signature of the interface variables is identified. Fig. 3.12 and Fig. 3.13 show samples of the dynamic behavior of the interconnections. The traces shown correspond to the three-machine nine-bus system as shown in Fig. 3.8. Machine # 1 is the reference machine, so one needs only to determine models for the interconnections of machines # 2 and #3.

It is the characteristic of power systems that the frequencies of oscillation modes change little when the operating condition changes if the power system structure does not change much. This characteristic is shown by two cases. In case 1, generator 2 generates 1 pu active power while generator 3 generates 1.7 pu active power. In case 2, generator generates 1.7 pu active power while generator 3 generates 1 pu active power. The inter-area oscillation modes are listed in Table 3.1.

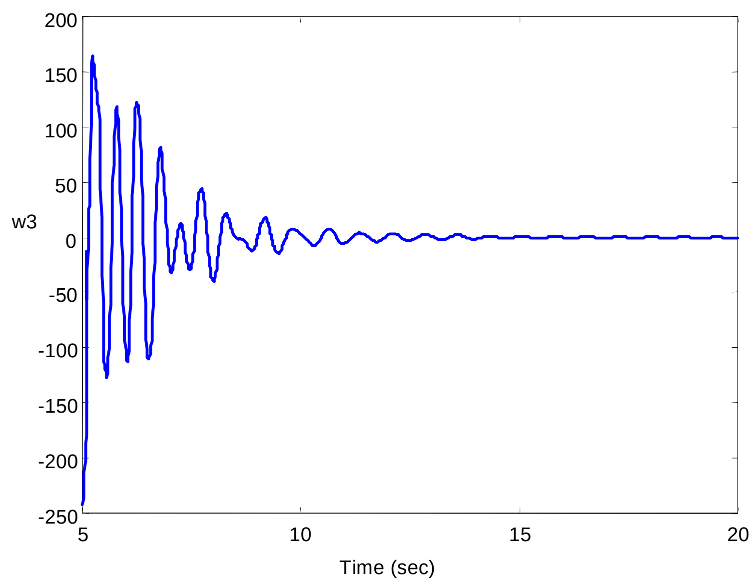

Figure 3.13: Interface variable w_3

Table 3.1: Eigenvalues of Electromechanic Oscillation Modes

	λ_{12}	λ_{34}
case 1	-0.3555 ±13.6916i	-0.2440 ±13.1715i
case 2	-0.2164 ± 7.1251i	-0.5180 ± 7.4003i

The interface variable waveforms, in general, can be approximately expressed by exponential sinusoidal functions. The exponential coefficients may change with disturbances, but the frequencies remain about the same assuming that the topology of the system does not change much. Therefore, the frequencies, once identified, are assumed constant here while the exponential terms are left as unknown parameters. How to identify the frequencies? This can be done by data fitting. First assume $w(t)$ can be expressed in certain mathematical form with unknown parameters (frequencies). These parameters are initialized to certain values. Then minimize the error between the data and $w(t)$ by using Matlab Optimization Toolbox. The parameters will be given out as optimization results.

Based on the traces shown above, the interconnection term $w(t)$ is modeled in the following waveform

$$w(t) = c_1 \sin(\omega_1 t) + c_2 \cos(\omega_1 t) + c_3 \sin(\omega_2 t) + c_4 \cos(\omega_2 t) \tag{3.34}$$

where ω_1, and ω_2 are the frequencies that will remain about constant, c_{i1}, c_{i2}, c_{i3}, c_{i4} are unknown coefficients, which will change from time to time in an unknown random fashion.

A dynamic model for $w(t)$ is then obtained:

$$\frac{dw^4}{dt^4} + (\omega_1^2 + \omega_2^2)\frac{dw^2}{dt^2} + (\omega_1^2\omega_2^2)w = d(t) \tag{3.35}$$

where $d(t)$ is an external forcing function, which consists of a sequence of completely unknown, random functions.

A state space model for this waveform is then derived:

$$\begin{aligned} \dot{z}_1 &= z_2 + \sigma_1 \\ \dot{z}_2 &= z_3 + \sigma_2 \\ \dot{z}_3 &= z_4 + \sigma_3 \\ \dot{z}_4 &= -(\omega_1\omega_2)^2 z_1 - (\omega_1^2 + \omega_2^2) z_3 + \sigma_4 \\ w &= z_1 \end{aligned} \tag{3.36}$$

where $\sigma_1, \sigma_2, \sigma_3, \sigma_4$ are sequence of completely unknown, randomly arriving intensity impulse functions. The symbolic action of $d(t)$ has been represented equivalently in terms of the σ_i, $i = 1, 2, ..., 4$.

$$d(t) = (\omega_1^2 + \omega_2^2)(\dot{\sigma}_1 + \sigma_2) + (\dot{\sigma}_1)'' + (\dot{\sigma}_2)' + \dot{\sigma}_3 \tag{3.37}$$

The model in Eq. 3.36 can be written, in matrix form, as:

$$\begin{aligned} \dot{z} &= Dz + E\sigma \\ w &= Lz \end{aligned}$$

where $D = \begin{bmatrix} 0 & 1 & 0 & 0 \\ 0 & 0 & 1 & 0 \\ 0 & 0 & 0 & 1 \\ 0 & -(\omega_1^2+\omega_2^2) & 0 & (\omega_1\omega_2)^2 \end{bmatrix}$,

$L = \begin{bmatrix} 1 & 0 & 0 & 0 \end{bmatrix}$,

$E = \begin{bmatrix} 1 & 0 & 0 & 0 \\ 0 & 1 & 0 & 0 \\ 0 & 0 & 1 & 0 \\ 0 & 0 & 0 & 1 \end{bmatrix}$

Substituting this interconnection model in the feedback linearized model of the i-th machine a composite model is obtained:

$$\begin{aligned} \dot{\xi} &= A\xi + Hz + Bv \\ \dot{z} &= Dz + E\sigma \\ w &= Lz \\ y &= C\xi \end{aligned} \tag{3.38}$$

where y is the plant measurement, $y = \xi$, therefore C is a identity matrix.

3.7.3 Design of a disturbance-utilization controller for output regulator problem

The composite linear model of each subsystem is given in Eq. 3.38. Based on this stand-alone system, a completely decentralized controller is designed. This disturbance-utilization control scheme requires knowledge of the external interconnection terms [19]. It is called a full-information controller, which might not be a realistic design. Hence, a second controller, an observer-based controller, is designed. The observer is designed to reconstruct the information used by the control scheme. These two designs are presented next.

Full-information controller

For each subsystem, the objective is to design a local, or decentralized controller that minimizes the following performance index (subscript i has been omitted to simplify the notation):

$$J = \frac{1}{2}e^T(t)Se(t) + \frac{1}{2}\int_{t_0}^{T}\left[e^T(t)Qe(t) + v^T(t)Rv(t)\right] dt \tag{3.39}$$

where S, Q, R are positive-definite symmetric weighting matrices chosen by the designer,

$e(t)$ denotes the set point error $e(t) = y_{sp} - y(t)$ and

$$y(t) = \begin{bmatrix} \delta - \delta_0 \\ \omega_0(\omega - 1) \\ \frac{\omega_0}{2\pi}(P_m - P_e) \end{bmatrix} \tag{3.40}$$

where

δ is the rotor angle

ω is the rotor speed

$P_m - P_e$ is the accelerating power $P_m - P_e$, as P_m is the mechanical power and P_e is the generating power of the generator.

Here the set point y_{sp} is the initial condition, and $[t_0\ T]$ is the specified time interval of control. The presence of the positive penalty term $v^T(t)Rv(t)$ in the integral encourages the system to make maximum utilization of the "free energy" of the interconnection term $w(t)$ in achieving set point regulation forcing $e(t) \longrightarrow 0$.

The external interconnection w is actually not a real disturbance; thus, it is not realistic to expect to cancel it, nor to minimize it. In particular, it is entirely possible that at least some of the action of the external interconnection can be constructively used as an aid in carrying out the primary control objective. To achieve this primary control objective and simultaneously make maximum utilization of the interconnection term $w(t)$, the designer can choose $v(t)$ to minimize the quadratic performance criterion given in Eq. 3.39.

Now one can introduce the augmented state vector $\tilde{x} = \begin{bmatrix} \xi & y_{sp} & z \end{bmatrix}^T$. Then the composite set of equations with the condition $\dot{y}_{sp} = 0$ can be written as :

$$\dot{\tilde{x}} = \begin{bmatrix} A & 0 & H \\ 0 & 0 & 0 \\ 0 & 0 & D \end{bmatrix}\begin{pmatrix} \xi \\ y_{sp} \\ z \end{pmatrix} + \begin{bmatrix} B \\ 0 \\ 0 \end{bmatrix} v + \begin{bmatrix} 0 \\ 0 \\ \sigma(t) \end{bmatrix} \tag{3.41}$$

And the set point error e can be expressed in terms of $\tilde{x}$ as

$$e = \begin{bmatrix} -C & I & 0 \end{bmatrix} \tilde{x} \tag{3.42}$$

Eq. 3.39 can be rewritten in terms of $\tilde{x}$. To determine the control $v(t)$ to minimize Eq. 3.39 subject to Eq. 3.41, the well-known results of linear quadratic optimal control theory are used. The final expression for the interconnection term utilization controller v is obtained as:

$$v(\xi, z, y_{sp}, t) = (-R^{-1}B^T K_x)^T \xi - (R^{-1}B^T K_y)^T y_{sp} - (R^{-1}B^T K_z)^T z \tag{3.43}$$

where matrices K_x, K_y and K_z are time-varying and may be computed, once and for all, by off-line numerical solution of the set of matrix differential equations (K_x is symmetric and nonnegative definite):

$$\begin{aligned} \dot{K}_x &= (-A + BR^{-1}B^T K_x)^T K_x - K_x A - C^T QC; K_x(T) = C^T SC \\ \dot{K}_y &= (-A + BR^{-1}B^T K_x)^T K_y + C^T QC; K_y(T) = -C^T S \\ \dot{K}_z &= (-A + BR^{-1}B^T K_x)^T K_z - K_z D - K_x H; K_z(T) = 0 \end{aligned} \tag{3.44}$$

K_x, K_y, K_z can be solved by integrating the differential equations in Eq. 3.44. The Matlab source codes are in Appendix. K_x, K_y, K_z are shown in Fig. 3.14, Fig. 3.15 and Fig. 3.16. Of course, when the variables ξ and z are available, then the controller is called a full-information controller. If these variables are not available, then they are replaced by $\hat{\xi}$ and $\hat{z}$ which are the outputs of the observer of state variables and interconnections. The observer is designed in the next section.

Observer-based design

The external interconnection is not measurable; therefore, an observer is needed to estimate this interconnection.

If the initial condition of y_{sp} is a zero vector, and $\dot{y}_{sp} = 0$, then Eq. 3.41 becomes Eq. 3.45.

$$\begin{bmatrix} \dot{\xi} \\ \dot{z} \end{bmatrix} = \begin{bmatrix} A & H \\ 0 & D \end{bmatrix} \begin{pmatrix} \xi \\ z \end{pmatrix} + \begin{bmatrix} B \\ 0 \end{bmatrix} v + \begin{bmatrix} 0 \\ \sigma(t) \end{bmatrix} \tag{3.45}$$

Let $\hat{\xi}$ and $\hat{z}$ be the "output" generated by the auxiliary linear dynamic system (observer) [10]

$$\begin{bmatrix} \dot{\hat{\xi}} \\ \dot{\hat{z}} \end{bmatrix} = \begin{bmatrix} A & H \\ 0 & D \end{bmatrix} \begin{pmatrix} \hat{\xi} \\ \hat{z} \end{pmatrix} + \begin{bmatrix} B \\ 0 \end{bmatrix} v + \begin{bmatrix} K_1 \\ K_2 \end{bmatrix} (y - \hat{y}) \tag{3.46}$$

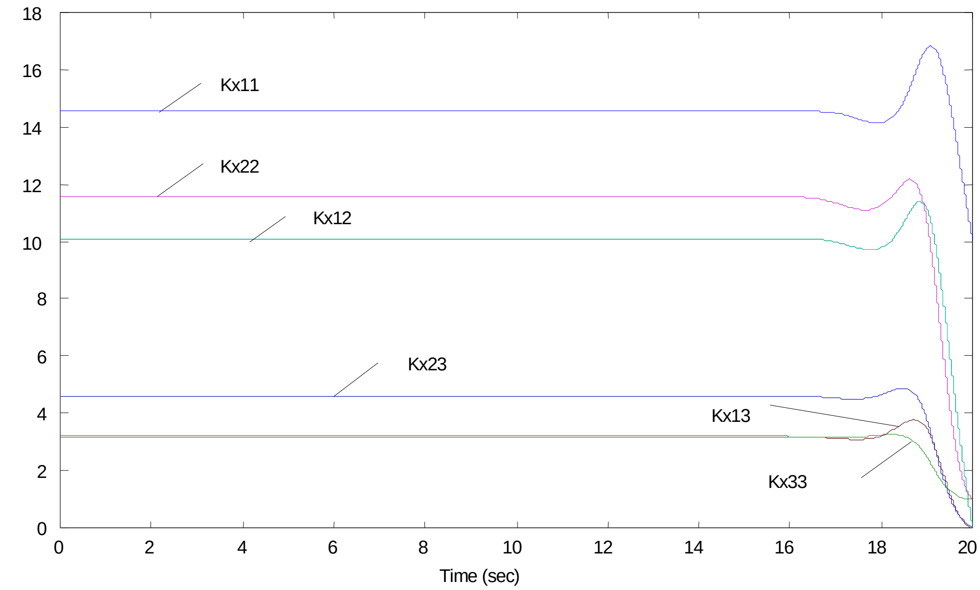

Figure 3.14: K_x versus time

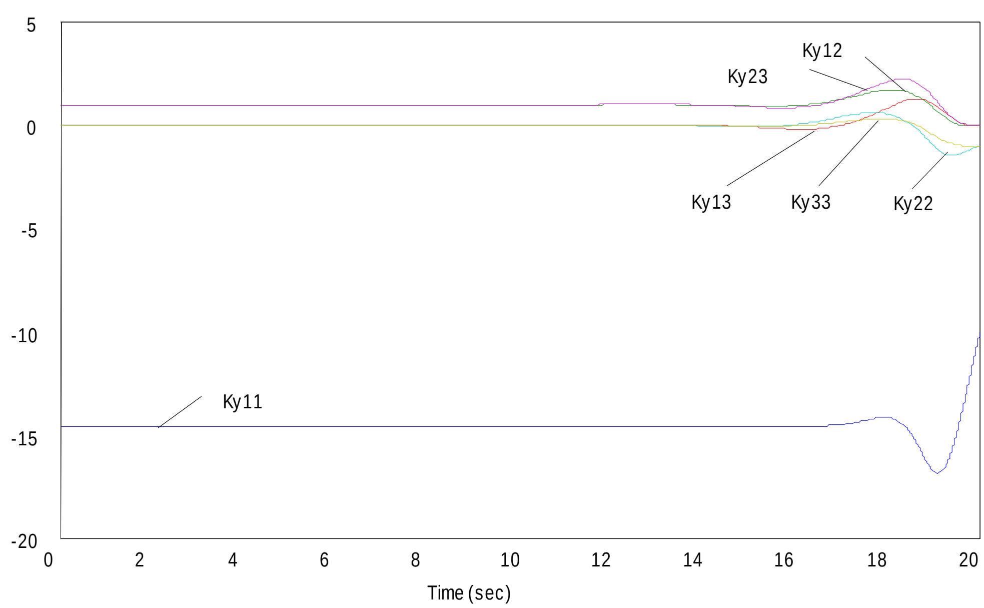

Figure 3.15: K_y versus time

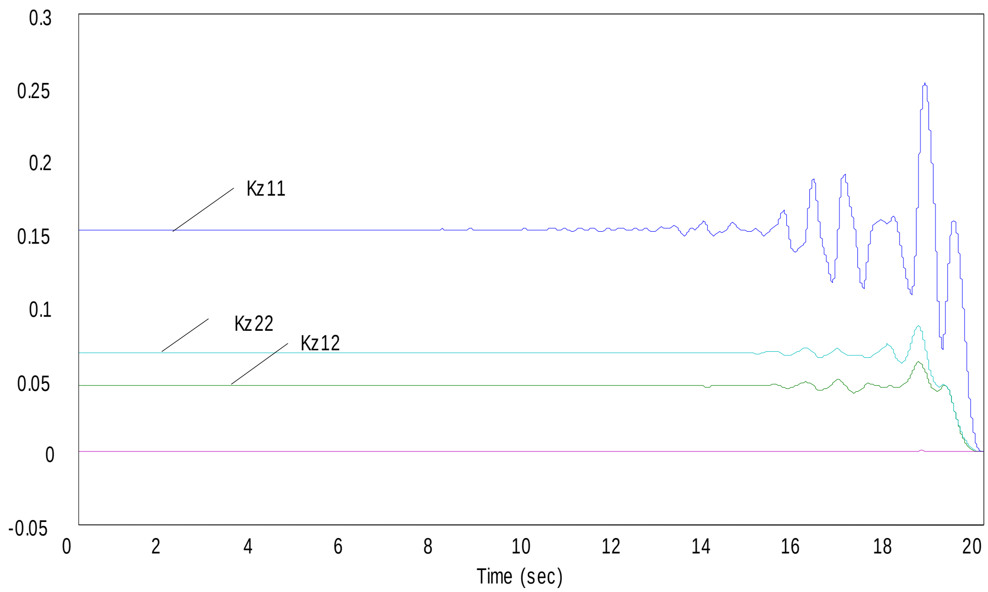

Figure 3.16: K_z versus time

where y and v are the actual output and control input of the original plant respectively and $\hat{y} = C\hat{\xi}$.

The gain matrices K_1 and K_2 are designed by customary procedures based on the error dynamics associated with the observer.

$$\begin{aligned} \varepsilon_\xi &= \xi - \hat{\xi} \\ \varepsilon_z &= z - \hat{z} \end{aligned} \tag{3.47}$$

The error dynamics can be obtained from Eq. 3.45 and Eq. 3.46.

$$\begin{bmatrix} \dot{\varepsilon}_\xi \\ \dot{\varepsilon}_z \end{bmatrix} = \begin{bmatrix} A + K_1 C & H \\ K_2 C & D \end{bmatrix} \begin{pmatrix} \varepsilon_\xi \\ \varepsilon_z \end{pmatrix} + \begin{bmatrix} 0 \\ \sigma \end{bmatrix} \tag{3.48}$$

K_1 and K_2 are chosen so that the transient solution of the above dynamic equations approache zero except at the isolated impulse times of $\sigma(t)$.

Linear observer design procedure can be found in reference [10]. In particular, pole-placement methodology is used here.

With observer designed, Eq. 3.43 becomes Eq. 3.49.

$$v(\hat{\xi}, \hat{z}, y_{sp}, t) = -(R^{-1}B^T K_x)\hat{\xi} - (R^{-1}B^T K_y)y_{sp} - (R^{-1}B^T K_z)\hat{z}. \tag{3.49}$$

Finally, the nonlinear excitation control law is given by

$$E_{fd} = \beta^{-1}(v(\hat{\xi}, \hat{z}, y_{sp}, t) - \alpha) \tag{3.50}$$

where α and β are given in Eq. 3.8.

3.7.4 Case study

The power system used in this case study consists of three machines and nine buses as shown in Fig. 3.8. Two designs are performed. First, design a controller for machine # 2 only. Second, design controllers for both machine #2 and machine # 3, using the methodology described in this dissertation. The output of the controller is E_{fd} while the inputs are rotor angle, rotor speed, and accelerating power. A three-phase to ground fault is applied at time t = 5 seconds and it is cleared at time t = 5.1 seconds.

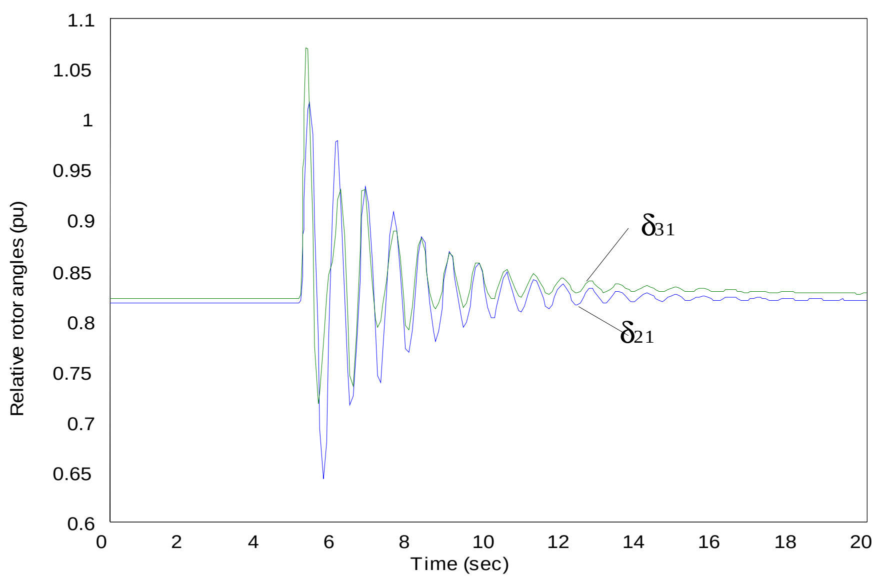

Figure 3.17: Time response of the relative rotor angles of the open-loop system

Case 1: At nominal conditions, machine #2 generates 1.33 pu active power while machine #3 generates 0.85 pu active power. With no excitation controller, the dynamic response of the system is shown in Fig. 3.17. If machine 2 is equipped with a nonlinear controller, the dynamics of machine angles are shown in Fig. 3.18.

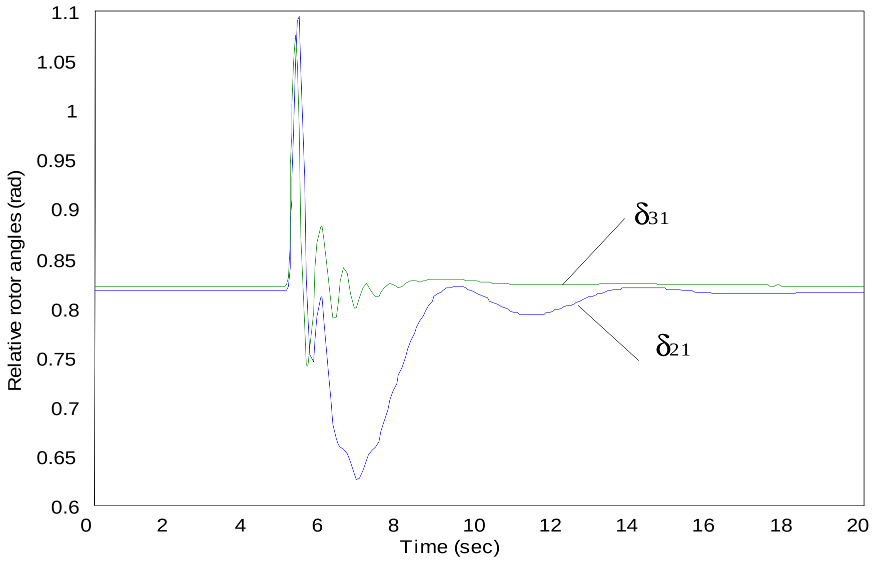

Figure 3.18: Machine angles when a nonlinear controller is installed at machine #2

If both machine #2 and machine #3 are equipped with nonlinear controllers, the dynamics of machine angles are shown in Fig. 3.20 and Fig. 3.21. The simulation results show that the controllers affect the dynamic responses much more by damping the oscillations, i.e., oscillations with original frequencies vanished quickly, while an oscillation component with much lower frequency appeared. Emergence of the low frequency oscillation is due to the estimation error of the interconnection terms.

Case 2: With operating conditions changing, (machine #2 generates 1.00 pu power and machine #3 generates 0.85 pu power), the dynamic responses of the power system are shown in Fig. 3.22 and Fig. 3.23.

The case study shows that with operating condition changing, the proposed controller can improve the dynamic performance. Therefore, the proposed controller is robust to operating conditions.

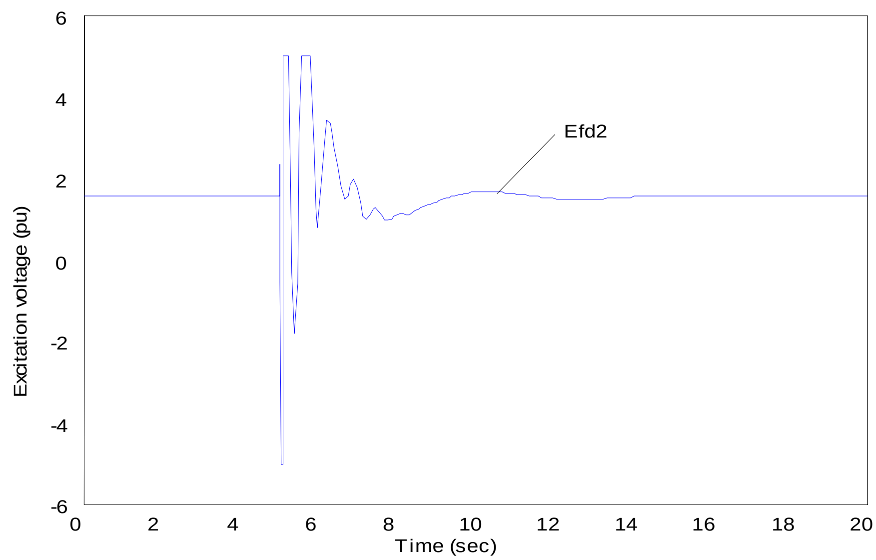

Figure 3.19: Excitation voltage of machine #2

3.8 Conclusion

In this chapter, mapped models of both one-axis generator model and subtransient generator model are derived when feedback linearization techniques are applied to the models. The mapped system model can be expressed as linear subsystems with nonlinear interconnection terms. The interconnection terms are modeled as bounded disturbances and linear robust control is then applied. The interconnection terms can also be modeled as wave-form type disturbances and disturbance accommodation control are designed. It seems that DAC has more advantage than static feedback H_∞ control since it can even deal with the interconnection term that is not bounded but has wave-form type structure. However, if we model the interconnection term as an unstable time-domain function, the inner-structure of the control is not stable too. That is not preferred in control engineering. Therefore, in DAC, the interconnection term should be modeled as bounded wave-form.

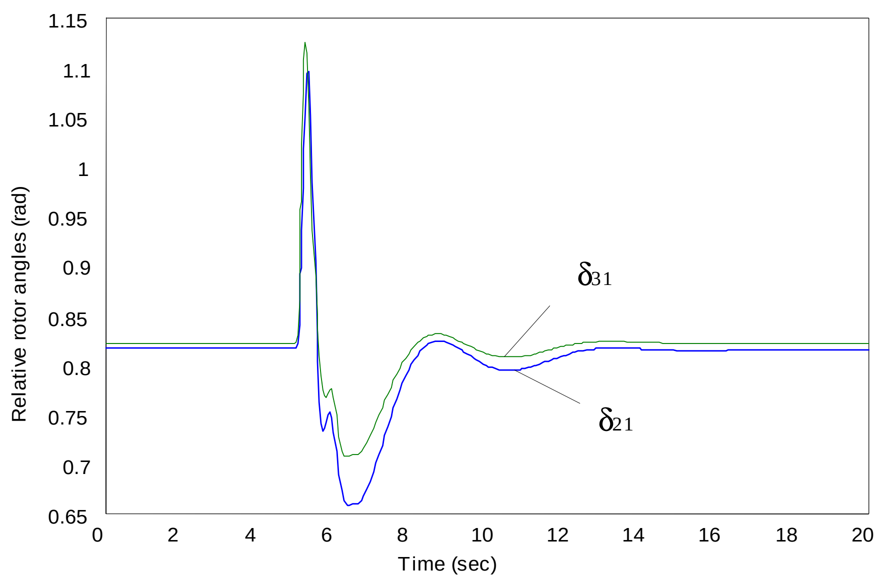

Figure 3.20: Machine angles when nonlinear controllers are installed at machines #2 and #3

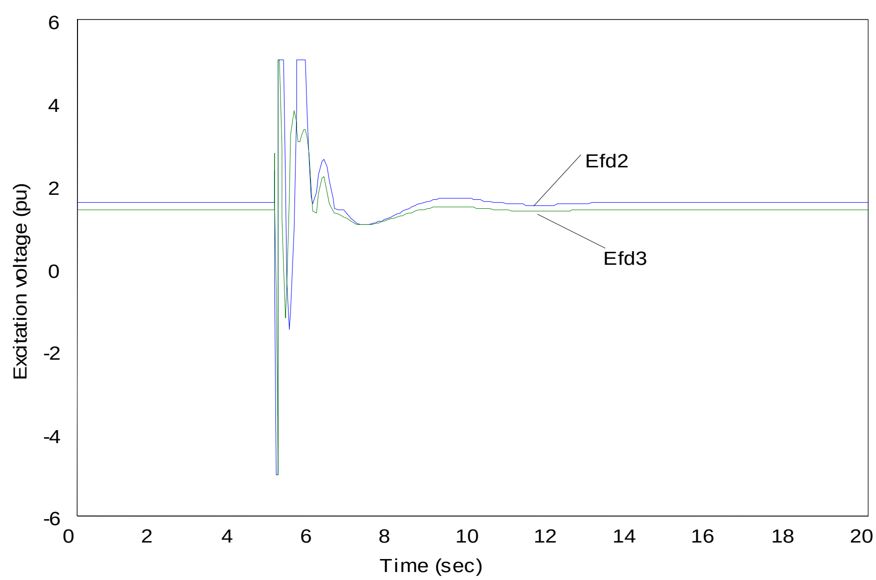

Figure 3.21: Excitation voltages of machines #2 and #3

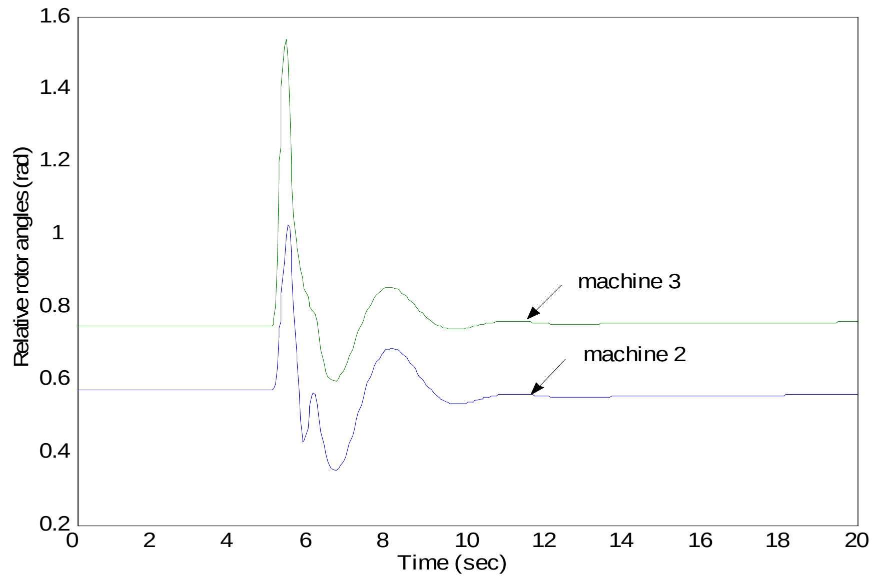

Figure 3.22: Machine angles when nonlinear controllers are installed at machines #2 and #3

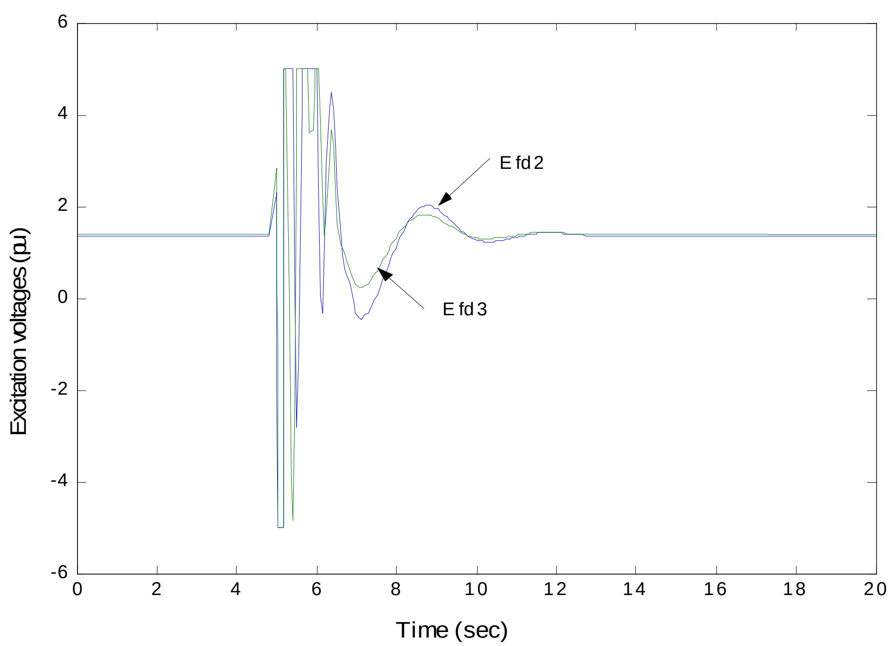

Figure 3.23: Excitation voltages of machines #2 and #3

Chapter 4

TCSC damping controller

4.1 Introduction

Thyristor controlled series capacitor (TCSC) is an important device in the FACTS family. It is placed on transmission lines rather than being connected in shunt. Advances in high-voltage, high-efficiency power electronics make it possible for the TCSC to flexibly adjust its equivalent reactance, and thus make it possible for a control scheme to be applied. The series connection scheme allows the TCSC to influence the power flow through changing the effective admittance linking two buses and is an approach to improve transient stability limits and increase transfer capabilities. It also has other roles such as mitigating subsynchronous resonance (SSR), damping the power oscillations, etc. In this dissertation, its ability to dampen oscillations is investigated.

A typical configuration of TCSC is shown in Fig. 4.1. TCSC is composed of a fixed capacitor, a thyristor-controlled reactance and metal oxide varistor (MOV) [24]. By varying the firing angle the overall admittance is changed and due to the series connection with the transmission line, the total admittance between the two power system buses changes too. The transmitted power is inversely proportional to the transfer reactance resulting in the possibility to increase the transfer limits through compensation. Assuming a 50% to 75 % series compensation, the steady-state power flow can be adjusted from twice to four times the original value. Nevertheless, a practical limit of a maximum compensation level of 70 % applies due to uncontrollable variations in power flow caused by only small changes in bus voltages otherwise.

Different expressions for the equivalent admittance can be found in the literature [11]. They depend on the choice of voltage or current as an ideal sine wave. In the TCSC case, it is more accurate to choose current through the device as sinusoidal. The equivalent reactance at the

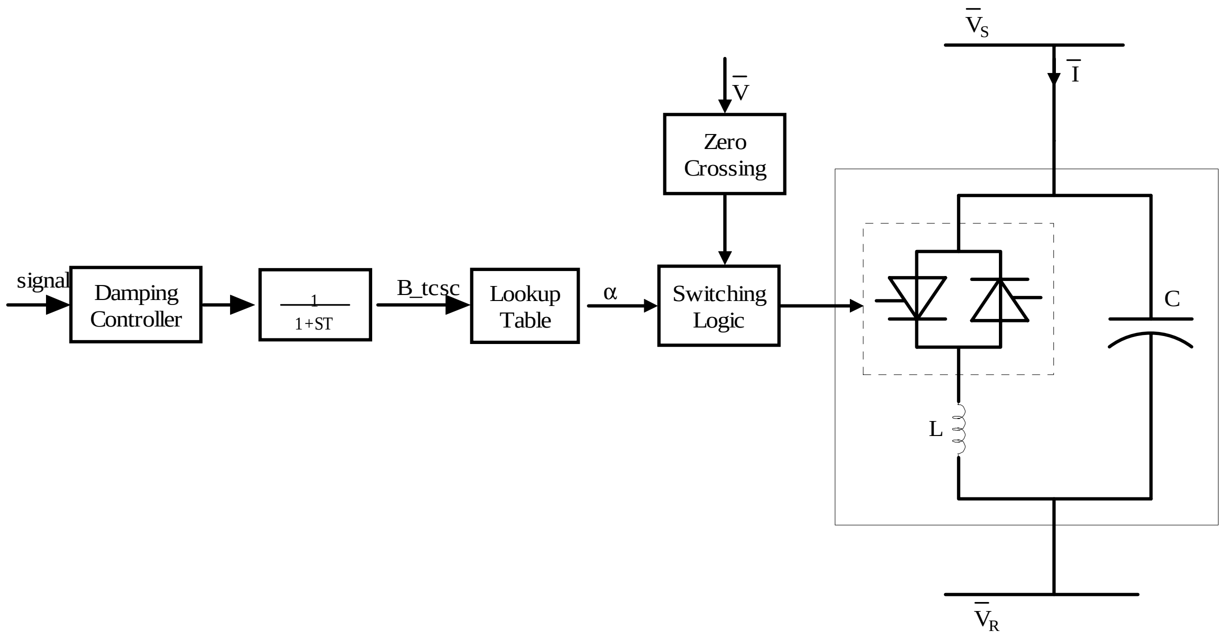

Figure 4.1: Configuration of a TCSC

fundamental frequency can be expressed as a variable inductance X_e given by [28]:

$$X_e = -X_c \left[1 - \frac{k_x^2}{k_x^2 - 1} \frac{\sigma + \sin \sigma}{\pi} + \frac{4k_x^2 \cos^2(\sigma/2)}{\pi(k_x^2 - 1)^2} (k_x \tan \frac{k_x \sigma}{2} - \tan \frac{\sigma}{2}) \right] \tag{4.1}$$

where α is the firing angle, $\sigma = 2(\pi - \alpha)$, $k_x = \sqrt{X_c/X_L}$, and X_c, X_L are the reactances of the capacitor and the inductor respectively.

TCSC can be controlled to work either in the capacitor or the inductor zones avoiding steady state resonance. This mode is called venire control mode. The inductive operation results in a high harmonic distortion which is undesirable in power systems. Therefore, if at all, this range is only permitted for a short period of time to improve transient damping. Most time the TCSC works in a capacitor mode and the firing angle will be $\alpha_r < \alpha < 180°$, where α_r is the critical angle that will cause resonance.

The fundamental reactance of the inductor tends to be much smaller than the capacitor reactance. A small X_L can provide well-defined charge reversal and control of the period time of the compensating voltage. It is also advantageous in facilitating an effective protective bypass for large surge current encountered during system faults.

In Fig. 4.2, X_c is selected to be 1.3 ohm while X_L is selected to be 0.18 ohm.

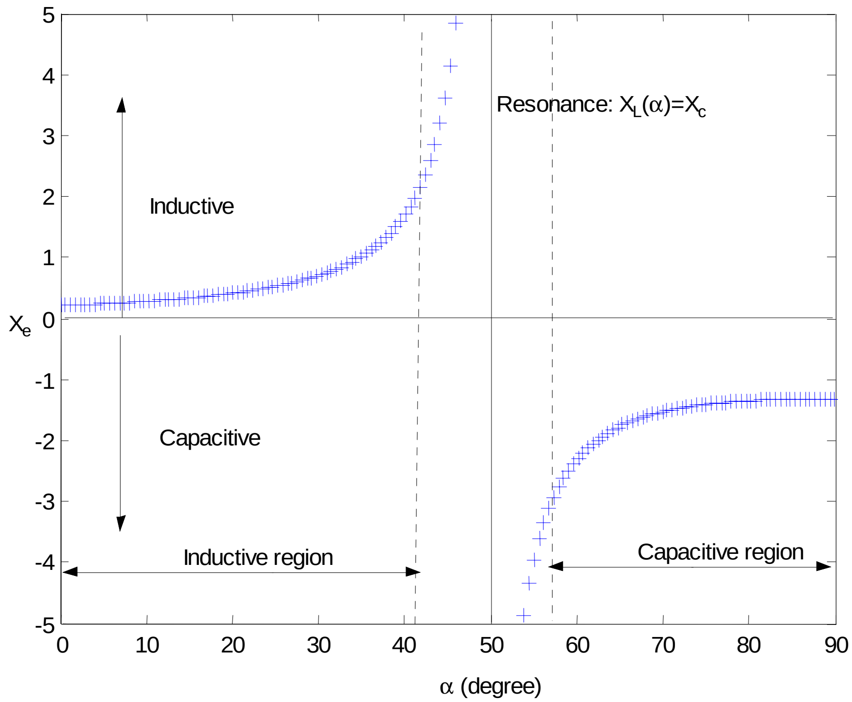

Figure 4.2: Impedance vs. firing angle α characteristic of the TCSC.

To simplify the control problem, the equivalent reactance X_e or admittance $B_{\_tcsc}$ is taken as the control output shown in Fig. 4.1 . An accurate characteristic curve of the TCSC's equivalent reactance with respect to the firing angle is available. Based on control output, firing angle could be immediately obtained through a lookup table which stores this nonlinear characteristic curve.

In this chapter, TCSC damping controller for inter-area oscillation is under investigation. Modal analysis method is chosen as the analysis tool. First of all, the linear power system model with TCSC damping controller is developed. Then conditions and indices for control signal selection are proposed. Finally, the controller is designed using lead-lag control design scheme or multi-stage design scheme.

4.2 Power system model with TCSC damping controller

Suppose that the k-th TCSC is installed on branch $i-j$, the branch current phasor $\bar{I}_{ij}$ is expressed by:

$$\bar{I}_{ij} = \frac{\bar{U}_i - \bar{U}_j}{Z_{ij} - jX_{ck}} \tag{4.2}$$

which can be linearized:

$$\Delta\bar{I}_{ij} = \frac{\Delta\bar{U}_i - \Delta\bar{U}_j}{Z_{ij} - jX_{ck0}} + \frac{\bar{U}_{i0} - \bar{U}_{j0}}{(Z_{ij} - jX_{ck})^2} j\Delta X_{ck} \tag{4.3}$$

where subscript 0 represents initial values. The second term in this equation can be considered as a controllable current source:

$$\Delta\bar{I}_{sk} = K_{ck}\Delta X_{ck} \tag{4.4}$$

where $K_{ck} = j\frac{\bar{U}_{\mathrm{i}0} - \bar{U}_{\mathrm{j}0}}{(Z_{\mathrm{ij}} - jX_{\mathrm{ck}})^2}$. Then the current injection at node i can be expressed by the following equations

$$\begin{aligned} \Delta\bar{I}_i &= \Delta\bar{I}_{fi} - \sum \Delta\bar{I}_{sk}, \text{when node } i \text{ is connected to a generator, or} \\ \Delta\bar{I}_i &= -\sum \Delta\bar{I}_{sk}, \text{when node } i \text{ is not connected to a generator.} \end{aligned} \tag{4.5}$$

For a system with n generators, n_c TCSCs and m TCSC nodes not connected to generators, the network equations, after nodes other than generator nodes and TCSC nodes are eliminated, are:

$$\begin{bmatrix} \mathbf{0} \\ \mathbf{\Delta\bar{I}}_f \end{bmatrix} - \begin{bmatrix} \mathbf{K}_{sm} \\ \mathbf{K}_{sf} \end{bmatrix} \mathbf{\Delta\bar{I}}_s = \begin{bmatrix} \mathbf{Y}_{mm} & \mathbf{Y}_{mf} \\ \mathbf{Y}_{fm} & \mathbf{Y}_{ff} \end{bmatrix} \begin{bmatrix} \mathbf{\Delta\bar{U}}_m \\ \mathbf{\Delta\bar{U}}_f \end{bmatrix} \tag{4.6}$$

where K_{sm} is mxn_c, K_{sf} is nxn_c and the controllable current source vector is:

$$\mathbf{\Delta\bar{I}}_s = diag\{K_{c1}, K_{c2}, ..., K_{cn_c}\} \begin{bmatrix} \Delta X_{c1} \\ \Delta X_{c2} \\ ... \\ \Delta X_{cn_c} \end{bmatrix}_s = \mathbf{K}_c\mathbf{\Delta X}_c \tag{4.7}$$

Eliminating all the TCSC nodes that are not connected to generators, the following equation can be obtained

$$\mathbf{\Delta\bar{I}}_s = \mathbf{Y}_s\mathbf{\Delta\bar{U}}_f + \mathbf{A}_c\mathbf{\Delta X}_c \tag{4.8}$$

where $\mathbf{Y}_f= (\mathbf{Y}_{ff}-\mathbf{Y}_{fm}\mathbf{Y}_{mm}^{-1}\mathbf{Y}_{mf})$
and $\mathbf{A}_c= (\mathbf{K}_{sf}-\mathbf{Y}_{fm}\mathbf{Y}_{mm}^{-1}\mathbf{K}_{sm})\mathbf{K}_c$

Eq. 4.8 can be transformed into common $dq0$ reference frames by the transformation matrix $T = \begin{bmatrix} \cos\delta & \sin\delta \\ \sin\delta & -\cos\delta \end{bmatrix}$. Substituting the simplified generator model into the transformed equations, after a series of tedious manipulations, the following equations can be obtained

$$\begin{aligned} \mathbf{\Delta I}_q &= \mathbf{L}_q\mathbf{\Delta E}'_q+\mathbf{S}_q\boldsymbol{\Delta\delta} + \mathbf{A}_q\mathbf{\Delta X}_c \\ \mathbf{\Delta I}_d &= \mathbf{L}_d\mathbf{\Delta E}'_q+\mathbf{S}_d\boldsymbol{\Delta\delta} + \mathbf{A}_d\mathbf{\Delta X}_c \end{aligned} \tag{4.9}$$

where $\mathbf{\Delta E}'_q$ is the transient EMF deviation vector; $\boldsymbol{\Delta\delta}$ is the power angle deviation vector. The order of coefficient matrices $\mathbf{L}_q, \mathbf{L}_d, \mathbf{S}_q$ and $\mathbf{S}_d$ is nxn, where $\mathbf{A}_\mathsf{q}$ and $\mathbf{A}_\mathsf{d}$ are nxn_c. All of them are determined by system parameters and initial operating conditions.

Linear differential equations describing the dynamic behavior of the system can be obtained:

$$\begin{bmatrix} \boldsymbol{\Delta\dot{\delta}} \\ \boldsymbol{\Delta\dot{\omega}} \\ \mathbf{\Delta\dot{E}}'_q \\ \mathbf{\Delta\dot{E}}_{\mathsf{fd}} \end{bmatrix} = \begin{bmatrix} \mathbf{0} & \boldsymbol{\omega}_0 & \mathbf{0} & \mathbf{0} \\ -\mathbf{T}_J^{-1}\mathbf{K}_1 & -\mathbf{T}_J^{-1}\mathbf{D} & -\mathbf{T}_J^{-1}\mathbf{K}_2 & \mathbf{0} \\ -\mathbf{T}_{d0}^{-1}\mathbf{K}_4 & \mathbf{0} & -\mathbf{T}_{d0}^{-1}\mathbf{K}_3 & -\mathbf{T}_{d0}^{-1} \\ -\mathbf{T}_A^{-1}\mathbf{K}_A\mathbf{K}_5 & \mathbf{0} & -\mathbf{T}_A^{-1}\mathbf{K}_A\mathbf{K}_6 & -\mathbf{T}_A^{-1} \end{bmatrix} \begin{bmatrix} \boldsymbol{\Delta\delta} \\ \boldsymbol{\Delta\omega} \\ \mathbf{\Delta E}'_q \\ \mathbf{\Delta E}_{\mathsf{fd}} \end{bmatrix} + \begin{bmatrix} \mathbf{0} \\ -\mathbf{T}_J^{-1}\mathbf{K}_p \\ -\mathbf{T}_{d0}^{-1}\mathbf{K}_q \\ -\mathbf{T}_A^{-1}\mathbf{K}_A\mathbf{K}_v \end{bmatrix} \mathbf{\Delta X}_c \tag{4.10}$$

where $\mathbf{T}_J, \mathbf{D}, \mathbf{T}'_{do}, \mathbf{K}_A$,and $\mathbf{T}_A$ are nxn order diagonal matrices, in which the corresponding symbols are

$\mathbf{T}_{Ji}$ —— Inertia time constant;

$\mathbf{D}_i$ —— Damping coefficient;

$\mathbf{T}'_{d0i}$ —— Field winding time constant;

$\mathbf{K}_{Ai}$ —— AVR gain;

$\mathbf{T}_{Ai}$ —— AVR time constant

The order of coefficient matrices $\mathbf{K}_1, \mathbf{K}_2, \mathbf{K}_3, \mathbf{K}_4, \mathbf{K}_5$ and $\mathbf{K}_6$ are nxn, and $\mathbf{K}_\mathsf{p}, \mathbf{K}_\mathsf{q}$ and $\mathbf{K}_\mathsf{v}$ are nxn_c. They have the following expressions

$\mathbf{K}_1 = \mathbf{I}_{q0}(\mathbf{x}_q - \mathbf{x}'_q)\mathbf{S}_d + \left[\mathbf{E}'_{q0} + \mathbf{I}_{d0}(\mathbf{x}_q - \mathbf{x}'_d)\right]\mathbf{S}_q$

$\mathbf{K}_2 = \mathbf{I}_{q0}(\mathbf{x}_q - \mathbf{x}'_q)\mathbf{L}_d + \left[\mathbf{E}'_{q0} + \mathbf{I}_{d0}(\mathbf{x}_q - \mathbf{x}'_d)\right]\mathbf{L}_q + \mathbf{I}_{q0}$

$\mathbf{K}_p = \mathbf{I}_{q0}(\mathbf{x}_q - \mathbf{x}'_q)\mathbf{A}_d + \left[\mathbf{E}'_{q0} + \mathbf{I}_{d0}(\mathbf{x}_q - \mathbf{x}'_d)\right]\mathbf{A}_q$

$\mathbf{K}_3 = \mathbf{1} + (\mathbf{x}_d - \mathbf{x}'_d)\mathbf{L}_d$

$\mathbf{K}_4 = (\mathbf{x}_d - \mathbf{x}'_d)\mathbf{S}_d$

$\mathbf{K}_q = (\mathbf{x}_d - \mathbf{x}'_d)\mathbf{A}_q$

$\mathbf{K}_5 = \mathbf{U}_{d0}\mathbf{x}_q\mathbf{S}_q + \mathbf{U}_{q0}\mathbf{x}'_d\mathbf{S}_d$

$\mathbf{K}_6 = \mathbf{U}_{d0}\mathbf{x}_q\mathbf{L}_q + \mathbf{U}_{q0}(\mathbf{x}'_d\mathbf{L}_d - \mathbf{1})$

$\mathbf{K}_v = \mathbf{U}_{d0}\mathbf{x}_q\mathbf{A}_q + \mathbf{U}_{q0}\mathbf{x}'_d\mathbf{A}_d$

In which $\mathbf{E}'_{q0}, \mathbf{I}_{q0}, \mathbf{I}_{d0}, \mathbf{U}_{q0}$ and $\mathbf{U}_{d0}$ are nxn order diagonal matrices.

The linear model can be expressed in a concise way as:

$$\begin{aligned} \dot{\mathbf{x}}(t) &= \mathbf{A}\mathbf{x}(t) + \mathbf{B}\mathbf{u}(t) \\ \mathbf{y}(t) &= \mathbf{C}\mathbf{x}(t) \end{aligned} \tag{4.11}$$

where $\mathbf{y}(\mathbf{t})$ is the output vector.

4.3 Modal analysis

Given an interconnected system P with N control stations:

$$\begin{aligned} \dot{\mathbf{x}}(t) &= \mathbf{f}(\mathbf{x}) + \sum_{k=1}^{N} \mathbf{g}_k(\mathbf{x})\mathbf{u}_k(\mathbf{x}) \\ \mathbf{y}_k(t) &= \mathbf{h}_k(\mathbf{x}),\ k = 1, 2, ..., N \end{aligned} \tag{4.12}$$

where $\mathbf{x}$ is a (Nx1) state vector;

$\mathbf{u}_k$ is a (r_kx1) control input vector at control station k;

r_k is the number of the control inputs at control station k;

$\mathbf{y}_k$ is a (l_kx1) output vector at control station k;

l_k is the number of the control outputs at control station k.

Let m be the number of the operating conditions. The objective is to control the system over a set of m operating conditions. With Eq. 4.12 linearized around these operating points, m linearized models $(P_1(s), P_2(s), \ldots, P_m(s))$ are obtained.

The state space representation of $P_i(s)$ ($i = 1, 2, ..., m$) is:

$$\begin{aligned} \dot{\mathbf{x}}^i &= \mathbf{A}^i\mathbf{x}^i + \mathbf{B}^i\mathbf{u}^i \\ \mathbf{y}^i &= \mathbf{C}^i\mathbf{x}^i \end{aligned} \tag{4.13}$$

where

$\mathbf{u}^i = \begin{bmatrix} u_1^i & u_2^i & ... & u_N^i \end{bmatrix}$

$\mathbf{y}^{iT} = \begin{bmatrix} y_1^{iT} & y_2^{iT} & ... & y_N^{iT} \end{bmatrix}$

The input vector $\mathbf{u}^i$ and output vectors $\mathbf{y}^i$ have dimensions rx1 and lx1, respectively, where $r = \sum_{k=1}^{N} r_k$ and $l = \sum_{k=1}^{N} l_k$.

The corresponding input and output matrices are:

$\mathbf{B}^i = \begin{bmatrix} B_1^i & B_2^i & ... & B_N^i \end{bmatrix}$

$\mathbf{C}^{iT} = \begin{bmatrix} C_1^{iT} & C_2^{iT} & ... & C_N^{iT} \end{bmatrix}^T$

The modal form of the model is:

$$\begin{aligned} \dot{\boldsymbol{\alpha}}^i &= \boldsymbol{\Lambda}^i\boldsymbol{\alpha}^i + \boldsymbol{\Gamma}^i\mathbf{u}^i \\ \mathbf{y}^i &= \boldsymbol{\Omega}^i\boldsymbol{\alpha}^i \end{aligned} \tag{4.14}$$

where

$\boldsymbol{\alpha}^i$ is a Nx1 vector

$\boldsymbol{\Lambda}^i = \mathbf{W}^i\mathbf{A}^i\mathbf{V}^i$

$\mathbf{V}^i = \begin{bmatrix} v_1^i & v_2^i & ... & v_N^i \end{bmatrix}$ is the matrix of the right eigenvectors

$\mathbf{W}^i = (\mathbf{V}^i)^{-1}$

$$\boldsymbol{\Gamma}^i = \mathbf{W}^i\mathbf{B}^i = \begin{bmatrix} w_1^{iH}\mathbf{B}^i \\ w_2^{iH}\mathbf{B}^i \\ ... \\ w_N^{iH}\mathbf{B}^i \end{bmatrix}$$

The controllability indices are obtained from the rows of $\boldsymbol{\Gamma}^i$. The j-th mode of the system is controllable if $w_j^{iH}\mathbf{B}^i$ is a nonzero vector. $|\boldsymbol{\Gamma}_{jk}^i|$ indicates the relative controllability of the j-th mode through the k-th input. Similarly, the observability indices are found from the columns of the matrix $\boldsymbol{\Omega}^i$, which is given by:

$\mathbf{\Omega}^{\mathsf{i}} = \mathbf{C}^i\mathbf{V}^i = \begin{bmatrix} \mathbf{C}^i v_1^i & \mathbf{C}^i v_2^i & \ldots & \mathbf{C}^i v_n^i \end{bmatrix}$

The j-th mode of the system is observable if $C^i v_j^i$ is a nonzero vector. $|\mathbf{\Omega}_{kj}^i|$ indicates the relative observability of the j-th mode in the k-th control output.

The oscillation modes can be identified using observability and controllability. For inter-area oscillation mode, it will not be both controllable and observable at one area.

Assume that all eigenvalues of the $\mathbf{A}$ matrix are distinct. Under this assumption, open-loop transfer function $\mathbf{G}^i(s)$ can be expressed in terms of the residue matrix:

$$G^i(s) = \sum_{j=1}^{m} \frac{R_j^i}{s - \lambda_j} \tag{4.15}$$

$\mathbf{R}_j^i$ is a (mxr) residue matrix associated with λ_j and it is given by:

$$\mathbf{R}_j^i = \mathbf{\Omega}_j^i \mathbf{\Gamma}_j^i = \mathbf{C}^i \mathbf{v}_j^i \mathbf{w}_j^{iH} \mathbf{B}^i \tag{4.16}$$

If the system model $P_i(s)$ is a SISO model, the residue of the j-th mode in control station k is a scalar defined by

$$\mathbf{R}_{kj}^i = \mathbf{\Omega}_{kj}^i \mathbf{\Gamma}_{jk}^i$$

The residue is proportional to the sensitivity of the j-th mode to the controller gain. It is also called functional sensitivity.

Consider a plant $G(s)$ and a feedback control loop:

$$H(s) = kh(s) \tag{4.17}$$

where k is a scalar representing the gain of the controller and $h(s)$ a given structure in SISO case.

To investigate the eigenvalue sensitivity, assume that the gain k has a small deviation ε which is very small; thus, the shift $\Delta\lambda_i$ of the eigenvalue λ_i is also very small.

By assuming that closed-loop system $G'(s) = \frac{G(S)}{1+kh(s)G(s)}$ has n distinct poles, $G'(s)$ can be expressed as:

$$\begin{aligned} G'(s) &= \frac{N(s)}{D(s)} = \frac{R_1}{s-\lambda_1} + \frac{R_2}{s-\lambda_2} + \ldots + \frac{R_n}{s-\lambda_n} \\ &= \frac{\sum_{i=1}^{n}(R_i \prod_{j \neq i}^{n}(s-\lambda_j))}{\prod_{j=1}^{n}(s-\lambda_j)} \end{aligned} \tag{4.18}$$

where R_i is the residue of the eigenvalue λ_i.

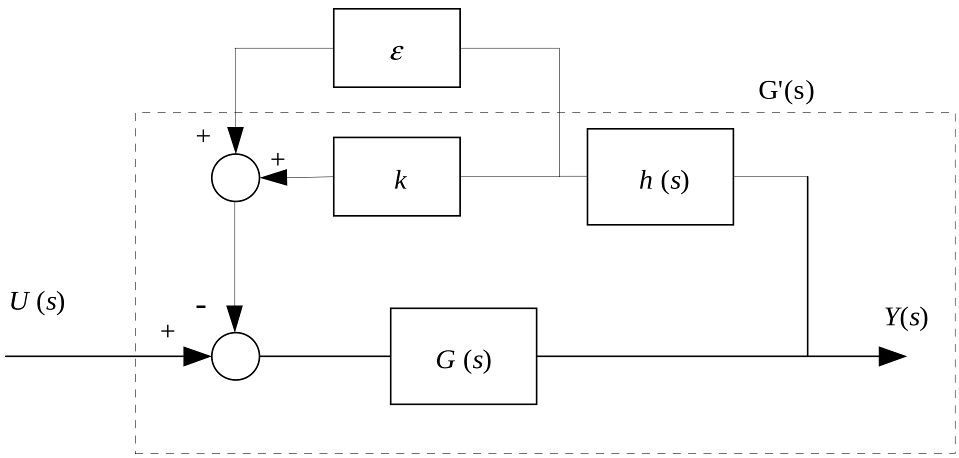

Figure 4.3: Closed-loop feedback system

Assume that the gain k has a small deviation ε which is very small, then the closed-loop feedback control system $G(s)''$ is:

$$G''(s) = \frac{Y(s)}{U(s)} = \frac{G'(s)}{1 + G'(s)\varepsilon h(s)} = \frac{N(s)}{D(s) + \varepsilon h(s) N(s)} \tag{4.19}$$

The closed loop system eigenvalues λ_c can be determined from $D(s) + \varepsilon h(s)N(s) = 0$:

$$\prod_{j=1}^{n}(\lambda_c - \lambda_j) + \varepsilon h(s) \sum_{i=1}^{n}(R_i \prod_{j \neq i}^{n}(\lambda_c - \lambda_j)) = 0 \tag{4.20}$$

The shift $\Delta\lambda_d$ of the eigenvalue λ_d can be expressed as:

$$\begin{aligned}
\Delta\lambda_d &= \lambda_{cd} - \lambda_d \qquad (4.21)\\
&= \frac{-\varepsilon h(\lambda_{cd}) \sum_{i=1}^{n}(R_i \prod_{j\neq i}^{n}(\lambda_{cd} - \lambda_j))}{\prod_{j\neq i}^{n}(\lambda_{cd} - \lambda_j)}\\
&= \frac{-\varepsilon h(\lambda_{cd}) R_d \prod_{j\neq d}^{n}(\lambda_{cd} - \lambda_j)}{\prod_{j\neq d}^{n}(\lambda_{cd} - \lambda_j)} - \frac{\varepsilon h(\lambda_{cd}) \sum_{i=1,i\neq d}^{n}(R_i \prod_{j\neq i}^{n}(\lambda_{cd} - \lambda_j))}{\prod_{j\neq d}^{n}(\lambda_{cd} - \lambda_j)}\\
&= -\varepsilon h(\lambda_{cd}) R_d - \frac{\varepsilon h(\lambda_{cd}) \sum_{i=1,i\neq d}^{n}(R_i \prod_{j\neq i}^{n}(\lambda_{cd} - \lambda_j))}{\prod_{j\neq d}^{n}(\lambda_{cd} - \lambda_j)}\\
&= -\varepsilon h(\lambda_{cd}) R_d - \frac{\varepsilon h(\lambda_{cd})(\lambda_{cd} - \lambda_d) \sum_{i=1,i\neq d}^{n}(R_i \prod_{j\neq i,j\neq d}^{n}(\lambda_{cd} - \lambda_j))}{\prod_{j\neq d}^{n}(\lambda_{cd} - \lambda_j)}\\
&= -\varepsilon h(\lambda_{cd}) R_d + M(\lambda_{cd})
\end{aligned}$$

where λ_{cd} is the eigenvalue of the closed-loop system $G''(s)$ corresponding to λ_d in $G'(s)$.

The second term $M(\lambda_{cd})$ of Eq. 4.21 includes $\varepsilon(\lambda_{cd}–\lambda_d)$. According to the assumption that both ε and $\Delta\lambda_d$ are very small, the second term is negligible; therefore, $M(\lambda_{cd}) \cong 0$.

Thus $\Delta\lambda_d$ can be expressed as

$$\Delta\lambda_d = -R_d \varepsilon h(\lambda_d) \tag{4.22}$$

Define the eigenvalue sensitivity as:

$$S_{\lambda_\mathrm{d}} = \frac{d\lambda_d}{dH(\lambda_d)} \tag{4.23}$$

Therefore, when the absolute value of scalar ε is very small, the eigenvalue sensitivity S_{λ_d} of the eigenvalue λ_d to the feedback loop can be represented as

$$S_{\lambda_\mathrm{d}} = |R_d| \tag{4.24}$$

which means that the eigenvalue shift is proportional to the magnitude of the residue.

4.4 Robust residue-based damping controller

4.4.1 Signal selection

Residue phase constraint

Residues relate an eigenvalue's sensitivity to the control parameters. Consider a dynamic controller with a transfer function $H(s) = kh(s)$, where k is the control gain. The sensitivity of a mode λ_d with respect to the gain of the controller is given by:

$$\frac{d\lambda_d}{dk} = R_d h(\lambda_d) \tag{4.25}$$

where R_d is the residue of this mode.

Changing the gain k of this controller, the mode λ_d will have a departure angle $\Delta\angle\lambda_d$ on the root locus given by:

$$\Delta\angle\lambda_d = \angle R_d + \angle h(\lambda_d) \tag{4.26}$$

The controller is to provide a phase compensation to make the eigenvalue shift toward the negative real-axis. There are two issues: (1) different eigenvalues might have close frequencies and affected by the same controller; in this case, their departure angles have to be such that all of

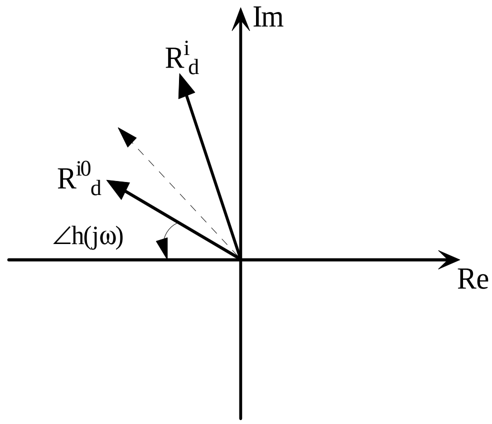

Figure 4.4: Residue plot

these eigenvalues are shifted to the left, and (2) for a single mode at different operating conditions (see Fig. 4.4), the departure angles have to be within a narrow angle. Therefore, the residue phases of oscillation modes at close frequencies are to be bundled together within a narrow angle (<90 degree). Meanwhile, the residue phases of a certain oscillation mode at different operating conditions are to be bundled together within a narrow angle (<90 degree). Then the controller can be effective to the close oscillation modes in different operating conditions [63].

The index to assess the effectiveness

As the operating point changes, the residue changes. Assume that $H(s)$ can compensate residue phase angle corresponding to the critical mode completely over the operating condition range. Then only the magnitude of the residue plays the role in effectiveness consideration.

An index of effectiveness proportional to residue magnitude is used in [20]. The different types of input signals have significant different base values of this index. By adjusting the gain of the controller, some shift of the eigenvalue can be achieved by the different types of input signals. Therefore, it is logical to use residue ratios of the critical modes as the index of signal effectiveness over a range. Assume eigenvalue λ_d is the critical mode; the residue magnitude of the mode at operating condition i of k-th control station $|R^i_{kd}|$ over the residue magnitude at the nominal condition i_0 $|R^{i0}_{kd}|$ is an index for the effectiveness of a control signal over a wide range of operating conditions. This index ρ_i, for operating condition i, is defined as:

$$\rho_i = \frac{S^i_{\lambda_\mathsf{d}}}{S^{i0}_{\lambda_\mathsf{d}}} = \frac{|R^i_{kd}|}{|R^{i0}_{kd}|}, \text{ at } k^{\text{th}} \text{ control station} \tag{4.27}$$

If ρ_i, $i \in \Re$, remains constant for a set of operating points $\Re = \{1, ..., m\}$, then it means that the corresponding signal is effective in the operating range $\Re$. On the other hand if the ratios change, then that signal is not effective for this set of operating conditions.

The index to assess the interaction

Assume that eigenvalue λ_d is the critical mode and define an index ,

$$SI^i_{\lambda_\mathsf{j}} = \frac{S^i_{\lambda j}}{S^i_{\lambda j}} = \frac{|R^i_{kj}|}{|R^i_{kj}|}, j \neq d \text{ at } k^{\text{th}} \text{ control station} \tag{4.28}$$

which is the ratio of the sensitivity of other mode to the critical mode. Thus this index assesses the interaction of the other modes with respect to the critical mode. It is independent of the coefficient of the input signals. The smaller the value of the index, the less the interaction between the controller and the other modes.

4.4.2 Controller design

Lead-lag controller

A dynamic compensator is needed in the case when static feedback control cannot provide adequate damping. The design of a dynamic compensator, as developed by Yang and Feliachi in [63], starts with residue phase compensation. To make the controller robust, different operating conditions should be considered, and the phase is compensated for all of these operating conditions.

The least damped critical modes should be considered first. To achieve this compensation, a local controller $K_k(s)$ at control station k with the following form may be used:

$$K_k(s) = k_l \frac{\tau_{wk} s}{1 + \tau_{wk} s} \prod_{j=1}^{m_\mathsf{k}} \frac{1 + a_{kj} \tau_{kj} s}{1 + \tau_{kj} s} \tag{4.29}$$

It consists of a gain k_l, a washout stage to eliminate the steady state error, and m_k phase lead/lag stages. In each phase-lead/lag stage, a_{kj} is determined by the maximal compensation angle (determined by residue) of this stage Φ_{kj} at frequency ω_{kj}:

$$\Phi_{kj}(\omega_{kj}) = \sin^{-1}\left(\frac{a_{kj} - 1}{a_{kj} + 1}\right) \tag{4.30}$$

where ω_{kj} can be either the imaginary part of a critical mode or a frequency where phase margin is needed. The time constant τ_{kj} is evaluated from

$$\tau_{kj} = \frac{1}{\omega_{kj}\sqrt{a_{kj}}} \tag{4.31}$$

The gain k_l is chosen according to the following criteria:

1. with this gain, the closed-loop system should have damping ratio of the critical modes greater than 5%,

2. small gain is preferred since large gain will induce nonlinearity and create an unstable limit cycle.

Multi-step controller design

Conventional lead-lag controller design is based on the residue of the open-loop system. However, with the gain of the controller increasing, the residue also changes and the controller may no longer provide accurate phase compensation. This problem can be overcomed by designing the controller in several steps [44]. At each step, the residue will be calculated and a controller designed based on this updated residue.

For example, in order to design a controller to achieve the damping of the critical mode (whose original damping is σ_0) to a certain value σ, n steps are needed.

$$\Delta\sigma_1 + \Delta\sigma_2 + \ldots\ + \Delta\sigma_n = \sigma - \sigma_0 \tag{4.32}$$

where $\Delta\sigma_i$ represents the damping increase at step i.

Then the design procedure is as the followings:

Step 1: Based on the residue of the open-loop system, design controller $k_1h_1(s)$ to improve the critical mode's damping by $\Delta\sigma_1$. Assume that with $h_1(s)$ the angle of the root locus of the critical mode will be -180°. Then

$$k_1 = \frac{\Delta\sigma_1}{|R_d|\,|h_1(\lambda_d)|} \tag{4.33}$$

where R_d is the residue of the critical mode of the open-loop system and λ_d is the eigenvalue of the critical mode of the open-loop system.

Step 2: The closed-loop system becomes $\frac{G(s)}{1+G(s)k_1h_1(s)}$ shown in Fig. 4.5.

Based on the residue of this closed-loop system, design controller $k_2h_2(s)$ to improve the critical mode's damping by $\Delta\sigma_2$, i.e., with $h_2(s)$ the angle of the root locus of the critical mode

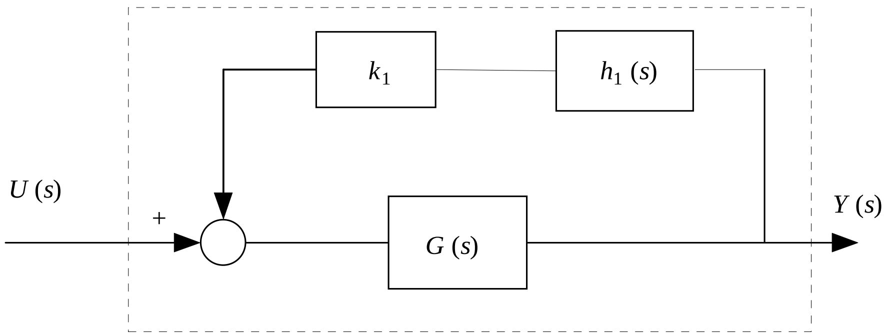

Figure 4.5: Closed-loop system diagram

will be -180°, and the gain k_2 will be

$$k_2 = \frac{\Delta\sigma_2}{|R'_d|\,|h_2(\lambda'_d)|} \tag{4.34}$$

where R'_d is the residue of the critical mode of the closed-loop system and λ'_d is the eigenvalue of the critical mode of the closed-loop system.

...

Step n: The critical mode's damping becomes improved by $\Delta\sigma_n$ for $k_n h_n(s)$.

The controller becomes:

$H(s) = k_1h_1(s) + k_2h_2(s) + \ldots\ + k_nh_n(s)$

Assume

$$h_i(s) = \frac{D_i(s)}{N_i(s)} = \frac{D_i(s)}{(1+T_1s)(1+T_2s)} \tag{4.35}$$

If $N_i(s)$ keeps unchanged, that means the time constants T_1 and T_2 are kept constant during all n steps, then the final realization is:

$$H(s) = \frac{K_{s0} + K_{s1}s + K_{s2}s^2}{(1+T_1s)(1+T_2s)} \tag{4.36}$$

4.5 Case study – a two-area four-machine power system

The two-area four-machine power system has a single tie-line connecting node 3 of area 1 to node 13 of area 2, see Fig. 4.6. All four machines have DC type exciters. The parameters

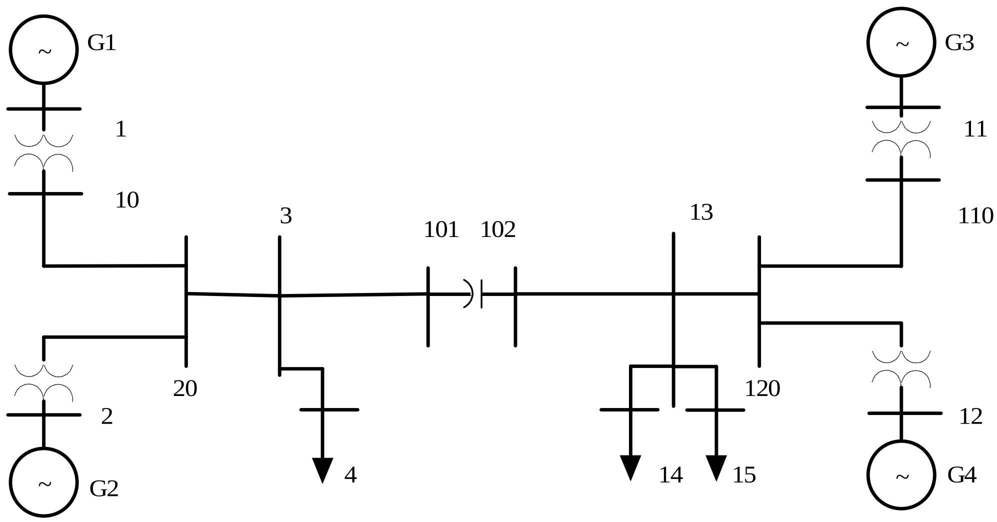

Figure 4.6: Two-area test power system

Table 4.1: The dominant oscillation modes

Number	Eigenvalues
$17, 18$	$-0.5186 \pm 6.8821i$
$19, 20$	$-0.5114 \pm 6.8404i$
$25, 26$	$-0.0286 \pm 3.0860i$
$31, 32$	$-0.6109 \pm 2.0368i$
$33, 34$	$-0.9741 \pm 2.0282i$
$40, 41$	$-0.2492 \pm 0.6450i$
$42, 43$	$-0.4202 \pm 0.4539i$
$44, 45$	$-0.4027 \pm 0.4501i$

and initial load flow solutions are shown in Appendix. A TCSC is installed in the mid-point of the transmission line, between nodes 101 and 102, providing a 40% compensation of the line reactance during steady state.

Under nominal conditions, when the tie-line active power, from area 1 to area 2, is 4 pu, and there is no TCSC damping signal, this system has the dominant eigenvalues shown in Fig. 4.7. The numerical values are shown in Table 4.1 There is an inter-area mode corresponding to eigenvalues No. 25 and 26, which is stable, but poorly damped, with a damping ratio of less than 0.05.

Several feedback signals have been investigated in the literature, amongst which are synthesized angle, tie-line active power, bus voltage magnitude and synthesized machine speed. The

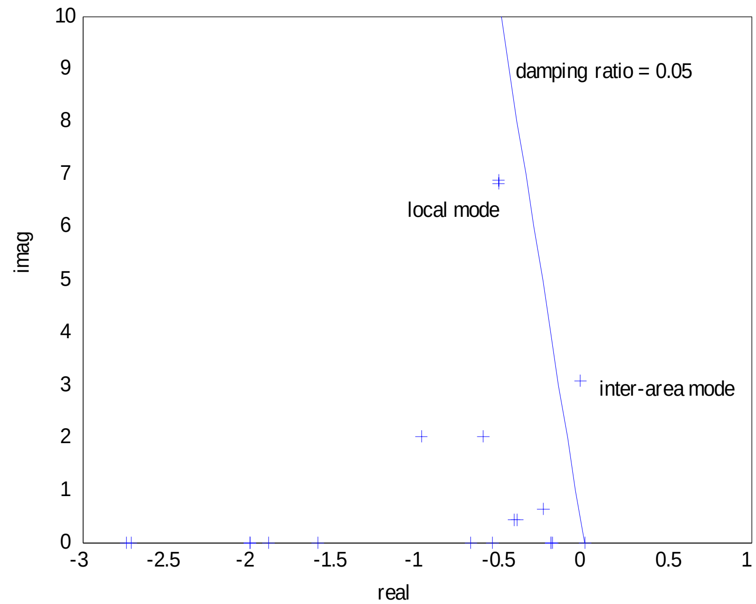

Figure 4.7: Eigenvalues of the open-loop system

Table 4.2: Three Operating Conditions (values in pu)

Case #	Load at Bus 4	Load at Bus 14	Tie-Line Power
1	9.76	17.17	4.010
2	11.76	15.17	1.865
3	16.76	10.17	-3.069

local measurements discussed here are voltage magnitude of bus 101, tie-line active power and current magnitude from bus 101 to bus 102.

4.5.1 Operating conditions

Three cases, described in Table 4.2, are investigated. Case 1 is the nominal condition when a 4 pu real power flows from area 1 to area 2. The second case corresponds to the tie-line carrying only half of the nominal power, i.e., 2 pu, and the third case is a reversal in the power flow direction.

For these three cases and using three different input signals, which are $|V|$, P and $|I|$, the residues of the inter-area mode, i.e., eigenvalue $-0.0286 \pm 3.0860i$, are given in Table 4.3.

Table 4.3: Residues' magnitude and phase of the inter-area mode

Case #	**Residue**					
	Input: |V|		Input: P		Input: |I|	
1	0.0113	74.12°	0.0938	-84.00°	0.1427	-90.95°
2	0.0012	55.01°	0.0837	-94.04°	0.0835	-94.79°
3	0.0155	66.41°	0.1496	87.16°	0.1915	-97.66°

From Table 4.3, the phase of residue did not change much for the three operating conditions when voltage magnitude or current magnitude is selected as the input signal. However, for the input signal corresponding to the active power flow, the angle of the residue in case 3 is (87°), with a big difference from that of case 1 (-84°) or case 2 (-94°). This is due to the reversed power flow in case 3. If the absolute value of active power flow is selected as the input signal, the residue phase in cases 1 and 2 will not change while in case 3 it becomes -93°. This makes the design of phase compensation controller much easier, see Table 4.4.

4.5.2 Indices for signal selection

Fig. 4.8 shows the effectiveness index for three input signals when the tie-line active power changes from 1.5 pu to 4.0 pu. In this range, the variation of the index corresponding to power flow is the smallest, i.e., the active power flow signal is much more robust when compared to the voltage and current magnitude signals.

Fig. 4.9 shows the interaction index SI_{λ_i} where λ_i corresponds to an oscillation mode 31, eigenvalue $-0.6109 + 2.0368i$. The maximum value of the index corresponding to $|V|$ as input signal is more than 0.8, that is, the controller has almost similar effects on mode 31 and inter-area oscillation mode 25. It is obvious that in this range using $|I|$ as input signal the control will have least interaction with this specified oscillation mode.

Fig. 4.10, Fig 4.11, Fig. 4.12 show the interaction index SI_{λ_i} where λ_i corresponds to oscillation mode 33 ($-0.9741+2.0282i$), mode 42 ($-0.4202+0.4539i$), mode 44 ($-0.4027\pm0.4501i$). Notice that the controller has little effects on mode 42 and 44 whatever the input signal is since the index has small scale (x 10^{-3}). For mode 33, at most conditions, the controller has small effects. Therefore the interaction that should be taken into consideration is between the controller and mode 31.

The effective index suggests that |P| is better than |V| and |I|, while interaction index suggests that |I| is the best. In this case, the effectiveness of the controller is treated with the

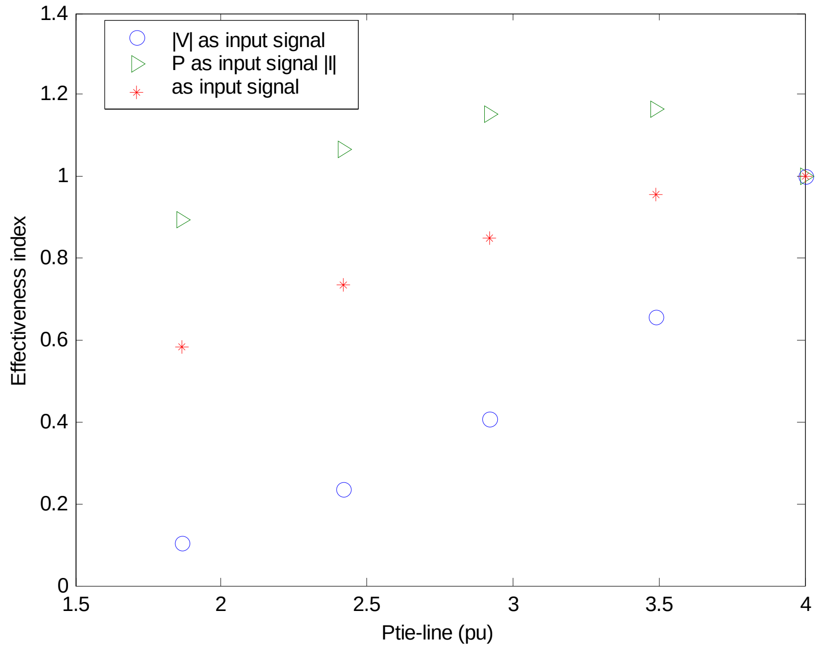

Figure 4.8: Variation of proposed effectiveness index vs. the tie-line active power

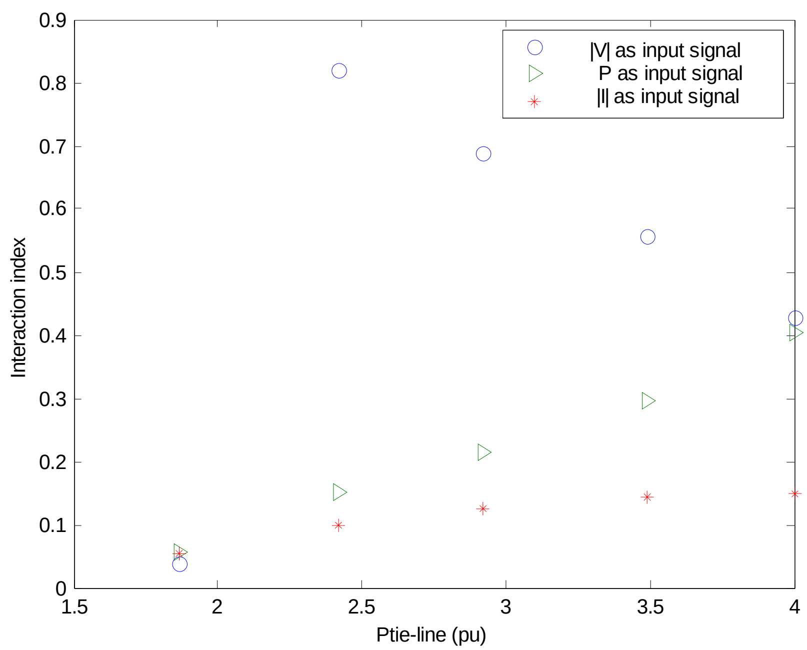

Figure 4.9: $SI^{i}_{\lambda 31}$ vs. the tie-line active power

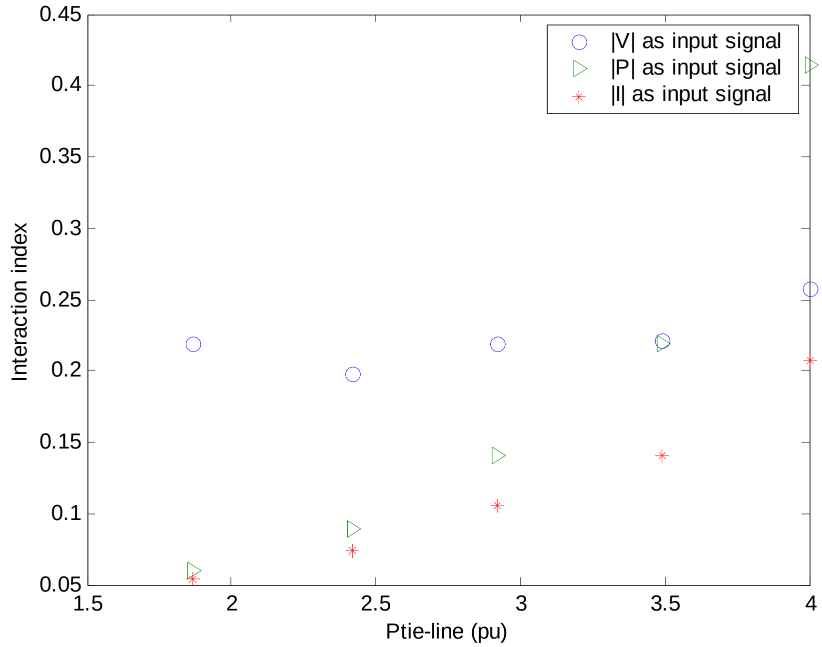

Figure 4.10: $SI^{i}_{\lambda 33}$ vs. the tie-line active power

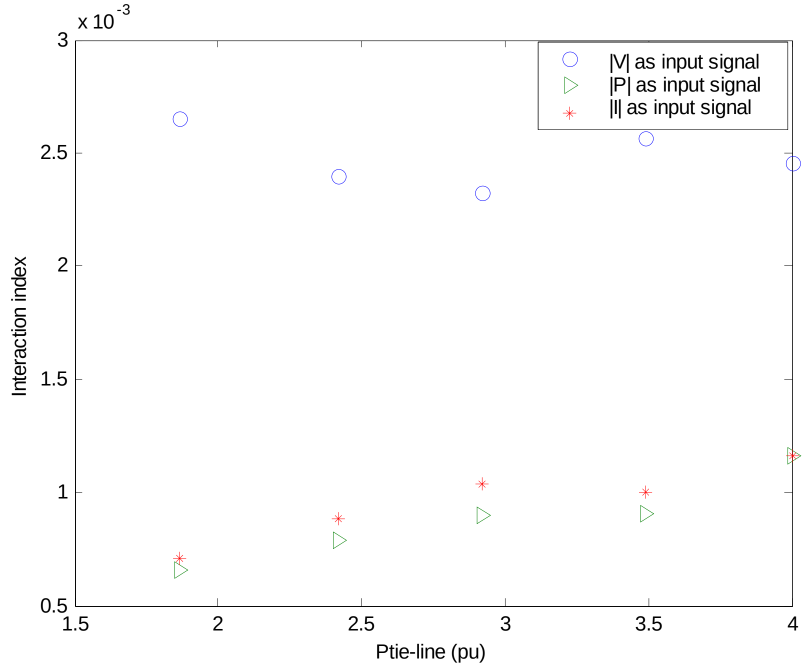

Figure 4.11: $SI^{i}_{\lambda 42}$ vs. the tie-line active power

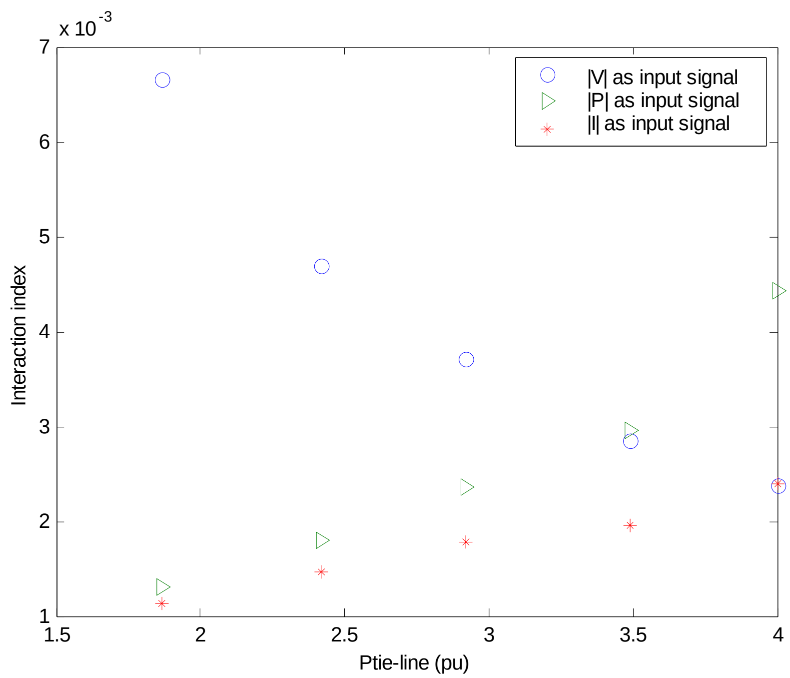

Figure 4.12: $SI^{i}_{\lambda 44}$ vs. the tie-line active power

Table 4.4: Angle of residues with input signal: |P|

Case #	Residue's angle
1	-84°
2	-94°
3	-93°

highest priority, therefore |P| is chosen as the best input signal for inter-area oscillation damping. In the following section, the damping controller will be designed based on input signal being the absolute value of tie-line power flow.

4.5.3 Damping controller design

Lead-lag controller

The damping controller is designed using the absolute value of the active tie-line power flow. It will then be compared to a design in [47] performed using the voltage signal. The angles of the residues of the inter-area mode are shown in Table 4.4.

Based on Table 4.4, the desired compensation phase is selected to be -90°. Two stages of lead-lag units are used with each providing 45° phase compensation. With these two stages of lead-lag units as a dynamic compensator, the root locus will leave the inter-area mode in the left half plane; thus, the control will dampen the mode.

The designed dynamic compensator is:

$$K(s) = k\frac{3s}{1+3s}\frac{1+0.69s}{1+0.15s}\frac{1+0.69s}{1+0.15s} \tag{4.37}$$

The bode plot of the open-loop system for the three operating conditions (solid lines) and controller (dotted line) are shown in Fig. 4.13. The compensator can provide satisfactory stability margins for all three cases.

Fig. 4.14 shows the root loci of the system with the proposed controller at three operating points. The root loci can be used to choose gain. The criteria to choose gain is (1) with this gain, the closed-loop system should have damping ratios greater than 5%, (2) small gain is preferred since high gain will induce nonlinearity and create an unstable limit cycle. Therefore, gain k is chosen to be 0.6 since in all three cases, the inter-area mode will have greater than 5% damping ratio.

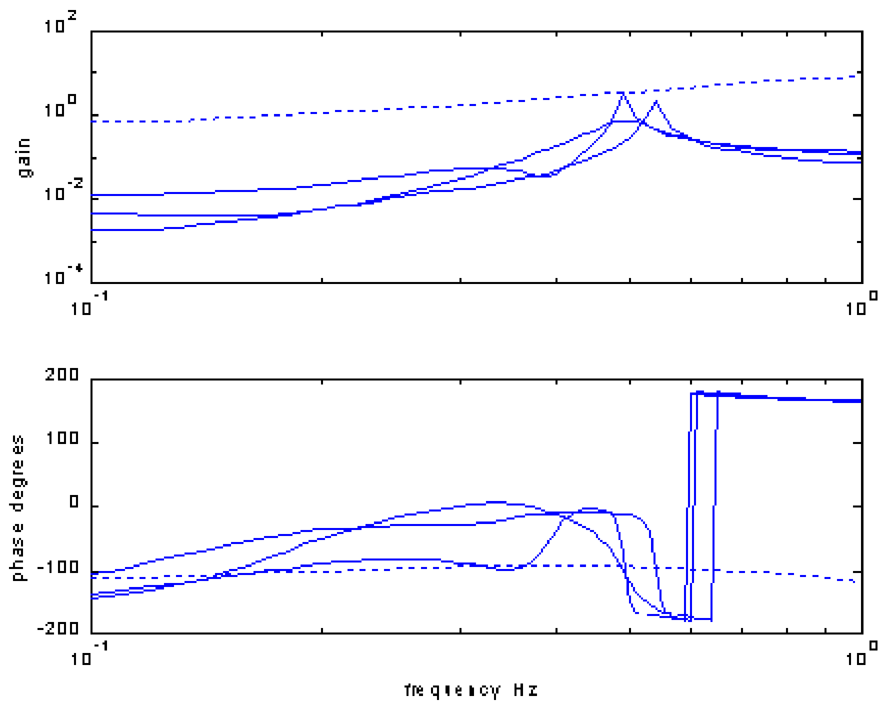

Figure 4.13: Robust desgin illustration

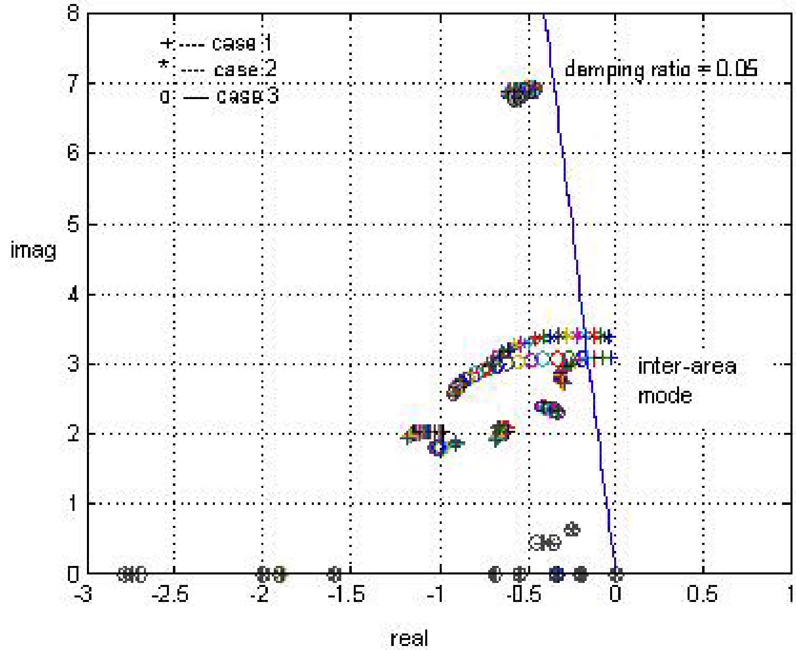

Figure 4.14: Root locus with absolute value of active power flow as variable (gain = 0 to 2, with a step of 0.1)

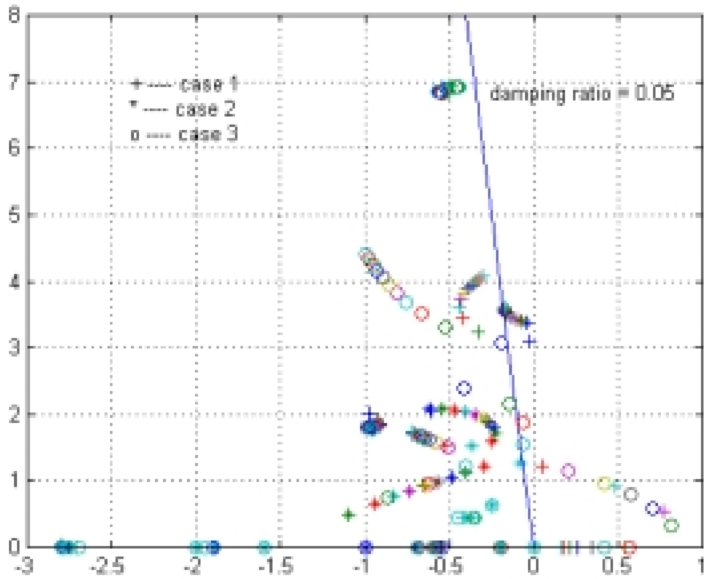

Figure 4.15: Root locus with voltage magnitude as variable, (gain = 0 to 10, each step 1)

For comparison, the transfer function for a controller using voltage magnitude as input signal [47] is:

$$K(s) = 100\frac{s}{1+s}\frac{1+0.1s}{1+0.5s}\frac{1+0.1s}{1+0.5s} \tag{4.38}$$

Fig. 4.15 shows the root loci of the system with this controller (Eq. 4.38) at three operating points. The inter-area mode is damped well at the nominal point, but this is not the case for the second operating condition.

Nonlinear simulation results are presented to illustrate the effectiveness of the proposed methodologies. At time t = 0.1 second, a three-phase line to ground fault is applied on line 3-15. The fault is cleared at time t = 0.15 second. Figs. 4.16, 4.17, 4.18, 4.19 show the simulation results for the nominal case and case 2 or 3 respectively when absolute value of the active tie-line power is used as a control signal. The simulation results demonstrate that the controller improves the damping of inter-area oscillations in all three cases.

Figs. 4.20, 4.21 and 4.22 show the simulations results for the nominal case 1 and case 2 respectively when voltage magnitude is used as a control signal.

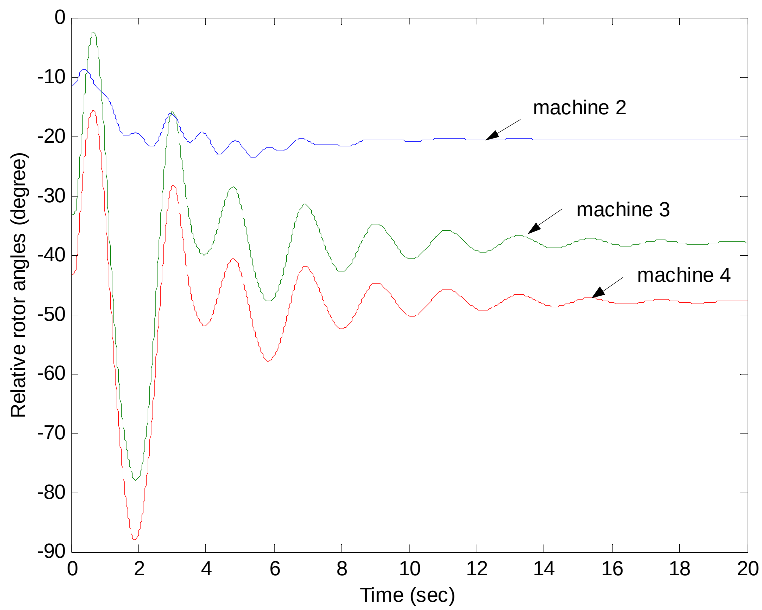

Figure 4.16: Dynamic response of relative rotor angles in case 1

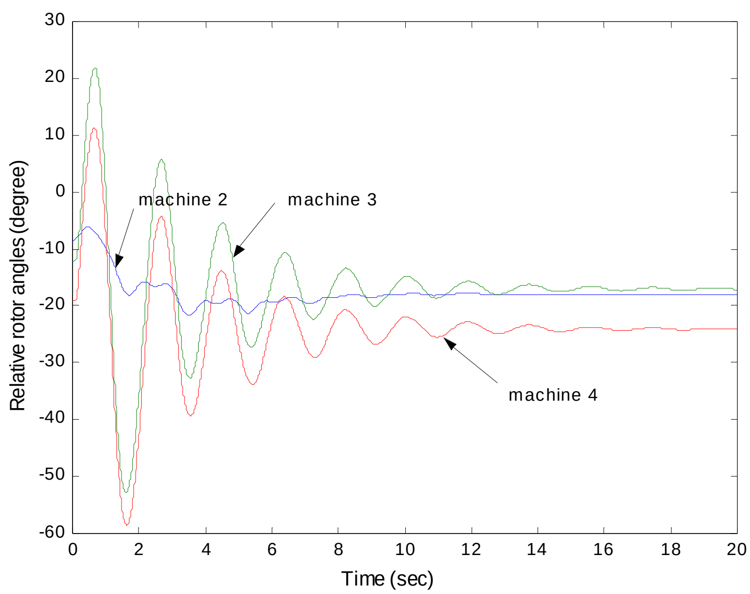

Figure 4.17: Dynamic response of relative rotor angles in case 2

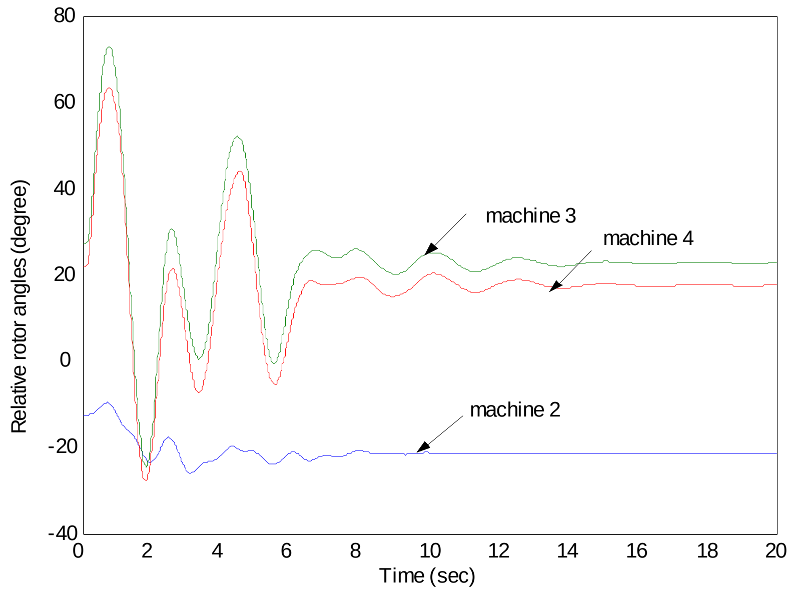

Figure 4.18: Dynamic response of relative rotor angles in case 3

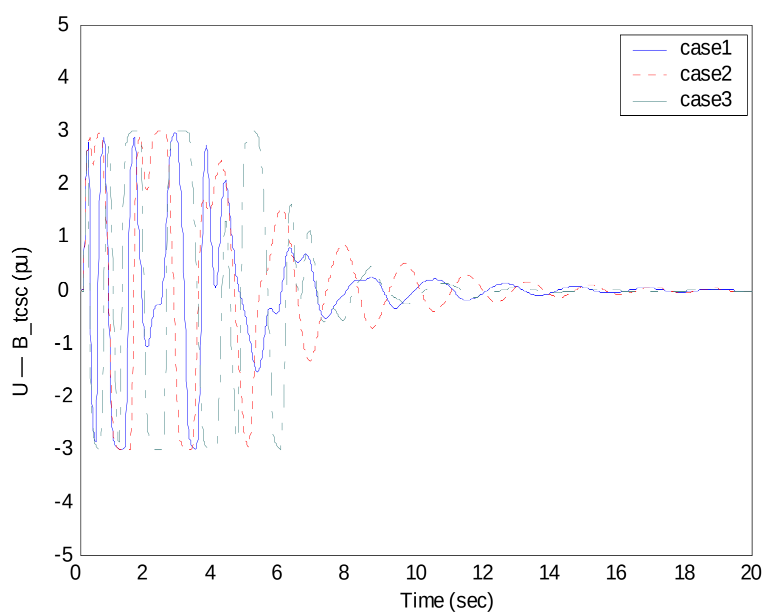

Figure 4.19: Dynamic response of u − B_tcsc

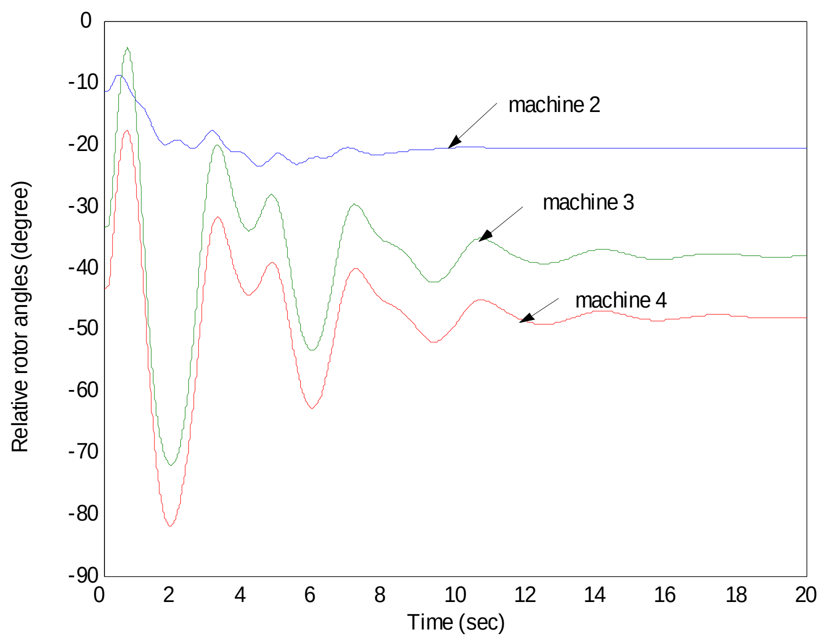

Figure 4.20: Dynamic response of relative rotor angles in case 1

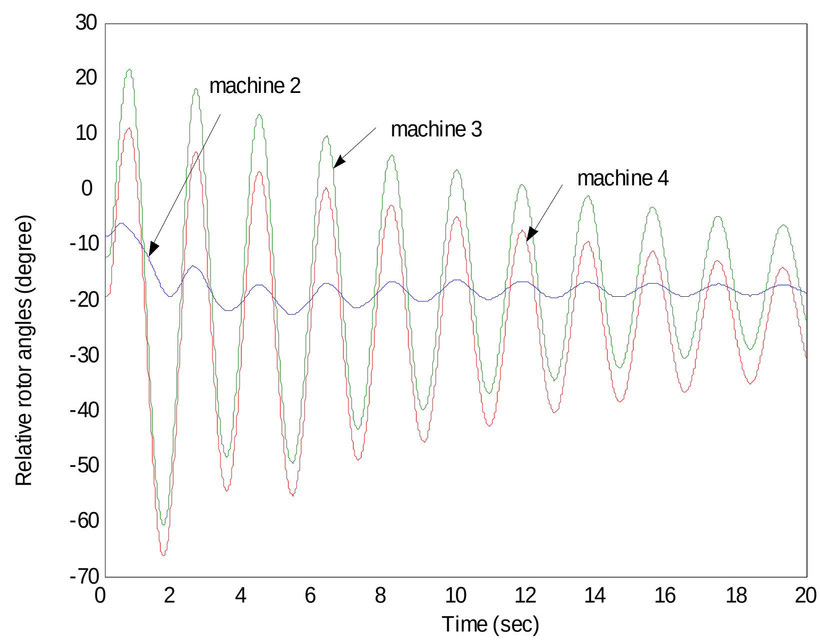

Figure 4.21: Dynamic response of relative rotor angles in case 2

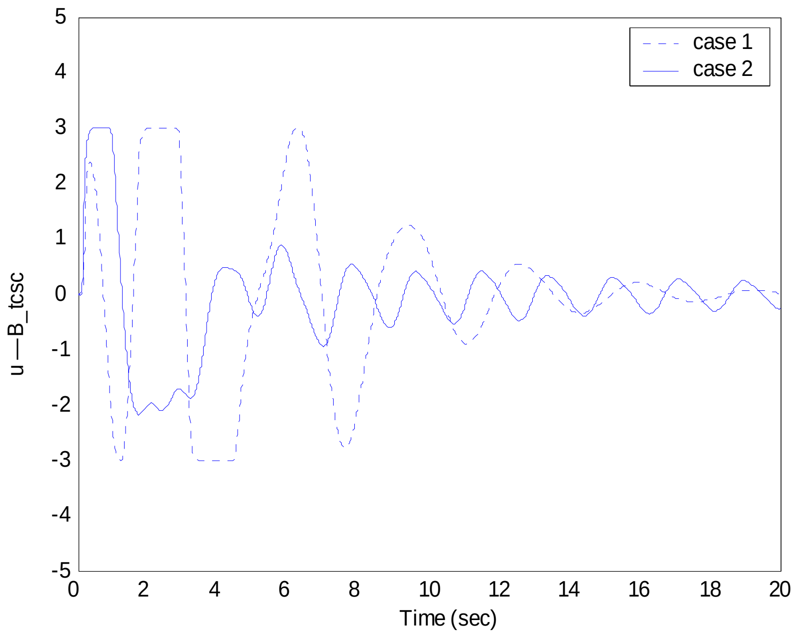

Figure 4.22: Dynamic response of u – B_tcsc

The simulation results in Fig. 4.20, 4.21, 4.22 show that the controller improves the damping of inter-area oscillations while in case 2 the controller loses its effectiveness.

Multi-step control design

The lead-lag controller using absolute value of active power is designed based on the residue of the open-loop system. To achieve better performance, multi-step controller design method is used. Without the controller, the open-loop system has an inter-area oscillation mode corresponding to eigenvalues $-0.0286 \pm j3.086$. The damping of the mode is expected to be improved to 0.2286. The open-loop system residue of the inter-area oscillation is already known as Table 4.3. The compensation angle is chosen to to 84° and the number of the lead units is two. Therefore, each unit will provide 42° leading angle. The parameters of the lead units are obtained through Eq. 4.30 and Eq. 4.31. With a washout unit, the transfer function of the lead units is

$$h_1(s) = \frac{s}{1+s}\left(\frac{1+5.0476*0.1294s}{1+0.1294s}\right)^2 \tag{4.39}$$

Table 4.5: One-step design approach

Original	Expected	Computed
$-0.0286 \pm j3.086$	$-0.2286 \pm j3.086$	$-0.1668 \pm j2.9825$

Table 4.6: Two-step design approach

Step	Expected	Computed	Gain k_i	a_i
1	$-.1286 \pm j3.086$	$-0.2286 \pm j3.086$	0.2562	5.0476
2	$-.2286 \pm j3.086$	$-.1952 \pm j2.9954$	0.5123	3.4197

Now the gain of the controller is

$$k_1 = \frac{\Delta\sigma}{|R_d|\,|h_1(\lambda_d)|} = \frac{0.2}{0.0938 * |-0.8938 + j4.0642|} = 0.5124$$

The controller is called Controller 1 and its transfer function is expressed in Eq. 4.40.

$$H_1(s) = 0.5124\frac{s}{1+s}\left(\frac{1+5.0476*0.1294s}{1+0.1294s}\right)^2 \tag{4.40}$$

Table 4.5 shows the one-step design approach results of eigenvalues. With the controller expressed in Eq. 4.40, the closed-loop system has an inter-area oscillation mode of eigenvalue $-0.1668 \pm j2.9825$. The damping of the mode differs from what is expected. To reduce the difference, two-step design is utilized.

Table 4.6 shows the two-step design approach. The two-step design approach gives a closer result to the expected value. The controller is called Controller 2 and its transfer function is

$$H_2(s) = 0.2562\frac{s}{1+s}\left(\frac{1+5.0476*0.1294s}{1+0.1294s}\right)^2 + 0.5123\frac{s}{1+s}\left(\frac{1+3.4197*0.1294s}{1+0.1294s}\right)^2 \tag{4.41}$$

The root locus with controllers are shown in Fig. 4.23. Compared with the one-step design based controller, the two-step design based controller has more ability to increase the damping of the mode.

4.6 Case study – the western U.S. power system

4.6.1 Introduction

The western U.S. power system (WSCC) has long been attracting researchers' interest. It is an interconnected power system that covers the western half of the United States, portions

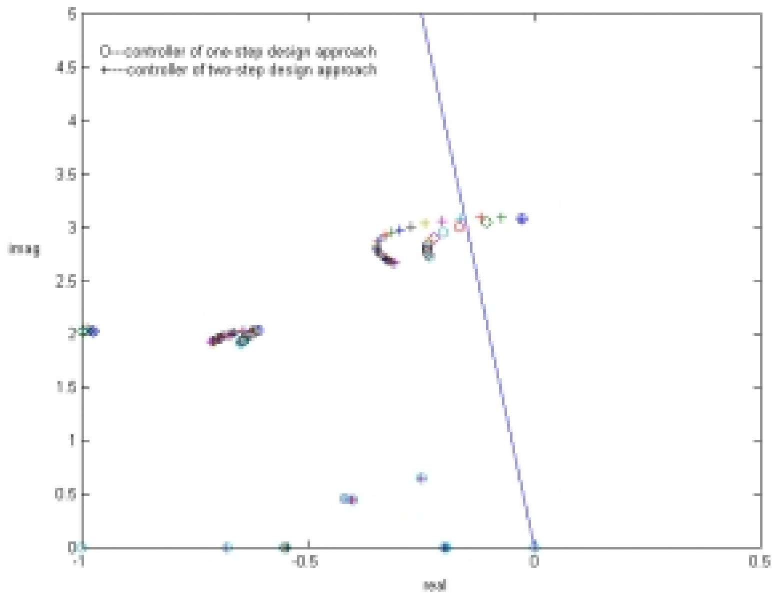

Figure 4.23: Root locus of two types of design

of western Canada and northern Mexico. The model used in this dissertation does not include northern Mexico. With some key transmission lines heavily loaded, disturbances have profound effects, e.g., the July 2, 1996 outage affected 3 percent of the customers [3]. Meanwhile, this system has been subjected to low frequency oscillations, especially oscillations around 0.7 Hz, when large power is transferred from Arizona and Nevada to Southern California. Power system stabilizers were designed to dampen this troublesome 0.7 Hz mode [63]. The InterMountain High Voltage Direct Current (HVDC) project has also aimed at dampening inter-area oscillations by power modulation of converter control [42].

In [29], a 19-generator 49-bus model exhibiting characteristics and structure similar to that of the WSCC system was studied. An energy approach is used to identify the two groups of machines that are involved in an inter-area oscillation. TCSC was then installed on a certain key transmission line for inter-area oscillation damping purpose. The paper focuses mainly on the identification of the generator groups involved in the oscillations.

In this case study, the damping enhancement by TCSC in the WSCC system is proposed. The proposed controller uses only a local signal so that communication links are avoided, which will reduce the cost and increase the reliability. The controller should be robust, i.e., the fixed controller structure that works well at various operating conditions. The proposed control signal selection index and the condition that deals with robustness are used as guidelines for siting and controller design.

4.6.2 WSCC system

The reduced WSCC model developed by Smith and co-workers [50] is used in this paper. It is a 19-machine, 46 bus power system. There are seven areas, Canada (CN), Arizona (AZ), South California and South (SS), Pacific Northwest and North (PN), Montana (MT), Utah (UT), and North California (NC). Two HVDC links, one from North West to South, the other from Utah to South, are modeled as injected power sources. Two cases of tie-line power flows are investigated in this paper. Case 1 is based on the power flow. Case 2 has a reversed flow between Utah and Arizona. The tie-line flows are shown in Figure 4.24.

Modal analysis is based on Case 1. Since there are 19 generators, the open-loop system has 18 electromechanical oscillation modes. 13 of them are local modes and five are inter-area oscillation modes. The eigenvalue analysis of these oscillation modes are shown in Table 4.7 and Table 4.8.

Mode shapes of observability vector [63] are used to identify oscillation patterns, which are shown in Table 4.9.

From Table 4.9, it is found that for oscillation mode 54 (0.96Hz), the SS, MT and PN areas swing against NC and UT areas; that is, the west and east ends of the system swing against the areas in between the two ends. For mode 56 (0.83 Hz), the SS, UT and CN areas swing against PN, AZ and MT areas. For mode 58 (0.73 Hz), SS and NC swing against AZ, CN, MT and UT; that is, the southwest against the east. For mode 60 (0.67Hz), AZ and CN in the north and the south ends of the system swing against the areas in between. For mode 62 (0.35 Hz), the south AZ and SS swing against the north.

It has been shown that inter-area mode 58 (0.73 Hz) has the largest residue at machine SOUTH_G1. The PSS on this machine can effectively improve the damping of this inter-area mode. Inter-area mode 56 (0.86 Hz) has the largest residue at machine BUTAH_G1, and therefore the PSS on BUTAH_G1 can improve the damping of this mode. However, inter-area mode 60 (0.67 Hz) has small value of its residues at all machines and therefore it is difficult to be dampened by PSSs using local signals. Hence mode 60 is the most critical oscillation mode.

A method is proposed in [63] to improve the damping of mode 60 by PSSs on machine

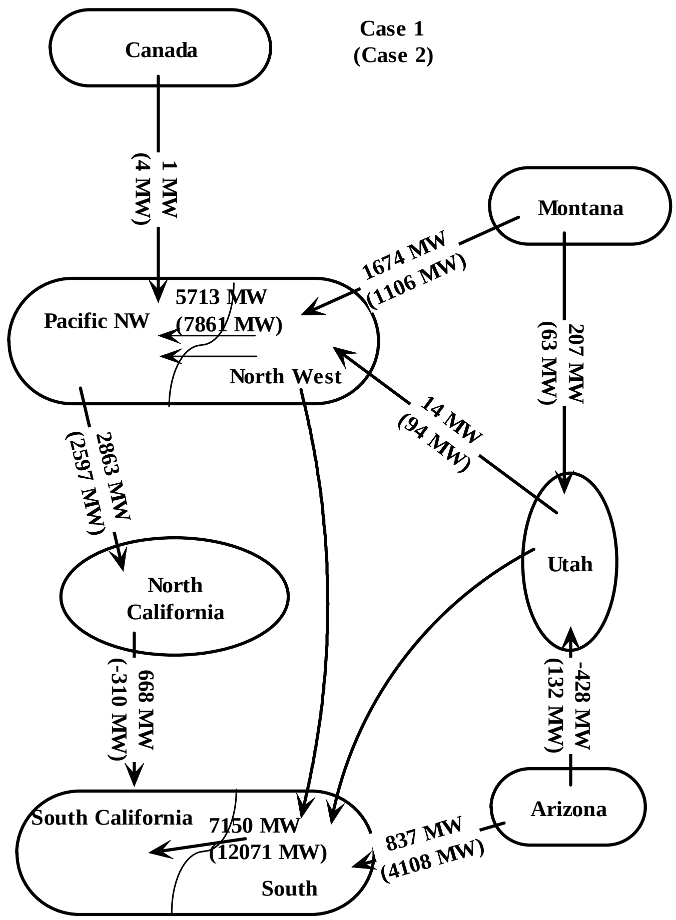

Figure 4.24: WSCC system

Table 4.7: Eigenvalue analysis results of local oscillation modes

Mode	Real part	Frequency	Observability (0.0001)	Main participating generators
4	-0.1955	2.3401	101	MONTA_GM
			26	MONTA_G1
16	-1.3161	2.2319	53	ARIZO_G2
20	-0.3303	2.2049	21	NORTH_G2
22	-0.2047	2.1082	14	BUTAH_G1
			6	BUTAH_GM
28	-0.1135	2.0127	26	PACNW_GM
			16	PACNW_G1
30	-0.8128	1.8560	26	ARIZO_G1
32	-0.4015	1.7987	26	NORTH_G1
34	-0.3289	1.7397	74	CANADA_G1
36	-0.2282	1.7081	146	PACNW_GM
			7	NORTH_G1
			6	PACNW_GM
38	-0.3463	1.6190	10	SOUTH_G1
			4	SOUTH_GM
46	-0.5141	1.4803	13	NOCAL_G1
			4	NOCAL_GM
48	-0.4205	1.3692	7	SOUTH_G2
			6	SOUTH_G1
52	-0.2296	1.1687	84	MONTA_G1
			39	MONTA_GM

Table 4.8: Eigenvalue analysis results of inter-area oscillation modes

Mode	Real part	Frequency (Hz)	Most Participant Machines
54	-0.0583	0.9606	NOCAL_GM, NOCAL_G1 SOUTH_G1, SOUTH_G2
56	0.0034	0.8293	ARIZO_GM, CANAD_GM NORTH_GM, MONTA_GM BUTAH_GM, BUTAH_G1 SOUTH_G1, SOUTH_G2
58	0.0009	0.7319	NOCAL_GM, NOCAL_G1 BUTAH_GM, BUTAH_G1 SOUTH_GM, SOUTH_G1, SOUTH_G2
60	0.0053	0.6741	MONTA_GM MONTA_G1 CANAD_GM CANAD_G1 BUTAH_GM BUTAH_G1
62	-0.0856	0.3514	ARIZO_GM ARIZO_G1 ARIZO_G2 CANAD_GM MONTA_GM MONTA_G1 NORTH_GM, NORTH_G1 NORTH_G2 SOUTH_G1, SOUTH_G2

Table 4.9: Mode shapes of inter-area oscillation modes

	Mode No.					
Machine	54	56	58	60	62	90
ARIOZO_GM	-5.6	27.6	-37.5	137.7	-23.2	28.1
CANAD_GM	-13.4	-155.4	-30.9	136.1	155.4	28.1
NOCAL_GM	-8.3	-139.1	141.1	-44.6	148.8	27.8
NORTH_GM	170.8	25.5	155.5	-43.6	154.7	27.9
MONTA_GM	168.6	26.5	-49.6	-43.7	154.4	27.6
BUTAH_GM	-16.4	-157.1	-37.8	-42.8	150.7	26.9
SOUTH_GM	174.4	-152.6	139.5	142.2	-23.2	27.9
PACNW_GM	169.1	25.1	148.8	-43.6	154.6	27.8
ARIZO_G1	-8.4	25.5	-38.4	135.7	-24.0	28.0
ARIZO_G2	-7.2	26.4	-37.7	136.2	-23.9	28.0
CANAD_G1	-16.3	-157.7	-32.7	134.5	154.8	28.0
NOCAL_G1	-18.3	-146.8	135.7	-48.9	147.6	27.8
MONTA_G1	162.2	21.5	-52.7	-47.0	153.5	27.6
BUTAH_G1	-17.7	-158.3	-38.8	-43.7	150.4	26.9
NORTH_G1	167.7	23.2	151.8	-45.2	154.1	27.9
NORTH_G2	169.0	24.4	153.0	-44.4	154.3	27.9
PACNW_G1	166.3	22.8	146.4	-45.2	154.1	27.9
SOUTH_G1	165.0	-159.5	134.4	138.8	-24.3	27.9
SOUTH_G2	169.5	-156.7	136.2	140.4	-24.0	27.8

PACNW_G1 and ARIZO_G1 using generator speed difference as input signals. Here, TCSC's ability to dampen the inter-area oscillation mode is analyzed and discussed.

4.6.3 Damping enhancement via TCSC

TCSC is used to enhance damping in the WSCC reduced system. Its siting, control signal selection and controller design are the issues to be addressed. Since the power system is a nonlinear system with loading conditions changing frequently, therefore, when linear systems tools are applied, different operating conditions have to be taken into account. The constraint and the index for effective and robust design are going to be used as a guideline for siting and signal selection.

4.6.4 TCSC siting and signal selection

A TCSC is to be installed on a key transmission line. The control signals for oscillation damping are chosen to be local measurements, such as active power or current magnitude. With PT and CT installed, the instantaneous waveforms of current and voltage can be obtained. The abc waveforms are transformed into qd-axis values which are easy for calculation of power and magnitude and hence easy for control purposes.

Tables 4.10 and 4.11 show the Case 1 and Case 2 residues of three inter-area oscillation modes near 0.7 Hz when active power flow is used as input control signal for TCSC installed on different transmission lines.

Table 4.10: Residues when active power through tie-lines used as input signal of the controller in case 1

Line	Mode 56	Mode 58	Mode 60
PACNW_MN–CANAD_MN	-.0000-.0000i	.0000-.0000i	.0000+.0000i
NORTH_MN–MONTA_MN	-.0004-.0011i	-.0011-.0045i	-.0019-.0080i
MONTA_TX–BUTAH_MN	.0000+.0000i	.0000+.0000i	.0000+.0000i
NORTH_MN–PACNW_MN	-.0000-.0000i	-.0000-.0000i	-.0000-.0000i
NORTH_TX–BUTAH_MN	-.0022-.0392i	-.0280-.1145i	.0000+.0000i
NOCAL_MN–SOCAL_TX	-.0000-.0000i	.0000-.0000i	.0000+.0000i
ARIZO_MN–SOUTH_MN	-.0353-.2335i	-.1182-.4752i	-.0021-.0064i
ARIZO_TX–BUTAH_MN	-.0118-.0383i	-.0018-.0102i	-.0050-.0255i

The greater the magnitude of the residues, the more effective is the controller. Although the transmission line between AZ and SS seems to be the best placement for mode 56 and mode 58,

Table 4.11: Residues when active power through tie-lines used as input signal of the controller in case 2

Line	Mode 56	Mode 58	Mode 60
PACNW_MN–CANAD_MN	.0000+.0000i	.0000+.0000i	.0000+.0000i
NORTH_MN–MONTA_MN	.0000+.0001i	-.0012-.0045i	-.0042-.0177i
MONTA_TX–BUTAH_MN	-.0098-.0298i	-.0109-.0478i	-.0029-.0160i
NORTH_MN–PACNW_MN	.0000+.0000i	.0000+.0000i	-.0000-.0000i
NORTH_TX–BUTAH_MN	-.0000-.0000i	.0000+.0000i	-.0000-.0000i
NOCAL_MN–SOCAL_TX	.0000+.0003i	.0027+.0124i	.0009+.0043i
ARIZO_MN–SOUTH_MN	-.0258-.1150i	-.0172-.0617i	-.0000-.0001i
ARIZO_TX–BUTAH_MN	.0198+.0625i	.0063+.0281i	.0153+.0764i

it is not a good place for mode 60. In Case 2, the residue of mode 60 is very small which means that the controller will hardly have any effect on this oscillation mode. Instead, the transmission line between AZ and UT has an effect on all three oscillation modes, especially on mode 60. Therefore, the transmission line between AZ and UT is chosen to be the place to install a TCSC.

Tables 4.12 and 4.13 show the residues of three inter-area oscillation modes near 0.7 Hz when current magnitude is used as an input control signal for TCSC installed on different transmission lines.

Table 4.12: Residues when current magnitude used as input signal of the controller in case 1

Line	Mode 56	Mode 58	Mode 60
PACNW_MN–CANAD_MN	-.0000-.0000i	.0000+.0000i	.0000+.0000i
NORTH_MN–MONTA_MN	-.0004-.0010i	-.0011-.0044i	-.0018-.0078i
MONTA_TX–BUTAH_MN	.0000+.0000i	.0000+.0000i	.0000+.0000i
NORTH_MN–PACNW_MN	-.0000-.0000i	-.0000-.0000i	-.0000-.0000i
NORTH_TX–BUTAH_MN	-.0024-.0409i	-.0289-.1171i	.0000-.0000i
NOCAL_MN–SOCAL_TX	-.0000-.0000i	.0000-.0000i	.0000+.0000i
ARIZO_MN–SOUTH_MN	-.0419-.2698i	-.1383-.5463i	-.0026-.0081i
ARIZO_TX–BUTAH_MN	-.0110-.0358i	-.0015-.0088i	-.0046-.0234i

According to the residue phase constraint, that is, the residue phases of close modes at different operating conditions are to be bundled together within a narrow angle, it is obvious that current magnitude as input control signal meets the requirement while active power does not. That is, because in Case 2, the line flow of AZ to UT is reversed. The residue phases of the channel when active power is used as an input signal have big differences. However, the residue phases of the channel when current magnitude is used as an input signal do not have significant differences.

Table 4.13: Residues when current magnitude used as input signal of the controller in case 2

Line	Mode 56	Mode 58	Mode 60
PACNW_MN–CANAD_MN	.0000+.0000i	.0000+.0000i	.0000+.0000i
NORTH_MN–MONTA_MN	-.0000-.0001i	-.0011-.0044i	-.0042-.0176i
MONTA_TX–BUTAH_MN	-.0095-.0289i	-.0105-.0459i	-.0028-.0152i
NORTH_MN–PACNW_MN	.0000+.0000i	.0000+.0000i	-.0000-.0000i
NORTH_TX–BUTAH_MN	-.0000-.0000i	.0000+.0000i	-.0000-.0000i
NOCAL_MN–SOCAL_TX	.0000-.0002i	-.0026-.0117i	-.0009-.0043i
ARIZO_MN–SOUTH_MN	-.0239-.1075i	-.0161-.0579i	-.0000-.0001i
ARIZO_TX–BUTAH_MN	-.0231-.0727i	-.0075-.0335i	-.0181-.0900i

TCSC controller design

Based on the previous analysis, the transmission line between AZ and UT is selected to be equipped with a TCSC. Also, the current magnitude is chosen as the best input control signal for inter-area oscillation damping. The task now is to design a controller. A simple controller, a lead-lag control structure, is designed in this case as the following.

$$H(s) = 10\frac{s}{1+s}\frac{1+0.4s}{1+0.108s}\frac{1+0.4s}{1+0.108s}$$

The root locus is shown in Fig. 4.25.

Root locus shows that all three roots near 0.7 Hz mode will move toward left plane when the gain increases.

Simulation results

Simulations are performed using Power System Toolbox. At 0.1 second, a three-phase fault is applied at bus PACNW_F1. It is cleared 50ms later.

Simulation results show that with TCSC damping controller, the tie line power flow has better performance.

This case study shows inter-area oscillation damping enhancement in the WSCC system by a TCSC. First, siting of the TCSC is investigated, and second a robust damping controller, i.e., a controller that operates at various loading conditions, was designed. The proposed methodologies are based on transfer function residues. An index is given to identify the most effective signal to feedback, and a condition to guarantee control robustness is derived based on the phases of the residues. A reduced order model of the WSCC system is used to demonstrate the proposed

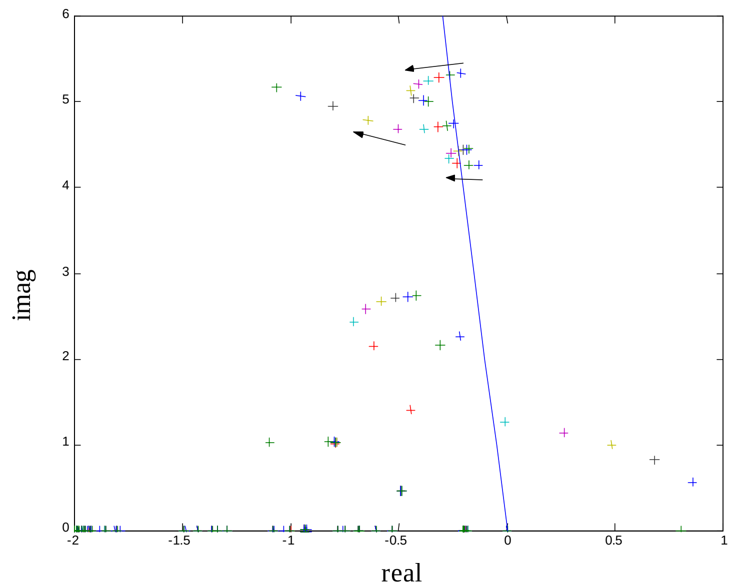

Figure 4.25: Root locus of the system with TCSC controller

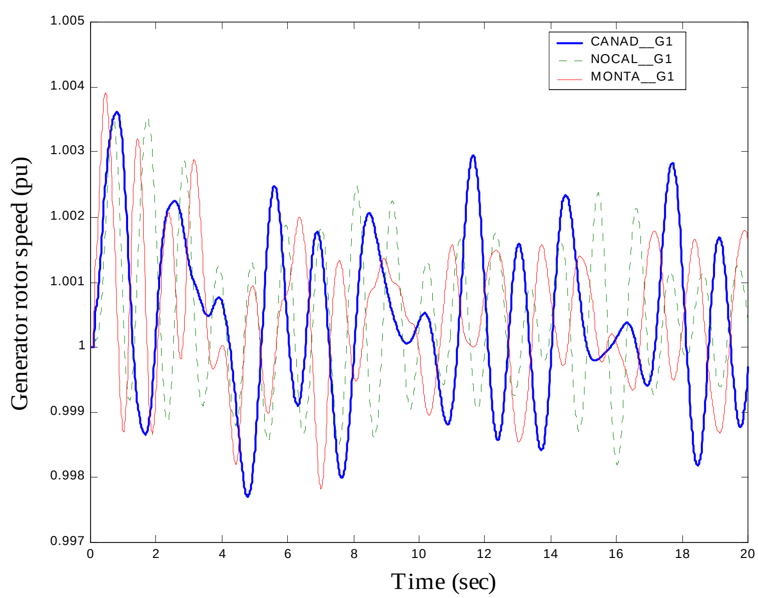

Figure 4.26: Generator rotor speeds of WSCC reduced system with no TCSC

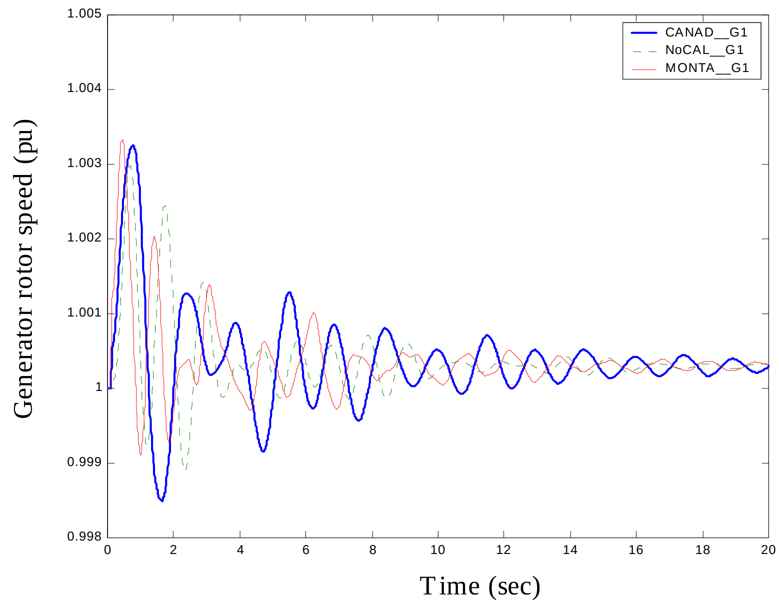

Figure 4.27: Generator rotor speeds of WSCC reduced system with TCSC

techniques. Specifically, a TCSC is recommended to dampen the WSCC's near 0.7 Hz inter-area modes. An optimal placement of TCSC is found and the effective control input was also found as current magnitude. Nonlinear simulations were performed and the system responses with and without the controller were compared. Both root locus and simulations results show the proposed methodology was effective.

4.7 Conclusion

In this chapter, TCSC damping controller for inter-area oscillation is studied. The conditions and indices for control signal selection are proposed and controller is designed using lead-lag control design scheme or multi-stage design scheme.

The proposed methodologies are tested in a two-area four-machine power system and demonstrated to be effective. A large-scale power system – WSCC system is also studied. The optimal location of TCSC and its control signal are chosen based on the proposed conditions and indices.

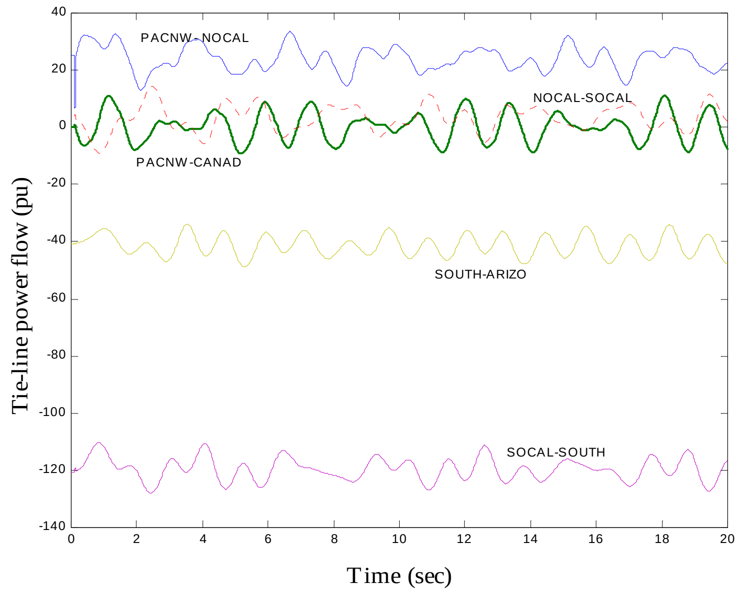

Figure 4.28: Tie-line power flow of WSCC reduced system with no TCSC

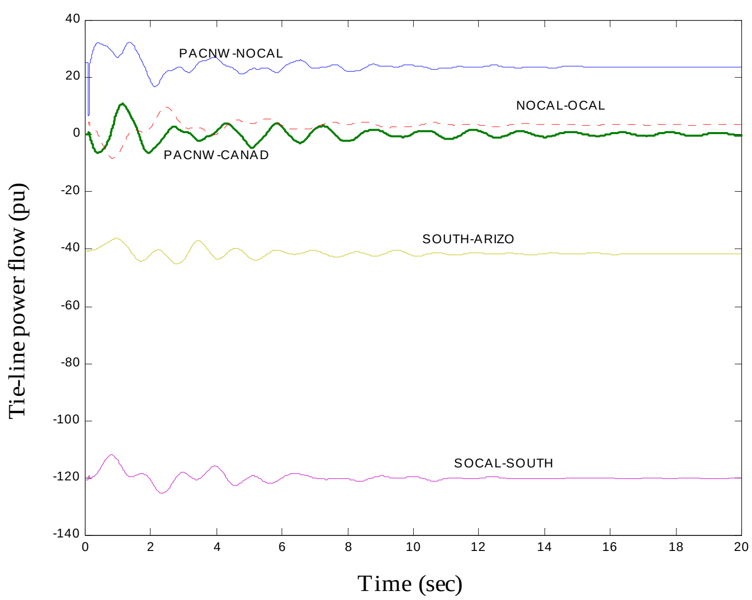

Figure 4.29: Tie-line power flow of WSCC reduced system with TCSC

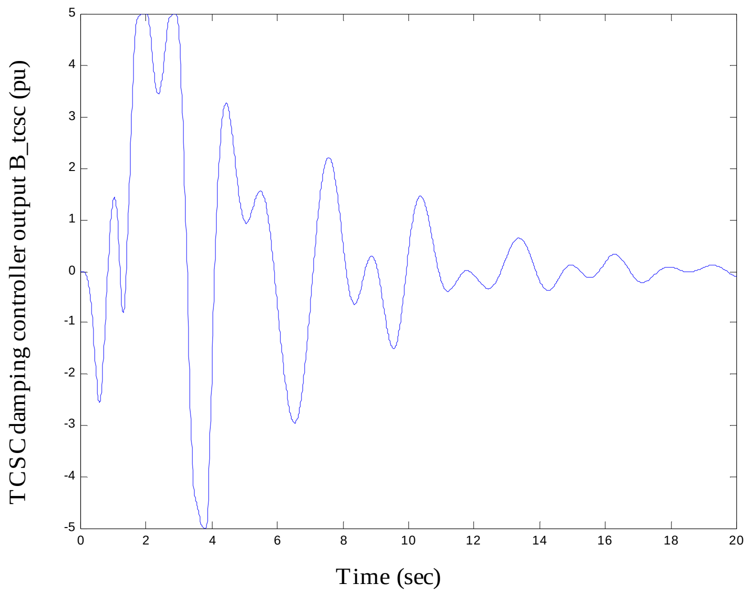

Figure 4.30: TCSC damping controller output

Chapter 5

Interaction between excitation and TCSC damping controllers

Two types of controller have been addressed and tested. They were not installed in power systems simultaneously. Theoretically, the nonlinear excitation control itself is already sufficient for transient stability control. Yet in reality, the nonlinear excitation control has to make compromise with decentralization and feasibility. For example, in this dissertation, the unmeasurable components in feedback linearization compensation law are treated as noise or disturbance. Hence, the nonlinear excitation control is not strict and itself may not be sufficient in some situation. It is worthwhile to see their combined function in power system. The two-area four-machine power system model is used here with subtransient generator model. First, nonlinear feedback linearization controller and TCSC damping controller are designed separately. Then the two types of controllers are installed in the power system simultaneously and their interactions are investigated.

The two-area four-machine power system has the same parameters as the one used in case studies in Chapter 3 except the exciters are different. Generator 1 and Generator 4 have DC type exciters, while Generator 3 has a simplified excitation system, and Generator 2 has a IEEE type ST3 compound source rectifier exciter. The open-loop system will be unstable when subject to a three-phase ground fault at bus 15. Nonlinear excitation control output will be added to the excitation system output to provide both rotor angle stability control and generator terminal voltage control. The nonlinear control is the combination of feedback linearization and linear robust control by feedback back the rotor angle offset.

Three tests are performed to show the interaction between the two types of controllers.

Table 5.1: Test descriptions

Test number	Description
1	open-loop system
2	power system with nonlinear excitation control solely
3	power system with both excitation and TCSC damping control

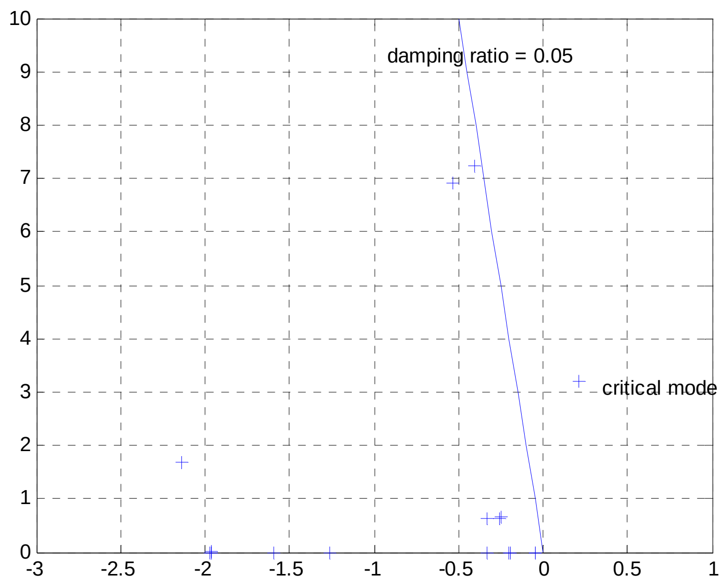

Figure 5.1: Open-loop system poles.

Fig. 5.1 gives the poles of the open-loop system. There is a pole located in the right half plane. The oscillation mode corresponding to this pole is the critical mode.

Fig. 5.2 gives the open-loop system performance. The system is unstable.

Fig. 5.3 and Fig. gives 5.4 the closed-loop system performance with nonlinear excitation controllers installed. The simulation results show that with nonlinear excitation controllers, the dynamic performance of the power system has been improved. However, the oscillation modes need to be dampened faster. Therefore, TCSC damping controller is designed.

Fig. 5.5 gives the root locus diagram with TCSC damping controller installed while the gain of the controller varies. Fig. 5.6 and Fig. gives 5.7 the closed-loop system performance with TCSC damping controller installed. TCSC damping controller is designed based on the residue of the critical mode while its control input is active power flow of the tie-line. The damping of the

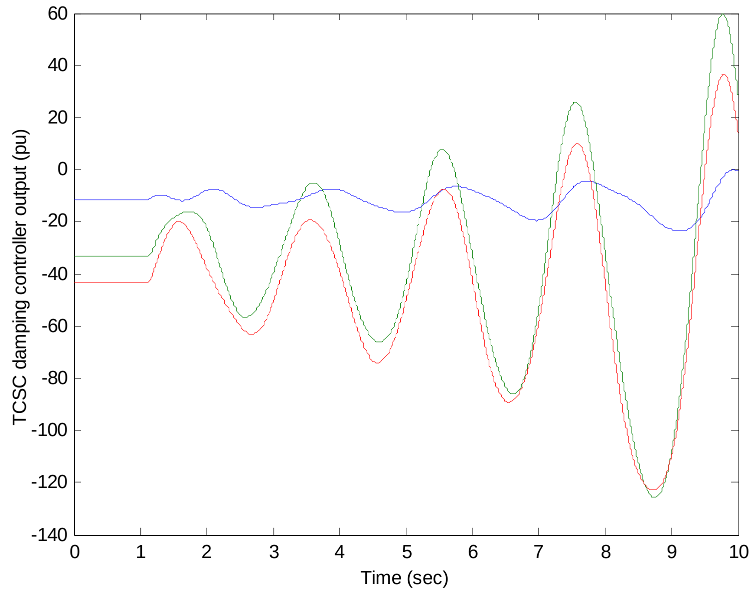

Figure 5.2: Open-loop power system dynamic performance.

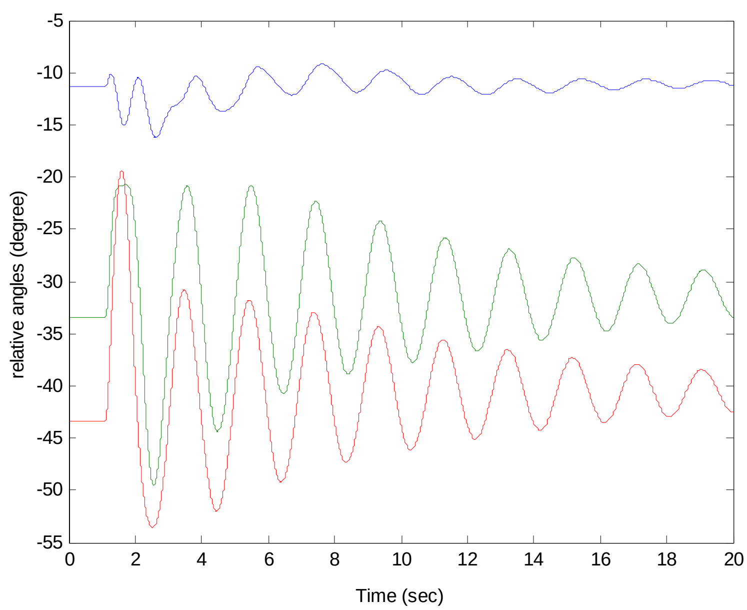

Figure 5.3: Dynamic performance of relative rotor angles.

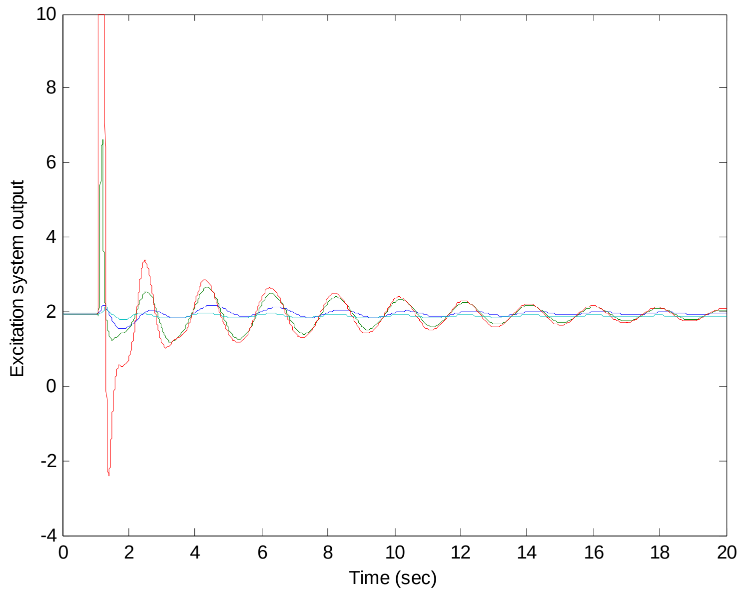

Figure 5.4: Dynamic response of excitation controller system output.

oscillations are greater than the damping of the oscillations in the system with excitation control only.

The conclusion drawn from the above tests is as follows:

The two types of controllers can work well with each other. If TCSC damping controller is needed, it should be designed based on the power system linearized model including the nonlinear excitation control.

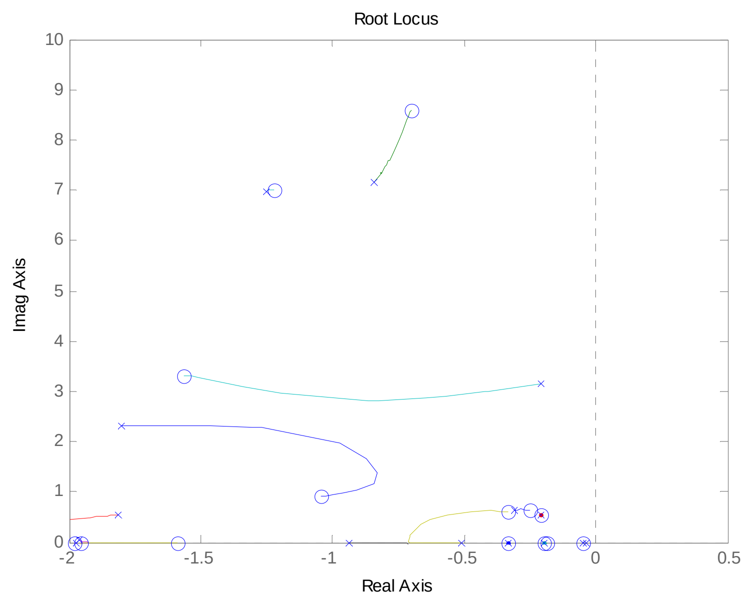

Figure 5.5: Root locus of the system with TCSC controller

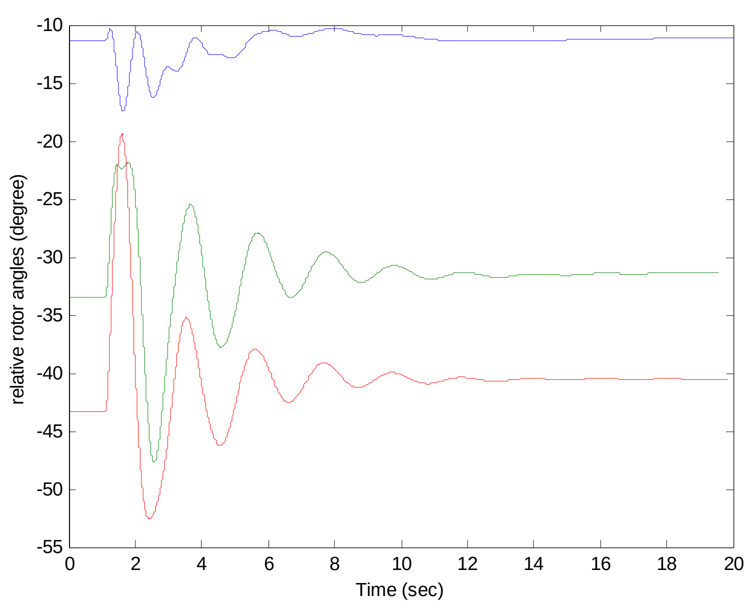

Figure 5.6: Dynamic performance of relative rotor angles.

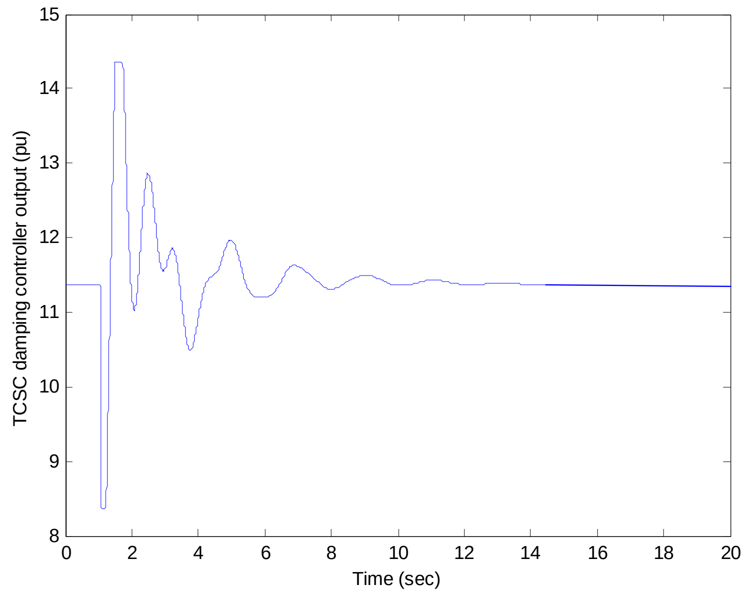

Figure 5.7: Dynamic response of TCSC damping controller output

Chapter 6

Conclusions

This dissertation addresses two categories of decentralized control design for power systems. One is excitation control to improve power system stability and the other is TCSC damping control to improve inter-area oscillation damping.

In the first part of the dissertation, an algorithm to design decentralized nonlinear controllers based on feedback linearization is developed. First, feedback linearization technique is applied in excitation control for each generator to obtain an interconnected system where subsystems have linear system matrices and interconnections are represented by nonlinear terms. Second, different ways of achieving decentralization are developed:

(1) linear robust control combined with observer decoupled state space

(2) disturbance accommodation control

While linear robust control guarantees the subsystem's stability when the interconnection terms are bounded within certain values, disturbance accommodation control is based on linear models of the interconnection terms. The offset of rotor angles from equilibrium point is an important variable to feed back into the controllers. However, since the post equilibrium point is usually unknown, observer decoupled state space concept is utilized to obtain a variable which can be calculated through local measurements to replace the offset of rotor angles. Thus the resulting controllers have decentralized structure.

Nonlinear simulations are performed on a three-machine nine-bus power system. The simulation results demonstrate the effectiveness of the proposed methodologies.

In the second part of the dissertation, indices for control signal selection and mode effectiveness and interaction are developed. A TCSC damping controller using a local signal is designed to dampen inter-area oscillations over a range of operating conditions. Residues not only represent the combination of state controllability and observability but also represent the eigenvalue sensitivity with respect to controller parameters. Therefore residues are utilized to develop criteria for control signal selection and controller siting. Conditions and indices for TCSC damping controller siting and signal selection are proposed. The indices are the effectiveness of the controller over a wide range of operating conditions and the interaction of the controller with other oscillation modes than critical modes. Controller configuration design is also investigated: one is lead-lag structure design and the other is multi-step design.

Two case studies are performed to explain and demonstrate the effectiveness of the proposed methodologies. The first power system is the two-area four-machine inter-area oscillation benchmark system. A poor damping oscillation can be observed in the tie-line. Three typical operating conditions are chosen to testify the robustness and effectiveness of the controller. The results show that for a TCSC installed on the tie-line, the better signal is the absolute value of active power which not only is robust but has less interaction with the other oscillation modes.

Besides this small system, a larger power system – a model of the WSCC system is used. The system has three inter-area oscillation modes near 0.7 Hz. The proposed conditions and indices are utilized to find the optimal placement, signal for a TCSC damping controller. Both root locus analysis and nonlinear simulation results show that TCSC damping controller is effective in stabilizing the most critical inter-area modes.

The indices proposed in this dissertation are general and can be used for signal selection and siting of other FACTS devices, such as Static Var Compensator, Unified Power Flow Controller and etc. The uncertainty shown in the case studies in this dissertation are variations of load conditions. It can also be variations of topologies. While the variation of load conditions can be considered as unstructured uncertainty the variations of the topologies can be considered as structured uncertainty. With variation of topologies included in case studies, the proposed indices are shown to be applicable to both structured and unstructured uncertainty. The damping controller proposed in this dissertation is to use local measurement as input signals. Local measurements can be obtained by phasor measurement units (PMU). The feasibility of these control schemes using PMU should be investigated using discrete control techniques. Meanwhile, the measurement errors, control signal delays are not considered in this dissertation. Further work can take above factors into consideration.

Further works can also include the implementation of the nonlinear excitation control schemes of this dissertation. The mapping process of Feedback Linearization is not detailed in this dissertation and the measurements used are assumed to be available and accurate. They may not however not be accurate and measurement errors should be taken into consideration. Hence the mapped linear subsystem will have multiple sources of uncertainties. This could be formulized as a robust control problem.

References

[1] M. E. Aboul-Ela, A. A. Sallam, J. D. McCalley, and A. A. Fouad, "Damping Controller Design for Power System Oscillations." IEEE Trans. Power Systems, Vol. 11, No. 2, pp. 767-773, May 1996

[2] O. Akhirif, F.A. Okou, L.A. Dessaint, and R. Champagne, "Application of Multivariable Feedback Linearization Scheme for Rotor Angle Stability and Voltage Regulation of Power Systems, " IEEE Trans. Power Systems, Vol. 14, No. 2, pp. 620-628, May 1999.

[3] C. Alsberg, "WSCC Unfolds Causes of the July 2 Disturbance." IEEE Power Engineering Review, pp.5-6, Sep. 1996.

[4] P. M. Anderson and A. A. Fouad, Power System Control and Stability, the Iowa State University Press, Ames, Iowa, 1977.

[5] S. Arabi, P. Kundur, and R. Adapa, "Innovative Techniques in Modeling UPFC for Power System Analysis", IEEE Trans. Power Systems, Vol.15, No. 1, pp. 336-341, Feb. 2000.

[6] J. Arrillaga, High Voltage Direct Current Transmission, 2nd edition, IEE Power Engineering Series 29, 1998.

[7] J. A. Bernard, "Use of a Rule-based System for Process Control", IEEE Control Systems Magazine, Vol. 8, No. 5, pp. 3-13, Oct. 1988.

[8] G. E. Boukarim, S. Wang, J. H. Chow, G. N. Taranto, and N. Martins, "A Comparison of Classical, Robust, and Decentralized Control Designs for Multiple Power System Stabilizers", IEEE Trans. Power Systems, Vol. 15, No. 4, pp. 1287-1292, Nov. 2000.

[9] H. Bourles, S. Peres, T. Margotin, and M. P. Houry, "Analysis and Design of a Robust Coordinated AVR/PSS." IEEE Trans. Power Systems, Vol. 13, No. 2, pp. 568-575, May 1998.

[10] W. L. Brogan, Modern Control Theory, Prentice Hall, 1974.

[11] C. A. Canizares, "Power Flow and Transient Stability Models of FACTS Controllers for Voltage and Angle Stability Studies", IEEE Power Engineering Winter Meeting, Vol. 2, pp. 1447 - 1454, 2000.

[12] Y. Cao, L. Jiang, S. Cheng, D. Chen, O. P. Malik, and G. S. Hope, "A Nonlinear Variable Structure Stabilizer for Power System Stability," IEEE Trans. Energy Conversion, Vol. 9, No. 3, pp. 489-495, Sep. 1994.

[13] J. W. Chapman, M. D. Ilic, and C. A. King, "Stabilizing a Multimachine Power System via Decentralized Feedback Linearizing Excitation Control." IEEE Trans. Power Systems, Vol. 8, No. 3, pp.830-839, Aug. 1993.

[14] J. H. Chow, J. J. Sanchez-Gasca, H. Ren, and S. Wang, "Power System Damping Controller Design Using Multiple Input Signals." IEEE Control Systems Magazine, pp.82-90, Aug. 2000.

[15] X. Z. Dai, D. He, L. L. Fan, N. H. Li, and H. Chen, "Improved ANN αth-order Inverse TCSC Controller for Enhancing Power System Transient Stability." IEE Proc. - Gener. Transm. Distrib., Vol. 46, No. 6, Nov. 1999.

[16] F. P. de Mello, "Measurement of Synchronous Machine Rotor Angle from Analysis of Zero Sequence Harmonic Components of Machine Terminal Voltage", IEEE Trans. Power Delivery, Vol. 9, No.4 , pp.1770 -1777, Oct. 1994.

[17] F. P. de Mello, C. Concordia, "Concepts of Synchronous Machine Stability as Affected by Excitation Control", IEEE Trans. PAS-87, pp. 190-201, 1968.

[18] L. Fan and A. Feliachi, "Decentralized Stabilization of Nonlinear Electric Power Systems Using Local Measurements and Feedback Linearization." The 40th Midwest Symposium on Circuit and System Theory, Aug. 2000.

[19] L. Fan and A. Feliachi, and A. Davari, "Decentralized Control of Power Systems Using Disturbance Accommodation Techniques " American Conference on Control, June 2001

[20] L. Fan, A. Feliachi, and H. Chen, "Improving Power System Damping Characteristics by Thyristor Controlled Series Compensation," Proceedings on North American Power Symposium, Oct. 2000.

[21] D. Q. Gan, Z. Qu, and H. Cai, "Multi Machine Power System Excitation Control Design via Theories of Feedback Linearization Control and Nonlinear Robust Control." International Journal of Systems Science, Vol 31, No. 4, pp.519-527, 2000.

[22] G. Guo, Y. Wang, and D. J. Hill, "Nonlinear Output Stabilization Control for Multimachine Power Systems." IEEE Trans. Circuit and Systems, Part 1, Vol. 47, No. 1, pp. 46-53, Jan. 2000.

[23] A. Heniche, H. Bourles, and M. P. Houry, "A Decentralized Controller for Voltage Regulation of Power Systems." IEEE Trans. Power Systems, Vol. 10, No. 3, pp 1461-1466, Aug. 1995.

[24] N. G. Hingorani and L. Gyugui, Understanding FACTS Concepts and Technology of Flexible AC Transmission Systems, IEEE Press, 2000.

[25] T. Hiyama, W. Hubbi, and T. Ortmeyer, "Fuzzy Logic Control Scheme with Variable Gain for Static Var Compensator to Enhance Power System Stability", IEEE Trans. Power Systems, Vol. 14, No. 1, pp.186-191, Feb. 1999.

[26] T. Hiyama, "Real Time Control of Micro-machine System using Micro-Computer based Fuzzy Logic Power System Stabilizer", IEEE Trans. Energy Conversion, Vol. 9, No. 4, pp. 724-730, Dec. 1994.

[27] M. Ilic and J. Zaborszky, Dynamics and Control of Large Electric Power Systems. John Wiley & Sons, Inc. 2000.

[28] S. G. Jalali, R. A. Hedin, M. Pereira, and K. Dadek, "A Stability Model for the Advanced Series Compensator (ASC)." IEEE Trans. Power Delivery, Vol. 11, No. 2, pp. 1128-1137, Apr. 1999.

[29] C. Jing, J. D. McCalley, and M. Kommareddy, "An Energy Approach to Analysis of Interarea Oscillations in Power Systems." IEEE Trans. Power Systems, Vol. 11, No. 2, pp. 734-740, May 1996.

[30] C. D. Johnson, "Theory of Disturbance Accommodation Controllers", Control and Dynamic Systems; Advances in Theory & Applications, Vol. 12, Academic Press, USA (1976).

[31] D. Kennedy, D. Miller, and V. Quintana, "A nonlinear geometric approach to power system excitation control and stabilization." Electrical Power & Energy Systems, Vol. 20, No. 8, pp. 501-514, 1998.

[32] H. K. Khall, Nonlinear Systems, Macmillan Publishing Company, New York, 1992.

[33] M. Klein, G. J. Rogers, and P. Kundur, "A Fundamental Study of Inter-Area Oscillations in Power Systems.", IEEE Trans. Power Systems, Vol. 6, No. 3, pp.914-921, Aug. 1991.

[34] P. V. Kokotovic and R. Marino, "On vanishing stability region in nonlinear systems with high-gain feedback," IEEE Trans. Automatic Control, Vol. 31, No. 10, pp. 967-970, Oct. 1986.

[35] E. V. Larsen, C. E. J. Bowler, B. L. Damsk, and S. L. Nilsson, "Benefits of Thyristor Controlled Series Compensation". CIGRE Paper 14/37/38-04, Paris, 1992

[36] E. V. Larsen, J. J. Sanchez-Gasca, and J. H. Chow, "Concepts of Design FACTS Controller to Damp Power Swing". IEEE Trans. Power Systems, Vol. 10, No. 2, pp. 948-955, May 1995.

[37] E. V. Larsen and D. A. Swann, "Applying power system stabilizers, Part I; General Concepts, Part II; Performance objectives and tuning concepts, Part III; Practical considerations," IEEE Trans. on Power Apparatus and Systems, Vol PAS-100, pp 3017-3046, 1981.

[38] B. Leirbukt, J. H. Chow, J. J. Sanchez-Gasca, and E. V. Larsen, "Damping Control Design Based on Time-Domain Identified Models." IEEE Trans. Power Systems, Vol. 14, No.1, pp. 172-178, Feb. 1999.

[39] Frank L. Lewis and Vassilis L. Syrmos, Optimal Control, Second Edition, John Wiley & Sons, Inc, 1995.

[40] J. Machowski, S. Robak, J. W. Bialek, J. R. Bumby, and N. Abi-Samra, "Decentralized Stability-Enhancing Control of Synchronous Generator." IEEE Trans. Power Systems, Vol. 15, No. 4, pp. 1336-1344, Nov. 2000,.

[41] R. Marino,"An example of a nonlinear regulator," IEEE Trans. Automatic Control, Vol. 29, No.3, pp.276-279, Mar. 1984.

[42] D. E. Martin, W. K. Wong, D. L. Dickmander, R. L. Lee, and D. J. Melvold, "Increasing WSCC Power System Performance with Modulation Controls on the Intermountain Power Project HVDC System", *IEEE Trans. Power Delivery*, Vol. 7, No. 3, pp. 1634-1642, 1992.

[43] M. Mohadjer and C.D.Johnson, "Load-frequency control with disturbance accommodation", *International Journal of Electrical Power & Energy System*, Vol. 6, No. 3, 1984.

[44] F. L. Pagola, L. Rouco, and I. J. Perez-Arriaga, "Analysis and Control of Small-Signal Stability in Electric Power System by Selective Modal Analysis", *Eigenvalue and Frequency Domain Methods for System Dynamic Performance*, IEEE Publication No. 90TH0292-3-PWR, New York, pp. 77-96, 1990.

[45] M. Parniani and M. R. Iravani, "Optimal Robust Control Design of Static VAR Compensator." *IEE Proc. -Gener. Transm. Distrib.*, Vol. 145, No. 3, pp.301-307, May 1998.

[46] H. Quinot and H. Bourles, "Robust Coordinated AVR+PSS for Damping Large Scale Power Systems." *IEEE Trans. on Power Systems*, Vol. 14, No. 4, pp 1446-1451, Nov. 1999.

[47] G. Rogers, *Power System Oscillations*, Kluwer Academic Publishers, Boston/ London/ Dordrecht, 2000.

[48] V. G. D. C. Samarasinghe and N. C. Pahalawaththa, "Stabilization of a Multi-Machine Power System using Nonlinear Robust Variable Structure Control." *Electric Power Systems Research* 43, pp. 11-17, 1997.

[49] J. E. Slotine and W. Li, *Applied Nonlinear Systems*, Prentice Hall, 1991.

[50] J. R. Smith, G. S. Woods, F. Fatechi, G. L. Keenan, and J. F. Hauer, "A Low Order Power System Model with Dynamic Characteristics of a High Order System," presented at WG on Oscillations, *IEEE PES Winter Meeting*, Columbus, OH, Feb. 1993.

[51] K. M. Son and J. K. Park, "On the Robust Control of TCSC for Damping Power System Oscillations." *IEEE Trans. Power Systems*, Vol. 15, No. 4, pp. 1306-1312, Nov. 2000.

[52] P. Shamsollahi and O. P. Malik,."Direct Neural Adaptive Control Applied to Synchronous Generator". *IEEE Trans. Energy Conversion*, Vol. 14, No. 4, pp. 1341 -1346, Dec. 1999.

[53] S. M. Shinners, *Modern Control System Theory and Application*, Addison-Wesley Publishing Company, 1978.

[54] Stoorvogel, *The H_∞ Control Problem - A State Space Approach*, Prentice Hall, 1992

[55] G. N. Taranto, *Robust Control Design for Power System Damping Controllers with Application to FACTS Devices*. Dissertation of Rensselarer Polytechnic Institute, Nov. 1994.

[56] G. N. Taranto, J.-K. Shiau, J. H. Chow, and H. A. Othman, "Robust Decentralized Design for Multiple FACTS Damping Controllers." *IEE Proc. -Gener. Transm. Distrib.*, Vol. 144, No. 1, pp. 61-67, Jan. 1997.

[57] Y. Wang, G. Guo, and D. J. Hill, "Robust Decentralized Nonlinear Controller Design for Multimachine Power Systems. " Automatica, Vol. 33, No. 9, pp 1725-1733, 1997.

[58] Y. Guo, D. J. Hill, and Y. Wang, "Nonlinear Decentralized Control of Large-Scale Power Systems", Automatica, Vol. 36, No. 9, pp. 1275-1289, 2000.

[59] C. Zhu, R. Zhou, and Y. Wang, "A New Decentralized Nonlinear Voltage Controller for Multimachine Power Systems," IEEE Trans. Power Systems, Vol. 13, No.1, pp. 211-216, Feb. 1998.

[60] G. Guo, Y. Wang, K. Y. Lim, and L. Gao, "Robust Nonlinear Controller for Power System Transient Stability Enhancement with Voltage Regulation," IEE Proc. -Gener. Transm. Distrib., Vol. 143, No. 5, pp. 407-412, Sep. 1996.

[61] H. F. Wang, "Selection of Robust Installing Locations and Feedback Signals of FACTS-based Stabilizers in Multi-machine Power Systems." IEEE Trans. Power Systems, Vol. 14, No. 2, pp. 569-574, May 1999.

[62] H. F. Wang, F. J. Swift, and M. Li, "Indices for Selecting the Best Location of PSSs or FACTS-based Stabilizers in Multimachine Power Systems: A Comparative Study," IEE Proc.- Gener. Transm. Distrib., Vol. 144, No. 2, pp.155-159, Mar. 1997.

[63] X. Yang and A. Feliachi, "Stabilization of Inter-area Oscillation Modes through Excitation Systems," IEEE Trans. Power Systems, Vol. 9, No. 1, pp. 494-502, Feb. 1994.

[64] N. Yang, Q. Liu, and J. D. McCalley, " TCSC Controller Design for Damping Interarea Oscillations." IEEE Trans. Power Systems. Vol. 13, No. 4, pp.1304 -1310, Nov. 1998.

[65] M. van de Wal and B. de Jager, "A Review of Methods for Input/Output Selection", Automatica, Vol 37, pp. 487-510, 2001.

[66] J. Zaborszky, K.W. Whang, K.V. Prasad, and I.N. Katz, "Local Feedback Stabilization of Large Interconnected Power Systems in Emergencies," Automatica, Vol. 17, No. 5, pp. 673-686, 1981.

[67] K. Zhou and J. C. Doyle, Essentials of Robust Control, Prentice Hall, 1998

Appendix A

Synchronous generator models

The swing equation is the most important part of a synchronous generator model. It describes the rotor motion in accordance with Newton's No.2 law, i.e., the acceleration of an object equals the force over the inertia. The swing equation is expressed in the following equations.

$$\begin{aligned} \frac{d\delta}{dt} &= \omega_0 (\omega - 1) \\ \frac{d\omega}{dt} &= \frac{1}{2H} (P_m - P_e) \end{aligned} \tag{A.1}$$

where ω_0 is the rated rotor angular speed $2\pi \cdot 60$ rad/s, δ is in rad, ω is in pu. P_m is the input mechanical power from the turbine to the generator in pu, P_e is the output electrical power of the generator in pu, and H is the constant angular moment of inertia in second.

Besides the swing equation, synchronous generator models include electrical equations which can be described in different ways from the simplified classical model to the most detailed 7th order model. By use of Park's transformation, the variables such as voltage and current are expressed in the d and q axis components as shown in Fig. A.1

In stability study, generator model can be classical model, transient models such as two-axis model or one-axis model.

A.1 Classical generator model

In classical representation, a synchronous generator is modeled as a constant voltage source behind transient reactance as shown in Fig. A.2, where x'_d is the direct axis transient reactance and δ is considered the angle between the rotor position and the terminal voltage $V_t\angle\alpha$. The magnitude of the voltage source E is kept constant during the transient.

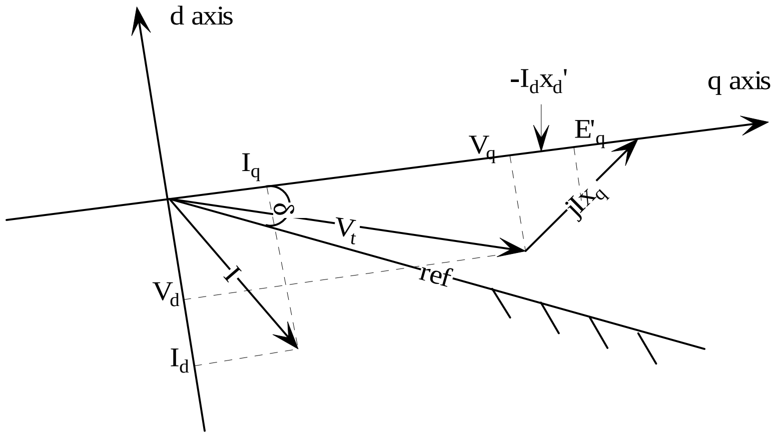

Figure A.1: Phasor diagram

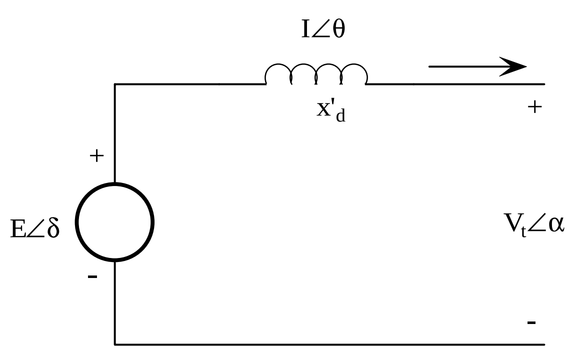

Figure A.2: Classical equivalent circuit of a generator

A.2 Two-axis generator model

In two-axis generator model, a synchronous generator is represented as voltage source behind transient reactance by assuming $x'_d \approx x'_q$. E'_q, E'_d are q and d axis stator voltage respectively. Besides swing equation, there are two differential equations that describe the field voltage and Q circuit as shown in Eq. A.2.

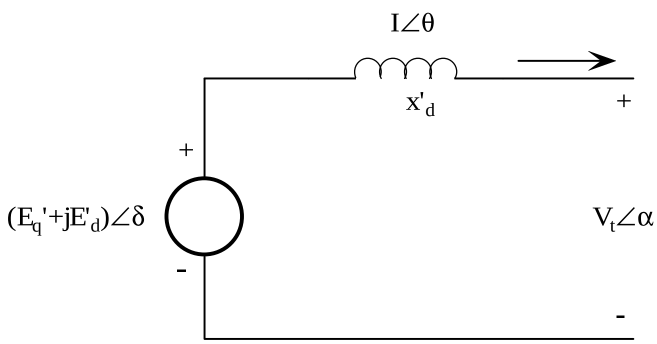

Figure A.3: Transient equivalent circuit of a generator

$$\begin{aligned} \frac{dE'_q}{dt} &= \frac{1}{T'_{d0}}\left(E_{fd} - E\right) \\ \frac{dE'_d}{dt} &= \frac{1}{T'_{q0}}(-E'_d - (x_q - x'_q)I_q) \end{aligned} \tag{A.2}$$

where E_{fd} is the excitation voltage, $E = E'_d + (x'_d - x_d)I_d$, $P_e = E'_d I_d + E'_q I_q - (x'_q - x'_d)I_d I_q$.

A.3 One-axis generator model

The one-axis generator model is similar to the two-axis generator model except the dynamics of E'_d are ignored. Without the assumption $x'_d \approx x'_q$, the generator and the network interface equations are:

$$\begin{aligned} E'_q &= V_q - x'_d I_d \\ 0 &= V_d + x_q I_q \end{aligned}$$

The electrical power equation can be expressed as $P_e = E'_q I_q - (x_q - x'_d)I_d I_q$.

Appendix B

Proof of Theorem 3.2

The proof of Theorem 3.2 are given detailly in Chapter 3 of [54]. Here the brief proof is given.

B.1 Intuitive proof of necessity part

The control objective is clearly to make the H_∞ norm as small as possible, which can be expressed in mathematical form as

$$\inf_f \sup_{w\neq 0} \left\{ \frac{\|z_{u,w}\|_2}{\|w\|_2} | w \in L_2^l, f : L_2^m \to L_2^n \text{ causal and } u = f(w) \right\}$$

for the initial condition x(0) $= 0$

If the norm is smaller than some bound $\gamma > 0$ then

$$\inf_f \sup_{w\neq 0} \left\{ \|z_{u,w}\|_2^2 - \gamma^2 \|w\|_2 \, | w \in L_2^l, f \text{ causal and } u = f(w) \right\} \leq 0$$

for the initial condition x(0) $= 0$. The internal stability of H_∞ control requires the control be stable for all initial conditions. Thus for an arbitrary initial condition x(0)=ξ, define

$$C(u,w,\xi) = \|z_{u,w}\|_2^2 - \gamma^2 \|w\|_2$$

$$C^*(\xi) = \sup_w \inf_u \left\{ C(u,w,\xi) | u \in L_2^m, w \in L_2^l \text{ such that } x_{u,w,\xi} \in L_2^n \right\}$$

for arbitrary initial state x(0)=ξ

It has been proved that $C^*(\xi) = \xi^T P \xi$ for all $\xi \in \Re^n$.

Define $C(u,w,\xi,t) = \int_t^{\infty} \|z_{u,w,\xi,t}(\tau)\|^2 - \gamma^2 \|w(\tau)\|^2 d\tau$, the system is time-invariant and therefore

$$\begin{aligned} C^*(\xi,t) &= \sup_w \inf_u \left\{ C(u,w,\xi,t) | u \in L_2^m, w \in L_2^l \text{ such that } x_{u,w,\xi,t} \in L_2^n \right\} \\ &= \xi^T P \xi \end{aligned}$$

u is indeed a casual function of w. Then the last "sup-inf" problem can be rewritten

$$\begin{aligned} 0 &= \sup_{w|_{[0,t]}} \inf_{u|_{[0,t]}} \sup_{w|_{(t,\infty)}} \inf_{u|_{(t,\infty)]}} \int_0^{\infty} \|z_{u,w,\xi,t}(\tau)\|^2 - \gamma^2 \|w(\tau)\|^2 d\tau - \xi^T P \xi \\ &= \sup_{w|_{[0,t]}} \inf_{u|_{[0,t]}} \int_0^{\infty} \|z_{u,w,\xi,t}(\tau)\|^2 - \gamma^2 \|w(\tau)\|^2 d\tau + x^T(t) P x(t) - \xi^T P \xi \end{aligned}$$

where $u \in L_2^n, w \in L_2^l$ should be such that $x_{u,w,\xi} \in L_2^n$. Differentiate this expression with respect to t and take the derivative at t=0, we then obtain

$$0 = \sup_{w(0)} \inf_{u(0)} \|z(0)\|^2 - \gamma^2 \|w(0)\|^2 + \frac{d}{dt} x^T(t) P x(t) \mid_{t=0}$$

Now we can obtain a static "sup-inf" problem which can be solved explicitly.

$$0 = \sup_{w(0)} \inf_{u(0)} \begin{pmatrix} \xi \\ u(0) \\ w(0) \end{pmatrix}^T \begin{pmatrix} A^T P + PA + C^T C & B^T P + C^T D & E^T P \\ PB + D^T C & D^T D & 0 \\ PE & 0 & -\gamma^2 I \end{pmatrix} \begin{pmatrix} \xi \\ u(0) \\ w(0) \end{pmatrix}$$

Next define $q = u + (D^T D)^{-1}(B^T P + D^T C)\xi$

$p = w - \gamma^{-2} E^T P \xi$

Denote the right hand side of the algebraic Riccati equation Eq. 3.19 by $R(P)$. By using Schur complements we can then rephrase the "sup-inf" problem in the form

$$0 = \sup_p \inf_q \begin{pmatrix} \xi \\ q \\ p \end{pmatrix}^T \begin{pmatrix} R(P) & 0 & 0 \\ 0 & D^T D & 0 \\ 0 & 0 & -\gamma^2 I \end{pmatrix} \begin{pmatrix} \xi \\ q \\ p \end{pmatrix}$$

The above equality should be true for all initial conditions $\xi \in \Re^n$. This implies $R(P) = 0$.

The optimal p and q are zero, i.e.

$w^*(t) = \gamma^{-2} E^T P x^*(t)$,

$u^*(t) = -(D^T D)^{-1}(B^T P + D^T C)x^*(t)$.

B.2 Proof of sufficiency part

This part will show if there exists a matrix P satisfying the condition in part (2) of Theorem 3.2, then the feedback suggested as the theorem satisfies condition (1). Assume that P satisfies the conditions in part (2) of Theorem 3.2. Moreover, set $\gamma = 1$. The implications will only be proven under this assumption.

Define the following system:

$$\Sigma_U : \begin{cases} \dot{x}_U = A_U x_U + B_U u_U + Ew, \\ y_U = C_{1,U} x_U + \qquad w, \\ z_U = C_{2,U} x_U + D_{21,U} u_U, \end{cases}$$

where

$$\begin{aligned} &A_U = A - B(D_1^T D_1)^{-1}(D_1^T C + B^T P), \\ &B_U = B(D_1^T D_1)^{-1/2}, \\ &C_{1,U} = -E^T P, \\ &C_{2,U} = C - D_1(D_1^T D_1)^{-1}(D_1^T C + B^T P), \\ &D_{21,U} = D_1(D_1^T D_1)^{-1/2} \end{aligned}$$

Lemma B.1 The system Σ_U is inner. Denote the transfer matrix of Σ_U by . We decompose GU:

$$G_U \begin{pmatrix} w \\ u_U \end{pmatrix} = \begin{pmatrix} G_{11,U} & G_{12,U} \\ G_{21,U} & G_{22,U} \end{pmatrix} \begin{pmatrix} w \\ u_U \end{pmatrix} = \begin{pmatrix} z_U \\ y_U \end{pmatrix}$$

compatible with the size of w, u_U, z_U, y_U. Then $G_{21,U}$ is invertible as a rational matrix and its inverse is in H_∞. Moreover $G_{22,U}$ is strictly proper.

The proof of the lemma will not be shown here.

Lemma B.2 Assume that the conditions in part (2) of theorem 3.2 are satisfied. In that case the compensator $\sum_F$ described by the feedback law $u = Fx$, where F is given by Eq. 3.20 satisfies condition (1) of theorem 3.2.

Proof: The transfer matrix G_F is equal to $G_{11,U}$ and moreover, $A + BF$ is equal to A_U. This implies that the compensator $\sum_F$ is internally stabilizing. Because $G_{21,U}$ is invertible over H∞ the following inequalities can be derived:

$$\|G_{11,U}\|_\infty^2 + \left\|G_{21,U}^{-1}\right\|_\infty^{-2} \leq \left\| \begin{pmatrix} G_{11,U} \\ G_{21,U} \end{pmatrix} \right\|_\infty^2 \leq 1$$

From the above inequalities, we have $\|G_F\|_\infty < 1$.

Appendix C

Solution of Riccati equation 3.19

The following procedure shows how to obtain the solution of Riccati equation 3.19 by use of Matlab Symbolic Toolbox.

First of all, the elements of matrix P and γ are defined as symbols. And the other matrices known are initialized.

```
syms P11 P12 P13 P21 P22 P23 P31 P32 P33 gama
P=[P11 P12 P13; P21 P22 P23; P31 P32 P33];
A = [0 1 0; 0 0 1; 0 0 0];
B = [0;0;1]; E = [0;0;1];
C = eye(3) ; D =[0;0;1];
```

Secondly, the right part of the Riccati equation are calculated.

```
x = A.'*P+P*A+C.'*C- [ B'*P + D'*C; E'*P].'*inv([D'*D, 0; 0,-gama^2])
*[ B'*P + D'*C; E'*P]
```

The result is shown as

```
x=[...
1-P31^2+P31^2/gama^2,                P11-P31*P32+P31/gama^2*P32,...
P12-P31*(P33+1)+P31/gama^2*P33;
P11-P31*P32+P31/gama^2*P32,          P12+P21+1-P32^2+P32^2/gama^2,...
P13+P22-P32*(P33+1)+P32/gama^2*P33;
P21-P31*(P33+1)+P31/gama^2*P33,      P22+P31-P32*(P33+1)+P32/gama^2*P33,...
P23+P32+1-(P33+1)^2+P33^2/gama^2];
```

Let $\gamma = 2$, and the right part of the Riccati equation are calculated again.

```
gama = 2;
```

```
x =[...
1-3/4*P31^2,      P11-3/4*P31*P32,      P12-P31*(P33+1)+1/4*P31*P33;
P11-3/4*P31*P32, P12+P21+1-3/4*P32^2,  P13+P22-P32*(P33+1)+1/4*P32*P33;
P21-P31*(P33+1)+1/4*P31*P33, P22+P31-P32*(P33+1)+1/4*P32*P33,...
P23+P32+1-(P33+1)^2+1/4*P33^2];
```

Now the results of the elements of matrix P are solved by function **solve.**

```
S = solve(...
'1-3/4*P31^2=0',...
'P11-3/4*P31*P32=0',...
'P12-P31*(P33+1)+1/4*P31*P33=0',...
'P11-3/4*P31*P32 =0',...
'P12+P21+1-3/4*P32^2 = 0', ...
'P13+P22-P32*(P33+1)+1/4*P32*P33=0',...
'P21-P31*(P33+1)+1/4*P31*P33=0',...
'P22+P31-P32*(P33+1)+1/4*P32*P33=0',...
'P23+P32+1-(P33+1)^2+1/4*P33^2=0');

P = [S.P11(1), S.P12(1), S.P13(1);
  S.P21(1), S.P22(1), S.P23(1);
  S.P31(1), S.P32(1), S.P33(1)];
P32= 3;
P =[ 1/2*P32*3^(1/2), -1/2+3/8*P32^2, 2/3*3^(1/2)
 -1/2+3/8*P32^2, 1/48*3^(1/2)*(-32-12*P32+9*P32^3),...
 -P32-13/12-3/8*P32^2+9/64*P32^4
 2/3*3^(1/2), P32, -1/3*3^(1/2)+1/4*3^(1/2)*P32^2-4/3];

P =[2.5981 2.8750 1.1547
  2.8750 6.3148 3.9323
 1.1547 3.0000 1.9864];
F=-inv(D.'*D)*(D.'*C+B.'*P)
```

And finnally the feedback gain matrix F is

```
F=[ -1.1547 -3.0000 -2.9864];
```

Appendix D

Solving Kx, Ky, Kz

Eq. 3.44 is a set of differential equations. To obtain K_x, K_y, and K_z, the differential equations will be integrated with respect of time. Matlab source codes are shown in this appendix.

```
a1=0.3312; w1=7;
a2=1.3669; w2=13;
A=[0 1 0;0 0 1; 0 0 0];
B=[0;0; 1];
H1=[0 0 0 0; 0 0 0 0; 1 0 0 0];
D=[0 1 0 0 ; 0 0 1 0; 0 0 0 1; -(w1*w2)^2 0 -(w1^2+w2^2) 0];
E=[1; 1 ; 1 ;1];
% S, Q, R, T are given
% Design a Disturbance-Utilization Controller for the Output Regulator Problem
C = [0,1,0];
S = 10;
Q=diag([100,100,10]);R=1;T=10;t=0;
Q= 100;
ysp=zeros(3,1);
dt=0.002; T=20;
% Initialization
Mx(:,:,1)=C.'*S*C;
My(:,:,1)=-C.'*S;
Mz(:,:,1)=zeros(3,4);
u(1)=0;
```

```
t=0;
for i=1:floor(T/dt)
 temp1= (-A+B*inv(R)*B.'*Mx(:,:,i)).'*Mx(:,:,i)-Mx(:,:,i)*A-C.'*Q*C;
 temp2= (-A+B*inv(R)*B.'*Mx(:,:,i)).'*My(:,:,i)+C.'*Q;
 temp3= (-A+B*inv(R)*B.'*Mx(:,:,i)).'*Mz(:,:,i)-Mz(:,:,i)*D-Mx(:,:,i)*H1;
 Mx(:,:,i+1)=-temp1*dt+Mx(:,:,i);
 My(:,:,i+1)=-temp2*dt+My(:,:,i);
 Mz(:,:,i+1)=-temp3*dt+Mz(:,:,i);

 end
 Kx=flipdim(Mx,3);
 Ky=flipdim(My,3);
 Kz=flipdim(Mz,3);
```

Appendix E

Two-area four-generator test system data

The two-area four-generator test system is used as the benchmark power system to investigate the nature of inter-area oscillations in [33]. The system data is collected in Table B.1, B.2, B.3 and B.4, with parameters in pu and $S_B = 100MVA$.

Table E.1: Bus Data

bus #	|V|	∠V	P_gen	Q_gen	P_load	Q_load	G_shunt	B_shunt	bus type
1	1.03	18.5	7.00	1.61	0.00	0.00	0.00	0.00	1
2	1.01	8.80	7.00	1.76	0.00	0.00	0.00	0.00	2
3	1.0	-6.1	0.00	0.00	0.00	0.00	0.00	3.00	3
4	0.97	-10	0.00	0.00	16.76	1.00	0.00	0.00	3
10	1.0103	12.1	0.00	0.00	0.00	0.00	0.00	0.00	3
11	1.03	-6.8	7.16	1.49	0.00	0.00	0.00	0.00	2
12	1.01	-16.9	7.00	1.39	0.00	0.00	0.00	0.00	2
13	1.0	-31.8	0.00	0.00	0.00	0.00	0.00	5.00	3
14	0.97	-38	0.00	0.00	10.17	1.00	0.00	0.00	3
15	0.97	-38	0.00	0.00	0.50	0.00	0.00	0.00	3
20	0.9876	2.1	0.00	0.00	0.00	0.00	0.00	0.00	3
101	1.05	-19.3	0.00	0.50	0.00	0.00	0.00	1.00	2
102	1.05	-19.3	0.00	0.50	0.00	0.00	0.00	1.0	2
110	1.0125	-13.4	0.00	0.00	0.00	0.00	0.00	0.00	3
120	0.9938	-23.6	0.00	0.00	0.00	0.00	0.00	0.00	3

Table E.2: Transformer and Line Data

From	To	R	X	B	Tap ratio	Tap phase
1	10	0.0	0.0167	0.00	1.00	0.00
2	20	0.0	0.0167	0.00	1.00	0.00
3	4	0.0	0.004	0.00	0.00	0.00
3	20	0.001	0.01	0.0175	1.0	0.00
3	101	0.011	0.11	0.1925	1.0	0.00
10	20	0.0025	0.025	0.0437	1.0	0.00
11	110	0.0	0.0167	0.0	1.0	0.00
12	120	0.0	0.0167	0.0	1.0	0.00
13	14	0.0	0.005	0.0	1.0	0.00
13	15	0.0	0.01	0.0	1.0	0.00
13	102	0.011	0.11	0.1925	1.0	0.00
101	102	0.00	-0.088	0.00	1.0	0.00
13	120	0.001	0.01	0.0175	1.0	0.00
110	120	0.0025	0.025	0.0437	1.0	0.00

Table E.3: Generator Data

x_d	x_q	x_l	x'_d	x'_q	x''_d	x''_q	R_a	T'_{d0} (s)	T'_{q0} (s)	T''_{d0} (s)	T''_{q0} (s)	H	D	Rating (MVA)
1.8	1.7	0.2	0.3	0.55	0.25	0.25	.0025	8.0	0.4	0.03	0.05	6.5	2.0	900

Table E.4: Exciter Data

Ka	Ta	Tb	Tc	Vrmax	Vrmin	Ke	Te	E1	E2
20	0.06	0	0	5	-5	1	0	-2	7

Appendix F

WSCC system data

The WSCC system reduced model was developed by J.R. Smith and co-workers [50].

Table F.1: Bus Data (1)

bus #	bus name	|V|	P_gen	Q_gen	P_load	Q_load	G_shunt	B_shunt	bus type
5	PACNW_GM	1.049	38.84	25	0	0	0	0	1
1	CANAD_GM	1.049	101.08	73.2	0	0	0	0	2
14	ARIZO_GM	1.049	110.11	62	0	0	0	0	2
17	SOUTH_GM	1.049	74.98	93.75	0	0	0	0	2
10	NOCAL_GM	1.049	65.93	78	0	0	0	0	2
7	NORTH_GM	1.049	117.09	101.80	0	0	0	0	2
3	MONTA_GM	1.049	8.31	25	0	0	0	0	2
12	BUTAH_GM	1.049	30.69	25	0	0	0	0	2
4	MONTA_G1	1.03	15.08	4.75	0	0	0	0	2
13	BUTAH_G1	1.04	16.79	16	0	0	0	0	2
15	ARIZO_G1	1.049	27.04	34	0	0	0	0	2
16	ARIZO_G2	1.049	5.60	16	0	0	0	0	2
11	NOCAL_G1	1.049	12.73	5	0	0	0	0	2
8	NORTH_G1	1.049	6.68	8	0	0	0	0	2
9	NORTH_G2	1.049	9.40	16	0	0	0	0	2
6	PACNW_G1	1.049	11.41	35	0	0	0	0	2
18	SOUTH_G1	1.049	25.40	7.5	0	0	0	0	2
19	SOUTH_G2	1.049	21.77	5.25	0	0	0	0	2

7

Table F.2: Bus Data (2)

bus #	bus name	|V|	P_gen	Q_gen	P_load	Q_load	G_shunt	B_shunt	bus type
20	ARIZO_MN	1.049	0	0	100.26	57.28	0	0	3
21	CANAD_MN	1.049	0	0	107.04	48	0	0	3
22	NOCAL_MN	1.049	0	0	104.99	43.25	10	0	3
23	MONTA_MN	1.049	0	0	11.68	4.00	0	0	3
24	BUTAH_MN	1.049	0	0	44.46	16.06	10	0	3
25	NOTRTH_MN	1.049	0	0	47.94	26.69	0	0	3
26	PACNW_MN	1.049	0	0	92.68	40.13	20	0	3
27	SOCAL_TX	1.049	0	0	117.61	54.03	70	0	3
28	SOUTH_MN	1.049	0	0	64.39	23.67	0	0	3
29	CLILO_DC	1.049	0	0	18.40	60	0	30	2
30	SYLMR_DC	1.049	0	0	-18.40	15	0	18	3
31	INTMT_DC	1.049	0	0	4.0	20	0	14	3
32	ADLAN_DC	1.049	0	0	-4.0	5	0	14	3
	FAULT BUSES								
33	ARIZO_F1	1.0	0	0	0	0	0	0	3
34	ARIZO_F2	1.0	0	0	0	0	0	0	3
35	CANAD_F1	1.0	0	0	0	0	0	0	3
36	NOCAL_F1	1.0	0	0	0	0	0	0	3
37	NORTH_F1	1.0	0	0	0	0	0	0	3
38	NORTH_F2	1.0	0	0	0	0	0	0	3
39	PACNW_F1	1.0	0	0	0	0	0	0	3
40	SOUTH_F1	1.0	0	0	0	0	0	0	3
41	SOUTH_F2	1.0	0	0	0	0	0	0	3
42	MONTA_F1	1.0	0	0	0	0	0	0	3
43	BUTAH_F1	1.0	0	0	0	0	0	0	3
	Other buses								
44	ARIZO_TX	1.049	0	0	0	0	0	0	3
45	MONTA_TX	1.049	0	0	0	0	0	0	3
46	NORTH_TX	1.049	0	0	0	0	0	0	3

Table F.3: Transformer Data

From	To	from bus name	To bus name	R	X	B	Tap ratio	Tap phase
20	44	ARIZO_MN	ARIZO_TX	0.0	0.02	0.00	1.0	0.00
20	33	ARIZO_MN	ARIZO_F1	0.0	0.002	0.00	1.0	0.00
20	34	ARIZO_MN	ARIZO_F2	0.0	0.005	0.00	1.0	0.00
20	14	ARIZO_MN	ARIZO_GM	0.0	0.0007	0.00	1.0	0.00
21	1	CANAD_MN	CANAD_GM	0.0	0.001	0.00	1.0	0.00
21	35	CANAD_MN	CANAD_F1	0.0	0.005	0.00	1.0	0.00
22	36	NOCAL_MN	NOCAL_F1	0.0	0.01	0.00	1.0	0.00
22	10	NOCAL_MN	NOCAL_GM	0.0	0.0008	0.00	1.0	0.00
23	42	MONTA_MN	MONTA_F1	0.0	0.005	0.00	1.0	0.00
23	45	MONTA_MN	MONTA_TX	0.0	0.02	0.00	1.0	0.00
24	43	BUTAH_MN	BUTAH_F1	0.0	0.004	0.00	1.0	0.00
25	29	NORTH_MN	CLILO_DC	0.0	0.0033	0.00	1.0	0.00
25	37	NORTH_MN	NORTH_F1	0.0	0.003	0.00	1.0	0.00
25	38	NORTH_MN	NORTH_F2	0.0	0.003	0.00	1.0	0.00
25	7	NORTH_MN	NORTH_GM	0.0	0.0009	0.00	1.0	0.00
25	46	NORTH_MN	NORTH_TX	0.0	0.02	0.00	1.0	0.0
26	39	PACNW_MN	PACNW_F1	0.0	0.0007	0.00	1.0	0.0
26	5	PACNW_MN	PACNW_GM	0.0	0.002	0.00	1.0	0.0
30	28	SYLMR_DC	SOUTH_MN	0.0	0.0033	0.00	1.0	0.0
28	40	SOUTH_MN	SOUTH_F1	0.0	0.005	0.00	1.0	0.0
28	41	SOUTH_MN	SOUTH_F2	0.0	0.008	0.00	1.0	0.0
28	17	SOUTH_MN	SOUTH_GM	0.0	0.0008	0.00	1.0	0.0
24	31	BUTAH_MN	INTMT_DC	0.0	0.0033	0.00	1.0	0.0
32	28	ADLAN_DC	SOUTH_MN	0.0	0.0033	0.00	1.0	0.0
23	3	MONTA_MN	MONTA_GM	0.0	0.0007	0.00	1.0	0.0
24	12	BUTAH_MN	BUTAH_GM	0.0	0.0007	0.00	1.0	0.0

Table F.4: Line Data

From	To	from bus name	To bus name	R	X	B	Tap ratio	Tap phase
21	26	PACNW_MN	CANAD_MN	0.0019	0.021	0.22	0.0	0.0
23	25	NORTH_MN	MONTA_Mn	0.0019	0.0155	0.0952	0.0	0.0
45	24	MONTA_TX	BUTAH_mM	0.0085	0.0995	0.50	0.0	0.0
25	26	NORTH_MN	PACNW_MN	0.00025	0.00282	0.018	0.0	0.0
25	26	NORTH_MN	PACNW_MN	0.0003	0.00279	0.009	0.0	0.0
24	26	NORTH_TX	BUTAH_MN	0.008	0.084	0.334	0.0	0.0
26	22	PACNW_MN	NOCAL_MN	0.003	0.018	0.018	0.0	0.0
27	22	NOCAL_MN	SOCAL_TX	0.0035	0.0246	0.292	0.0	0.0
27	28	SOCAL_TX	SOUTH_MN	0.0001	0.00075	0.04	0.0	0.0
20	28	SOUTH_MN	ARIZO_MN	0.002	0.0155	0.032	0.0	0.0
44	24	BUTAH_MN	ARIZO_TX	0.0092	0.109	0.5	0.0	0.0
34	16	ARIZO_F2	ARIZO_G2	0.00007	0.007	0.0	0.0	0.0
15	33	ARIZO_G1	ARIZO_F1	0.0001	0.002	0.0	0.0	0.0
2	35	CANAD_G1	CANAD_F1	0.0006	0.0073	0.0	0.0	0.0
36	11	NOCAL_F1	NOCAL_G1	0.00007	0.0055	0.0	0.0	0.0
37	8	NORTH_F1	NORTH_G1	0.00008	0.0053	0.0	0.0	0.0
38	9	NORTH_F2	NORTH_G2	0.00007	0.0063	0.0	0.0	0.0
39	6	PACNW_F1	PACNW_G1	0.00002	0.0005	0.0	0.0	0.0
40	18	SOUTH_F1	SOUTH_G1	0.00007	0.006	0.0	0.0	0.0
41	19	SOUTH_F2	SOUTH_G2	0.00007	0.004	0.0	0.0	0.0
42	4	MONTA_F1	MONTA_G1	0.00007	0.006	0.0	0.0	0.0
43	13	BUTAH_F1	BUTAH_G1	0.00007	0.006	0.0	0.0	0.0

Table F.5: Generator of Classical Model

Bus Name	x'_d	H	D	Rating (MVA)
ARIZO_GM	0.2561	6.11	0	9000
CANAD_GM	0.1875	5.5	0	9000
NOCAL_GM	0.25	4.375	0	8000
NORTH_GM	0.2561	6.67	0	9000
MONTA_GM	0.25	2.5	0	2000
BUTAH_GM	0.25	2.67	0	6000
SOUTH_GM	0.25	4.44	0	9000
PACNW_GM	0.25	4	0	3000

Table F.6: Generator of Detail Model

Bus Name	x_d	x_q	x_l	x'_d	x'_q	R_a	T'_{d0} (s)	T'_{q0} (s)	H	D	Rating (MVA)
ARIZO_G1	1.7	1.6	0.0	0.25	0.5	.0	6.0	0.8	3.83	0	3118
ARIZO_G2	1.7	1.6	0.0	0.25	0.5	.0	6.0	0.8	3.23	0	640
CANAD_G1	0.9	0.6	0.0	0.25	0.5	.0	8.0	1.0	5.1	0	880
NOCAL_G1	1.7	1.6	0.0	0.25	0.5	.0	6.0	0.8	5.36	0	1500
MONTA_G1	1.7	1.6	0.0	0.25	0.5	.0	6.0	0.8	4.1	0	2398
BUTAH_G1	0.9	0.6	0.0	0.25	0.5	.0	8.0	1.0	2.88	0	1982
NORTH_G1	0.9	0.6	0.0	0.25	0.5	.0	8.0	1.0	2.4	0	737
NORTH_G2	0.9	0.6	0.0	0.25	0.5	.0	8.0	1.0	2.98	0	1137
PACNW_G1	1.7	0.9	0.0	0.37	0.75	.0	8.0	1.0	4.82	0	2208
SOUTH_G1	1.7	1.6	0.0	0.25	0.5	.0	6.0	0.8	5.156	0	3004
SOUTH_G2	1.7	1.6	0.0	0.25	0.5	.0	6.0	0.8	3.8044	0	2500

Table F.7: Exciter Data

Generator	Ka	Ta	Tb	Tc	Vrmax	Vrmin	Ke	Te	E1	E2
ARIZO_G1	15	0.02	0	0	5	-5	1	0	-2	7
ARIZO_G2	15	0.02	0	0	5	-5	1	0	-2	7
CANAD_G1	10	0.02	0	0	5	-5	1	0	-3	6
NOCAL_G1	15	0.02	0	0	5	-5	1	0	-2	7
MONTA_G1	10	0.02	0	0	5	-5	1	0	-3	6
BUTAH_G1	20	0.02	0	0	5	-5	1	0	-3	6
NORTH_G1	10	0.02	0	0	5	-5	1	0	-3	6
NORTH_G2	10	0.02	0	0	5	-5	1	0	-3	6
PACNW_G1	10	0.02	0	0	5	-5	1	0	-3	6
SOUTH_G1	20	0.02	0	0	5	-5	1	0	-3	6
SOUTH_G2	20	0.02	0	0	5	-5	1	0	-3	6

Vita

Lingling Fan was born in December 1973 in Qidong County, Jiangsu Province, P. R. China. She entered Southeast University (Nanjing, China) in 1990, majoring in Power System and its Automation. She got her bachelor degree in 1994 and master degree in 1997 from Dept. of Electrical Engineering, Southeast University. She enrolled in West Virginia University in Aug. 1998 as a Ph. D. candidate and worked as a research assistant for three years. The projects she was involved are Distribution Generation project, National Science Foundation funded Robust Decentralized Power System Control project. Since Oct. 2001, She worked with Mid-Continent Area Power Pool Contractor in St. Paul, Minnesota and works with Midwest Independent System Operator since Dec. 2001. Lingling Fan was married with Zhixin Miao in 1997.